

MASS TRANSPORT AND FOULING OF NOVEL FORWARD OSMOSIS THIN-FILM COMPOSITE MEMBRANES

Marc Sauchelli Toran

Per citar o enllaçar aquest document:

Para citar o enlazar este documento:

Use this url to cite or link to this publication:

<http://hdl.handle.net/10803/670169>

ADVERTIMENT. L'accés als continguts d'aquesta tesi doctoral i la seva utilització ha de respectar els drets de la persona autora. Pot ser utilitzada per a consulta o estudi personal, així com en activitats o materials d'investigació i docència en els termes establerts a l'art. 32 del Text Refós de la Llei de Propietat Intel·lectual (RDL 1/1996). Per altres utilitzacions es requereix l'autorització prèvia i expressa de la persona autora. En qualsevol cas, en la utilització dels seus continguts caldrà indicar de forma clara el nom i cognoms de la persona autora i el títol de la tesi doctoral. No s'autoritza la seva reproducció o altres formes d'explotació efectuades amb finalitats de lucre ni la seva comunicació pública des d'un lloc aliè al servei TDX. Tampoc s'autoritza la presentació del seu contingut en una finestra o marc aliè a TDX (framing). Aquesta reserva de drets afecta tant als continguts de la tesi com als seus resums i índexs.

ADVERTENCIA. El acceso a los contenidos de esta tesis doctoral y su utilización debe respetar los derechos de la persona autora. Puede ser utilizada para consulta o estudio personal, así como en actividades o materiales de investigación y docencia en los términos establecidos en el art. 32 del Texto Refundido de la Ley de Propiedad Intelectual (RDL 1/1996). Para otros usos se requiere la autorización previa y expresa de la persona autora. En cualquier caso, en la utilización de sus contenidos se deberá indicar de forma clara el nombre y apellidos de la persona autora y el título de la tesis doctoral. No se autoriza su reproducción u otras formas de explotación efectuadas con fines lucrativos ni su comunicación pública desde un sitio ajeno al servicio TDR. Tampoco se autoriza la presentación de su contenido en una ventana o marco ajeno a TDR (framing). Esta reserva de derechos afecta tanto al contenido de la tesis como a sus resúmenes e índices.

WARNING. Access to the contents of this doctoral thesis and its use must respect the rights of the author. It can be used for reference or private study, as well as research and learning activities or materials in the terms established by the 32nd article of the Spanish Consolidated Copyright Act (RDL 1/1996). Express and previous authorization of the author is required for any other uses. In any case, when using its content, full name of the author and title of the thesis must be clearly indicated. Reproduction or other forms of for profit use or public communication from outside TDX service is not allowed. Presentation of its content in a window or frame external to TDX (framing) is not authorized either. These rights affect both the content of the thesis and its abstracts and indexes.



Doctoral Thesis

Mass Transport and Fouling of Novel Forward Osmosis Thin-film Composite Membranes

Marc Sauchelli Toran

2019

Doctoral Program: Water Science and Technology

Supervisors: Dr. Wolfgang Gernjak and
Dr. Ignasi Rodriguez-Roda

Thesis submitted in fulfilment of the requirements for the degree
of: "Doctor of the University of Girona"



Dr. Wolfgang Gernjak, ICREA Research Professor at the Catalan Water Research Institute and Dr. Ignasi Rodriguez-Roda, Full Professor of the Department of Chemical and Agricultural Engineering and Agrifood Technology of the University of Girona

WE DECLARE:

That the thesis "Mass transport and fouling of novel forward osmosis thin-film composite membranes", presented by Marc Sauchelli Toran to obtain a doctoral degree, has been completed under our supervision and meets the requirements to opt for an International Doctorate.

For all intents and purposes, we hereby sign this document.

Wolfgang Gernjak

Ignasi Rodriguez-Roda

A handwritten signature in blue ink, appearing to read "Wolfgang Gernjak".

A handwritten signature in black ink, appearing to read "Ignasi Rodriguez-Roda".

Girona, 27th of June of 2019

Authors acknowledge the support from the European Regional Development Fund (FEDER) under the Catalan FEDER Operative Program 2007-2013 and MINECO through the DA3^a of the Catalan Statute of Autonomy and PGE2010, and also acknowledge the Catalan Government through Consolidated Research Group (2014 SGR 291) - Catalan Institute for Water Research and (2017 SGR 01318) - ICRA-TECH (Tecnologies i avaluació del cicle de l'aigua).

Acknowledgements

Sitting in my office I look out at the window and watch the sun set behind the Gavarres. I wonder, out of all the places I have lived throughout my life, how lucky I am to have come to Girona and completed this PhD in such a wonderful place. Nonetheless, it is the people around you that make the experience truly worthy and therefore I'd like to thank everyone with whom I've crossed paths in ICRA and the gorgeous city of Girona for making this period of my life unforgettable.

Starting something new needs a lot of motivation and Wolfgang, your drive towards cleaner waters, launched me into this project with great enthusiasm. Your guidance and advice was often recalled outside the workplace and I hope that together with Ignasi you learnt as much as I did from these three and a half years. Both of you had enormous patience with me and I'm only left with admiration. I would also like to thank Gaetan for kick-starting my experimental part. I hope to keep in touch with all of you in the future!

I've realized that sharing an office is so much more than chatting coffee breaks and lunches away. The people I had sitting next to me at work were frequently found drinking and dancing next to me in the late hours of the night, from resounding laughs in the terrace to the spilling beers on top of rocking boats. We've had so many great moments together that I'll reminisce about in the upcoming years. This big thank you goes to the oldies Lucia, Pau, Jess, Fede, Zhiyuan, Giuseppe and Natalia as well as the newbies Giannis, Esther, Jose Miguel and Aleksandra. Without a doubt I'm forgetting many more friends, from RiE and Qualitat, who make ICRA anything but boring.

Time has never passed so quickly as during my research stay in beautiful Ghent. I'll remember most of all the friendship I found in Arnout, the relaxed atmosphere of the PalnT group, Giel and Tymen's shenanigans in Hoogstraat and the freakishly good weather that enabled many beers to be drunk at the Koepuur.

Arriving home to a warm meal and huge smiles was more than I hoped for after spending long hours in the lab. To Gabe, Charrisse and Yasmin, you're like a second family, the vegetarian one. This flat has hosted countless nationalities, from the far reaches of Iran to the plains of Riuderenes, and all the scents and spices marked my daily life. They also fuelled me to cycle to work every morning with a huge grin on my face.

Sometimes you're in need of a good talk and there's nothing better than having friends like Anna and Eliza show up at your front door, ready to listen and sing the night away. To take a break there were the weekend escapades and never-ending phone calls with university mates, Josh, Luca and George. Thank you all very much for being there!

Life in two has been an amazing adventure, filled with travelling and support for each other, especially in these last few months. A huge thank you, Andrea, for encouraging me forward and for brightening up every day!

Last but not least, always there to give me a morale boost when needed, I'd like to thank with all my gratitude, my family for offering absolutely all of their help throughout these years. This thesis is dedicated to you!

Table of Contents

List of publications.....	i
List of acronyms	ii
List of figures.....	iv
List of tables.....	viii
Summary.....	x
Resumen	xii
Resum.....	xv
1 Introduction	1
1.1 The Advent of Potable Water Reuse.....	1
1.2 Osmotic membrane processes.....	1
1.3 FO in the context of Water Reuse.....	3
1.4 Challenges in FO membrane innovation	4
2 Literature Review	6
2.1 Mass Transport in FO	6
2.1.1 Modelling mass transport	7
2.1.2 Active layer	8
2.1.3 Boundary Layers	9
2.1.4 Support layer	11
2.2 FO Membrane development.....	11
2.3 Membrane Characterisation	12
2.4 Rejection of Trace Organic Contaminants (TrOCs).....	14
2.4.1 Role of the draw solution on the rejection of TrOCs	15
2.5 Fouling propensity in FO	17
2.5.1 Modelling the effects of fouling on solute and water flux.....	18
2.5.2 Roles of osmotic and hydraulic pressure on fouling	20
3 Research Objectives	23
4 Materials and Methods	25
4.1 Membranes	25
4.2 Chemicals	26

4.3	Experimental Set-up.....	28
4.4	Chemical Analysis.....	29
4.4.1	Low-concentration TrOCs analysis	29
4.4.2	High-concentration TrOCs analysis	30
4.4.3	SEM Characterisation	31
4.5	Characterisation experiments.....	31
4.6	Long-term operation TrOCs rejection experiments.....	32
4.7	TrOCs permeability experiments	33
4.7.1	Diffusion experiments	33
4.7.2	FO experiments	34
4.8	Fouling experiments.....	35
4.8.1	Effect of constant osmotic pressure.....	35
4.8.2	Effect of hydraulic pressure.....	35
5	FO-only characterisation of novel TFC membranes	37
5.1	Experimental Design and Evaluation.....	38
5.1.1	Characterisation experiments	38
5.1.2	Model implementation	38
5.2	Results and Discussion	41
5.2.1	Characterisation experiments	41
5.2.2	Assessing model accuracy	43
5.2.3	Membrane Performance parameters	44
6	Transport of trace organic contaminants through novel TFC membranes	50
6.1	Experimental Design and Evaluation.....	51
6.1.1	Fate and rejection of TrOCs in FO	51
6.1.2	Effect of DS on permeability of TrOCs.....	52
6.1.3	Determining solute-membrane interactions	53
6.2	Results and Discussion	53
6.2.1	Fate of TrOCs in system set-up.....	53
6.2.2	Rejection of TrOCs by novel TFC membranes	55
6.2.3	Effect of DS on permeability of TrOCs.....	58
7	Fouling propensity of novel TFC membranes with different driving forces.....	66
7.1	Experimental Design and Evaluation.....	67
7.1.1	Effect of constant osmotic pressure on fouling	67
7.1.2	Effect of feed hydraulic pressure on fouling	67
7.2	Modelling cake structural parameter	68

7.3	Results and Discussion	70
7.3.1	Effect of constant osmotic pressure as driving force	70
7.3.2	Effect of hydraulic pressure as driving force	74
7.3.3	Effect of draw salt reverse flux.....	79
7.3.4	Effect of membrane surface properties	81
8	Conclusions and recommendations for future research	84
8.1	FO-only characterisation of novel TFC membranes.....	84
8.2	Transport of TrOCs through novel TFC membranes	84
8.3	Fouling propensity of novel TFC membranes with different driving forces	85
8.4	General discussion and recommendations for future research	85
9	References	89

List of publications

Marc Sauchelli, Giuseppe Pellegrino, Arnout D'Haese, Ignasi Rodriguez-Roda, Wolfgang Gernjak. 2018 Transport of trace organic compounds through novel forward osmosis membranes: Role of membrane properties and the draw solution. *Water Research*: 141, 65-73.

Marc Sauchelli, Arnout D'Haese, Ignasi Rodriguez-Roda, Wolfgang Gernjak. Alginate fouling of novel TFC membranes and the impact of different driving forces. *In preparation*

List of acronyms

The following acronyms and abbreviations can be found in this thesis.

ACE	Acetaminophen
ATE	Atenolol
BEZ	Bezafibrate
CBZ	Carbamazepine
CECP	Cake-Enhanced Concentration Polarisation
CFV	Crossflow Velocity
CM1	Characterisation Method 1
CM2	Characterisation Method 2
CP	Concentration Polarisation
CTA	Cellulose Triacetate
CV	Coefficient of Variation
DI	De-ionised
DIC	Diclofenac
DS	Draw Solution
ECP	External Concentration Polarisation
EPS	Extracellular Polymeric Substance
ERY	Erythromycin
FO	Forward Osmosis
FS	Feed Solution
FUR	Furosemide
GEM	Gemfibrozil
HPLC	High-Performance Liquid Chromatography
IBU	Ibuprofen
ICP	Internal Concentration Polarisation
IND	Indomethacine
I-PAO	Intermittent Pressure Assisted Osmosis
MBR	Membrane bioreactor
MF	Microfiltration
MPSA	Minimal Projected Surface Area
MW	Molecular Weight
MWCO	Molecular Weight Cut-Off
NAD	Nadolol
NF	Nanofiltration
NI	Negative Ionisation
ODMP	Osmotically Driven Membrane Process
OMBR	Osmotic membrane bioreactor
PALS	Positron Annihilation Lifetime Spectroscopy
PAO	Pressure Assisted Osmosis
PHE	Phenazone
PI	Positive Ionisation
PLC	Programmable Logic Controller
PRO	Pressure Retarded Osmosis
PVDF	Polyvinylidene difluoride
RO	Reverse Osmosis
RSF	Reverse Salt Flux
S-D	Solution-Diffusion
SEM	Scanning Electron Microscopy

SFX	Sulfamethoxazole
SPE	Solid Phase Extraction
TFC	Thin-Film Composite
THI	Thiabendazole
TRI	Trimethoprim
TrOCs	Trace Organic Contaminants
UPLC	Ultrahigh-Performance Liquid Chromatography
UV	Ultraviolet
VEN	Venlafaxine
VER	Verapamil

List of figures

- Figure 1.1** A holistic scheme of the thesis, showing how water scarcity motivates water reuse in urban areas, employing FO as a possible solution and the main topics researched in this thesis: 1) mass transport modelling, 2) rejection of trace organic contaminants (TrOCs) and 3) membrane fouling. 2
- Figure 2.1** Draw solute concentration profile across all the transport layers showing the detrimental effects of ECP and ICP on the effective driving force. On the feed side, ECP is concentrative, whereas on the draw side both ICP and ECP are dilutive. The effective driving force across the active layer determines the water (J_w) and reverse solute fluxes (J_s). 8
- Figure 2.2** Draw solute concentration profile across all the transport layers, including the foulant cake layer, and showing the effects of ECP, ICP and CECP. 20
- Figure 4.1** Diagram of the experimental set-up, showing the circulation of the feed and draw solutions from the reservoirs, through the membrane cell unit and back into the reservoirs. Conductivity (CC) of both solutions and the weight (W) of the feed solution were monitored via a PLC connected to a PC. The draw re-concentration system used to maintain the draw solution concentration constant is also shown on the right. 29
- Figure 5.1** Flowchart of the optimisation procedure for the characterisation methods. Additional input parameters for CM2 include the mass transfer coefficients and concentration-dependent diffusivity. 40
- Figure 5.2** Graphs A, B and C illustrate water fluxes, reverse salt fluxes and the ratio of water to reverse salt flux (J_w/J_s) for the four selected membranes for a range of DS concentrations. These were taken from a single characterisation experiment for each of the membranes and are not averaged values. Graph D shows the averaged coefficient of variation (CV) as a percentage for the four membranes. 42
- Figure 5.3** Fitting of modelled water and reverse salt fluxes to the experimental fluxes obtained. The better fit of the CM1 method compared to the CM2 method is clearly seen, particularly for the water flux. 44
- Figure 5.4** Impact of the different concentration polarisation effects on the overall driving force and the resulting effective driving for the four selected membranes at increasing DS concentrations. The numbers represent the stages, with stage 4 having the highest DS concentration. The CP effects and effective driving force were modelled using CM1. 45

Figure 5.5 Modelled water and reverse salt fluxes for a varying range of <i>A</i> , <i>B</i> and <i>S_s</i> values. CM1 was used to model these fluxes for the TFC-2 membrane only. When changing one parameter, the other parameters were kept constant at the values obtained from the characterisation of TFC-2: <i>A</i> = 1.30 Lm-2h-1bar-1, <i>B</i> = 0.19 Lm-2h-1, <i>S</i> = 81 μm.	46
Figure 5.6 SEM images of the cross-section of TFC-2 (top) and TFC-3 (bottom) showing the average thickness of the membranes and the woven structure of the support layer.	49
Figure 6.1 Schematic illustrations of the different permeability experiments; on the left the diffusion experiment without any salt and only DI water, in the middle the diffusion at increasing ionic strength (<i>i</i> stands for the different concentrations of NaCl or MgCl ₂ , either 0.1M or 0.5M) and on the right the normal FO experiment with added NaCl in the draw solution only.	52
Figure 6.2 Graph A shows the changing concentration of six TrOCs in the feed solution as a function of experimental duration. Only six TrOCs are shown for clarity, some adsorb or degrade in the FO system and therefore decrease in concentration. Graph B depicts the loss of mass for most of the selected TrOCs in the FS and DS at the end of the long-term experiment.	54
Figure 6.3 Rejection percentages of the selected TrOCs at the different sampling intervals; after 3 hours and then in 10 hour intervals. Besides the rejection of phenazone by TFC-3, the rejection of all the other compounds increased as the experiment progressed.	55
Figure 6.4 Rejection percentages of the 16 TrOCs for TFC-2 and TFC-3 membranes are shown by the triangle and circle symbols, respectively. Ranitidine and Verapamil were omitted due to their poor analysis by HPLC. The MW of the compounds is shown by the bar charts below. The first 7 TrOCs on the left are negatively charged, the 6 in the middle are neutral and the 4 on the right are positively charged.	57
Figure 6.5 Permeability of TrOCs through TFC-2 and TFC-3 as a function of molecular weight for the diffusion tests without salt and with 0.5M NaCl and 0.5M MgCl ₂ ionic strength. Positive, negative and neutral compounds are marked with a positive sign, negative sign and a square, respectively.	61
Figure 6.6 Permeability coefficients of TrOCs through TFC-2 and TFC-3 as a function of molecular weight obtained for the diffusion tests without salt, at 0.1M NaCl ionic strength the FO tests. Positive, negative and neutral compounds are marked with a positive sign, negative sign and a square, respectively.	63

Figure 6.7 Graphical summary of the solute-membrane interactions for TFC-2 and TFC-3 in the different scenarios tested in this study. A) Diffusion tests with DI water: sterics dominated TrOCs transport through TFC-2 whereas electrostatic attraction/repulsion interactions were strongly present in TFC-3. B) At higher membrane ionic strength, a reduction of membrane pore sizes and shielding of membrane surface charges were observed for TFC-2 and TFC-3, respectively. C) In the FO experiments, convective transport of solutes towards the membrane facilitated the permeability of TrOCs whereas reverse salt flux had little impact on their transport.	64
Figure 7.1 Schematic illustrations of the different fouling experiments. From left to right: baseline test without added alginate, fouling with a non-constant osmotic pressure difference, fouling with a constant osmotic pressure difference and PAO mode with a constant osmotic pressure and an applied hydraulic pressure in the feed.	68
Figure 7.2 Flowchart of the optimisation procedure for the modelling of the cake structural parameter.	70
Figure 7.3 Water flux profiles for the baseline and fouling tests, with non-constant and constant DS concentrations and for TFC-2 and TFC-3.	71
Figure 7.4 Contribution of the different concentration polarisation effects and hydraulic resistance on the overall driving force. The components were calculated for the TFC-3 membrane at three different stages of the experiment, at the beginning, after 4 hours and at the end after 8 hours. The experiments compared are FO fouling with non-constant and constant DS concentrations.	73
Figure 7.5 Water flux profiles for the baseline and fouling tests, with constant DS concentrations, in FO and PAO experiments and for TFC-2 and TFC-3.	75
Figure 7.6 Modelled cake structural parameter and pore hydraulic diameter as a function of time for a case in which the pore size remains constant (as assumed in the model) and for a decreasing pore size that is expected during compaction of the alginate gel. This plot was generated using the model. On the right, an illustration of how the pore size (D_h) and the alginate layer thickness (δ_c) would decrease if compaction occurred.	77
Figure 7.7 Contribution of the different concentration polarisation effects, hydraulic resistance and hydraulic pressure on the overall driving force. Again, these components were calculated for the TFC-3 membrane at three different stages of the experiment, at the beginning, after 4 hours and at the end after 8 hours. The experiments compared are FO mode with constant DS concentration, PAO mode with 1 bar of hydraulic pressure and PAO mode if the real hydraulic pressure is 5 bar.	78

Figure 7.8 Water flux profiles for the baseline and fouling tests, with constant DS concentrations, in FO experiments with NaCl and Na ₂ SO ₄ as draw salts and for TFC-2 and TFC-3.	79
Figure 7.9 Contribution of the different concentration polarisation effects and hydraulic resistance on lowering the overall driving force to the resulting effective driving force. Again, these components were calculated for the TFC-3 membrane at three different stages of the experiment, at the beginning, after 4 hours and at the end after 8 hours. The experiments compared are FO mode with constant NaCl DS concentration and FO mode with constant Na ₂ SO ₄ DS concentration.	81
Figure 7.10 First derivative of water flux plotted against time, showing the initial effect of foulant-membrane interactions on the water flux decline. These were calculated from the FO experiments at constant DS concentration.	83

List of tables

Table 2.1 Summary of recent fouling studies which compare fouling behaviour in FO, PAO and RO mode. Flux decline rates vary significantly whereas flux recovery is usually greater in FO mode. Comparing all the studies is difficult because different membranes, experimental set-ups, foulants and feed pressures are used.	22
Table 4.1 Membrane performance parameters and physico-chemical properties for the selected membranes, obtained with the RO-FO characterisation method and further characterisation from literature. Membrane providers of TFC-2 and TFC-3 are kept undisclosed.	25
Table 4.2 List of the selected organic compounds with the purity and product reference. The physico-chemical properties of the TrOCs are also summarised.	27
Table 4.3 A list of the three groups of TrOCs that were analysed independently by HPLC-UV with the corresponding retention times and mobile phase mixtures. These were chosen based on retention times, polarity and charge.	31
Table 4.4 Starting conditions for the long-term fate of TrOCs in the FO system and the membrane rejection experiments.	33
Table 4.5 Starting conditions for the diffusion experiments with DI water, the diffusion experiments at higher ionic strength and for the FO experiments	35
Table 4.6 Starting conditions for the fouling experiments designed to determine the effect of a constant osmotic pressure as driving force and the fouling experiments designed to determine the effect of hydraulic pressure as driving force	36
Table 5.1 Coefficients of the determination of water and reverse salt fluxes for the selected membranes obtained from the two different characterisation methods	43
Table 5.2 Summary of the membrane performance parameters obtained from the two FO-only characterisation methods (CM1 and CM2) used herein for the selected membranes. Also listed are the parameters reported from other FO-only and RO-FO methods in the literature on the same membranes.	48
Table 6.1 Pearson and Spearman's rank correlations between the rejection of the TrOCs by TFC-2 and TFC-3 membranes and their physico-chemical parameters.	57

Table 6.2 TrOCs permeability coefficients for all the diffusion and FO experiments and for both novel TFC membranes.	59
Table 6.3 Pearson and Spearman's rank correlations between solute physico-chemical properties and the permeability coefficients of the TrOCs for both TFC-2 and TFC-3 membranes. The feed and draw solution compositions are also shown. The physico-chemical properties include: MW (Molecular weight), MPSA (Minimal projected surface area), LogD (Hydrophobicity) and charge.	60
Table 7.1 Results of the water flux decline, final alginate surface density and the final calculated cake structural parameter for both TFC membranes and for experiments with non-constant and constant DS concentrations.	72
Table 7.2 Water flux decline, final alginate surface density and the final calculated cake structural parameter for both TFC membranes and for FO mode and PAO mode experiments.	76
Table 7.3 Water flux decline, final alginate surface density and the final calculated cake structural parameter for both TFC membranes and for experiments with NaCl as the DS and experiments with Na ₂ SO ₄ as the DS.	80

Summary

Forward osmosis (FO) is known to be particularly efficient at treating impaired water sources with a high fouling potential. In the context of water reuse FO is being introduced as a robust pre-treatment process, usually as a first barrier prior to a reverse osmosis (RO) step. The commercialisation of FO however hinges on the development of higher permeability membranes and a recent breakthrough came with the introduction of thin-film composite (TFC) membranes. While promising state-of-the-art TFC membranes have been successfully fabricated and tested at the pilot-scale, their performance in FO is yet to be determined by comprehensive characterisation under the changed, elevated transmembrane water flux conditions.

Despite FO's apparent lower fouling propensity compared to RO, membrane fouling remains a major concern, limiting the long term efficiency of the process. Numerous studies have been carried out to determine the factors and complex mechanisms governing the fouling behaviour in FO membranes. However, since most of the fouling studies have been performed with the same benchmark cellulose triacetate (CTA) membrane, there is a need to investigate the fouling phenomena at the changed operating conditions with novel TFC membranes. Another challenge associated with the reclamation of impaired water for potable use is the presence of emerging trace organic contaminants (TrOCs) in wastewater. Seeing that a main benefit of FO is the high rejection of a number of organic pollutants, FO has received increasing attention as a potential barrier for these compounds. In this respect, the removal mechanisms of organic compounds are still not fully understood, particularly regarding the role of reverse draw salt diffusion and the influence of sorption saturation behaviour on the rejection of TrOCs by TFC membranes.

To fill these gaps, in this thesis mass transport through novel TFC membranes was initially studied and modelled using two FO-only characterisation methods. Improvements in membrane water permeability were clearly observed for the two selected TFC membranes, with water fluxes exceeding $20 \text{ L m}^{-2} \text{ h}^{-1}$ even at low draw solution concentrations, and these were attributed to a greater active layer free volume and thinner support layers. Although the applied characterisation methods successfully predicted the transport and structural parameters of conventional membranes, novel TFC membranes were found to be more sensitive to experimental errors during characterization and therefore require a more rigorous approach to be able to compare their performance. Greater water permeability of the TFC

membranes was accompanied by a lower rejection of neutral and positively charged organic compounds. Whilst negatively charged solutes were rejected above 90%, some neutral and positively charged solutes had rejections of less than 60%. It was found that electrostatic interactions between these solutes and the strong membrane surface charge of novel TFC membranes played a crucial role in the rejection of trace organic contaminants. Moreover, the use of draw solution concentrations typical in FO operation was found to alter solute-membrane interactions, indirectly affecting the forward transport of trace organic compounds.

Also in this study, alginate fouling in novel TFC membranes was thoroughly examined under different driving forces. Significantly more fouling occurred when the osmotic pressure difference was maintained constant, with more than 3 times the alginate surface density deposited on the membrane, contrasting the premise of low fouling tendency in the FO process. On the other hand, the thinner but denser foulant cake layer observed at an applied hydraulic pressure of 1 bar was partly attributed to the commonly reported pressure-induced compaction along with the different response of the membrane to hydraulic pressure and the presence of membrane defects. In quantifying the cake layer structural parameter, the current model based on the water flux decline was found to lack more accurate structural-related parameters of alginate gels to allow a better description of fouling behaviour.

Overall, the knowledge obtained from this thesis on the complex mass transport phenomena through novel TFC FO membranes is highly relevant for membrane developers who aim to enhance membrane performance whilst maintaining a high rejection of feed solutes and improve anti-fouling properties. In advancing the application of FO in wastewater treatment and reuse more efficient system designs and membrane modules are needed. These will depend on accurate water flux and fouling models that take into account the impacts of hydraulic pressure and higher permeability on membrane performance.

Resumen

La ósmosis directa (OD) es particularmente eficaz en tratar aguas residuales con un alto potencial de contaminación y ensuciamiento. En el contexto de la reutilización del agua, la OD se está consolidando como un proceso de tratamiento robusto, generalmente como pretratamiento de la ósmosis inversa (OI). Sin embargo, la comercialización de la OD depende del desarrollo de membranas de mayor permeabilidad. Un avance reciente se produjo con la introducción de membranas thin-film composite (TFC). Aunque las membranas de TFC se han fabricado y probado con éxito a escala piloto, su rendimiento en OD aún no se ha determinado mediante una caracterización completa con condiciones de flujo de agua elevado.

A pesar de la aparente menor propensión al ensuciamiento de la OD en comparación con la OI, el ensuciamiento de la membrana sigue siendo una restricción importante, limitando la eficacia del proceso a largo plazo. Se han realizado numerosos estudios para determinar los factores y complejos mecanismos que rigen el comportamiento del ensuciamiento de las membranas de OD. Sin embargo, dado que la mayoría de los estudios de ensuciamiento se han realizado con la misma membrana de tri-acetato de celulosa (CTA) de referencia, existe la necesidad de investigar los fenómenos de ensuciamiento en las condiciones operativas modificadas con las nuevas membranas de TFC. Otro desafío asociado con la recuperación de agua residual para uso potable es la presencia de micro-contaminantes orgánicos emergentes (TrOC). Un beneficio principal de la OD es el alto rechazo de una serie de contaminantes orgánicos. Por lo tanto, la OD ha recibido mucha atención como proceso de rechazo de estos compuestos. A este respecto, los mecanismos de eliminación de los compuestos orgánicos aún no se conocen del todo. En particular con respecto al papel de la difusión de sal inversa y la influencia de saturación de sal en el rechazo de los TrOCs por las membranas de TFC.

En esta tesis, el transporte de masa a través de las nuevas membranas de TFC se ha estudiado y modelado inicialmente utilizando dos métodos de caracterización de OD. Las mejoras en la permeabilidad de agua de la membrana se observaron claramente para las dos membranas TFC seleccionadas. Los flujos de agua de las nuevas

membranas de TFC excedieron los $20 \text{ L m}^{-2} \text{ h}^{-1}$, incluso a bajas concentraciones de sal en solución de extracción. Esto se atribuyó a un mayor tamaño de poros de la capa activa y capas de soporte más delgadas. Aunque los métodos de caracterización aplicados determinaron con éxito el transporte y los parámetros estructurales de las membranas convencionales, se descubrió que las nuevas membranas de TFC eran más sensibles a los errores experimentales durante la caracterización y, por lo tanto, requieren un enfoque más riguroso para poder comparar su rendimiento. La mayor permeabilidad de agua de las membranas de TFC fue acompañada por un menor rechazo de compuestos orgánicos neutros y cargados positivamente. Mientras que los solutos con carga negativa se rechazaron por encima del 90%. Algunos solutos con carga positiva y neutra tuvieron rechazos menores al 60%. Se observó que las interacciones electrostáticas entre los solutos orgánicos y la carga superficial de las nuevas membranas de TFC afectaron fuertemente el rechazo de los solutos. Además, se vio que el uso de concentraciones típicas de la solución de extracción en la operación de la OD altera las interacciones entre los solutos y la membrana, afectando indirectamente el transporte de compuestos orgánicos.

En este estudio también se examinó el ensuciamiento con alginato de las nuevas membranas de TFC bajo diferentes fuerzas impulsoras (presión osmótica y presión hidráulica). Se produjo mayor ensuciamiento cuando la diferencia de presión osmótica se mantuvo constante, triplicando la cantidad de alginato depositado en la membrana. Este resultado contrasta con la premisa de una baja tendencia al ensuciamiento en el proceso de la OD. Por otro lado, una capa de ensuciamiento más delgada pero más densa fue obtenida a una presión hidráulica aplicada de 1 bar. Esto se atribuyó en parte a la compactación inducida por presión hidráulica junto con los efectos degenerativos de la integridad de la membrana bajo presión hidráulica. Al cuantificar el parámetro estructural de la capa de ensuciamiento, se encontró que el modelo actual carece de parámetros estructurales más precisos relacionados con los geles de alginato para permitir una mejor descripción del comportamiento de ensuciamiento de membranas.

En general, el conocimiento obtenido de esta tesis sobre los complejos fenómenos de transporte de masa a través de las nuevas membranas de TFC es muy relevante para

los desarrolladores de membranas, que buscan mejorar el rendimiento de la membrana, mantener un alto rechazo de TrOCs y mejorar las propiedades para evitar el ensuciamiento. Además, para avanzar en la aplicación de la OD en el tratamiento y reutilización de aguas residuales, se necesitan sistemas y módulos de membrana más eficientes. Estos dependerán de modelos precisos de flujo de agua que tengan en cuenta los impactos del ensuciamiento, de la presión hidráulica y una mayor permeabilidad en el rendimiento de la membrana.

Resum

L'osmosi directa (OD) és especialment eficaç per tractar aigües residuals amb un alt potencial de contaminació i embrutiment. En el context de la reutilització de l'aigua, la OD s'està mostrant com un procés de tractament robust, generalment abans d'una etapa d'osmosi inversa (OI). No obstant això, la comercialització de la OD depèn del desenvolupament de membranes de major permeabilitat. Un avanç significatiu recent es va produir amb l'aparició de membranes thin-film composite (TFC). Tot i que les membranes de TFC s'han fabricat i provat amb èxit a escala pilot, el seu rendiment en OD encara no s'ha determinat mitjançant una caracterització completa sota condicions de flux d'aigua elevat.

Tot i l'aparent menor propensió a l'embrutiment de la OD en comparació de la OI, l'embrutiment de la membrana segueix sent una restricció important, limitant l'eficàcia del procés a llarg termini. S'han realitzat nombrosos estudis per determinar els factors i mecanismes complexos que regeixen el comportament de l'embrutiment de les membranes d'OD. No obstant això, atès que la majoria dels estudis d'embrutiment s'han realitzat amb la mateixa membrana de tri-acetat de cel·lulosa (CTA) de referència, hi ha la necessitat d'investigar els fenòmens de embrutiment en les condicions operatives modificades amb les noves membranes de TFC. Un altre desafiament associat amb la recuperació d'aigua residual per a ús potable és la presència de micro-contaminants orgànics emergents (Troc). Un benefici principal de la OD és l'alt rebuig d'una sèrie de contaminants orgànics. Per tant, la OD ha rebut molta atenció com a procés d'eliminació d'aquests compostos. Referent a això, els mecanismes d'eliminació dels compostos orgànics encara no es coneixen del tot. En particular pel que fa al paper de la difusió de sal inversa i la influència de saturació de sal en el rebuig dels TroCs a les membranes de TFC.

En aquesta tesi, el transport de massa a través de les noves membranes de TFC s'ha estudiat i modelat inicialment utilitzant dos mètodes de caracterització d'OD. Les millores en la permeabilitat d'aigua de la membrana es van observar clarament per a les dues membranes TFC seleccionades. Els fluxos d'aigua de les noves membranes de TFC van excedir els $20 \text{ L m}^{-2} \text{ h}^{-1}$, fins i tot a baixes concentracions de sal a la solució

d'extracció. Això es va atribuir a una major grandària de porus de la capa activa i a que les capes de suport són més primes. Tot i que els mètodes de caracterització aplicats van determinar amb èxit el transport i els paràmetres estructurals de les membranes convencionals, es va descobrir que les noves membranes de TFC eren més sensibles als errors experimentals durant la caracterització i, per tant, requereixen un enfocament més rigorós per poder comparar el seu rendiment. La major permeabilitat d'aigua de les membranes de TFC va ser acompanyada per un menor rebuig de compostos orgànics neutres i carregats positivament. Mentre que els soluts amb càrrega negativa es van rebutjar per sobre del 90%, alguns soluts amb càrrega positiva i neutra van tenir rebutjos de menys del 60%. Es va observar que les interaccions electrostàtiques entre els soluts orgànics i la càrrega superficial de les noves membranes de TFC va afectar fortament el rebuig dels soluts. A més, es va veure que l'ús de concentracions típiques de la solució d'extracció en l'operació de la OD altera les interaccions entre els soluts i la membrana, afectant indirectament el transport de compostos orgànics.

En aquest estudi també es va examinar l'embrutiment d'alginat de les noves membranes de TFC sota diferents forces impulsores (pressió osmòtica i pressió hidràulica). Es va produir més embrutiment quan la diferència de pressió osmòtica es va mantenir constant, amb més del triple de la quantitat d'alginat dipositat a la membrana. Aquest resultat contrasta amb la premissa d'una baixa tendència a l'embrutiment en el procés de la OD. D'altra banda, una capa d'embrutiment més prima però més densa va ser obtinguda a una pressió hidràulica aplicada d'1 bar. Això es va atribuir en part a la compactació induïda per pressió hidràulica juntament amb els efectes degeneratius de la integritat de la membrana sota pressió hidràulica. Al quantificar el paràmetre estructural de la capa d'embrutiment, es va trobar que el model actual no té paràmetres estructurals prou precisos relacionats amb els gels d'alginat per permetre una millor descripció del comportament d'embrutiment de membranes.

En general, el coneixement obtingut d'aquesta tesi sobre els complexos fenòmens de transport de massa a través de les noves membranes de TFC és molt rellevant per als desenvolupadors de membranes que busquen millorar el rendiment de la membrana, mantenir un alt rebuig dels TrOCs i millorar les propietats per evitar l'embrutiment. A

més, per avançar en l'aplicació de la OD en el tractament i reutilització d'aigües residuals, es necessiten sistemes i mòduls de membrana més eficients. Aquests dependran de models precisos de flux d'aigua que tinguin en compte els impactes del embrutiment i de la pressió hidràulica, així com una major permeabilitat en el rendiment de la membrana.

1 Introduction

1.1 The Advent of Potable Water Reuse

Global water-related problems are expected to exacerbate in the coming decades, with water scarcity occurring in developed and developing regions which were previously considered water-rich (Shannon et al., 2008). In order to augment fresh water supplies in these water-scarce regions, water reuse initiatives are increasingly being put into practice. These include non-potable (e.g. agricultural and landscape irrigation), indirect potable (e.g. groundwater and surface water re-charge) and direct potable reuse (Guo et al., 2014). Although direct potable reuse is the least implemented, it has many benefits over other water reuse options. These are highlighted by Leverenz et al. (2011) and include i) a high yield of produced water which is used entirely compared to indirect potable reuse, where a significant share of the reclaimed water is simply lost in the environmental buffer (evaporation or seepage into the ground), ii) a high quality of produced water without the risk of recontamination from the environmental buffer iii) ease of integration with existing drinking water infrastructure, iv) a lesser demand on drinking water treatment facilities, particularly at peak times and lastly, v) a continuous supply of water, independent of droughts and other environmental factors.

Generally, non-potable reuse applications use water treated by conventional treatment methods. For example, activated sludge systems and membrane bioreactors, are two commonly used technologies in the removal of organics and nutrients (Bixio et al., 2006). This is not the case for potable reuse, which requires a more comprehensive wastewater treatment approach, involving a combination of conventional treatment systems and more advanced processes to achieve safe drinking water. Current tertiary treatment often includes reverse osmosis (RO) followed by ultra-violet disinfection as two of several barriers to dissolved species and contaminants. However, high energy requirements and membrane fouling are some of the drawbacks that limit the efficiency of reverse osmosis.

1.2 Osmotic membrane processes

To tackle the challenge of treating wastewater for direct potable reuse, novel water treatment technologies and operating schemes have been proposed. One class of these technologies is osmotically-driven membrane processes (ODMPs) which rely on an osmotic pressure gradient to drive water across a semi-permeable membrane (Cath et al., 2006). In these processes, solutes have a much lower permeability through the membrane than water, therefore a water

flux establishes from a solution of low osmotic pressure to a solution of high osmotic pressure. Forward Osmosis (FO) is an ODMP in which water spontaneously permeates from a feed solution to a more saline draw solution (Mccutcheon and Elimelech, 2006).

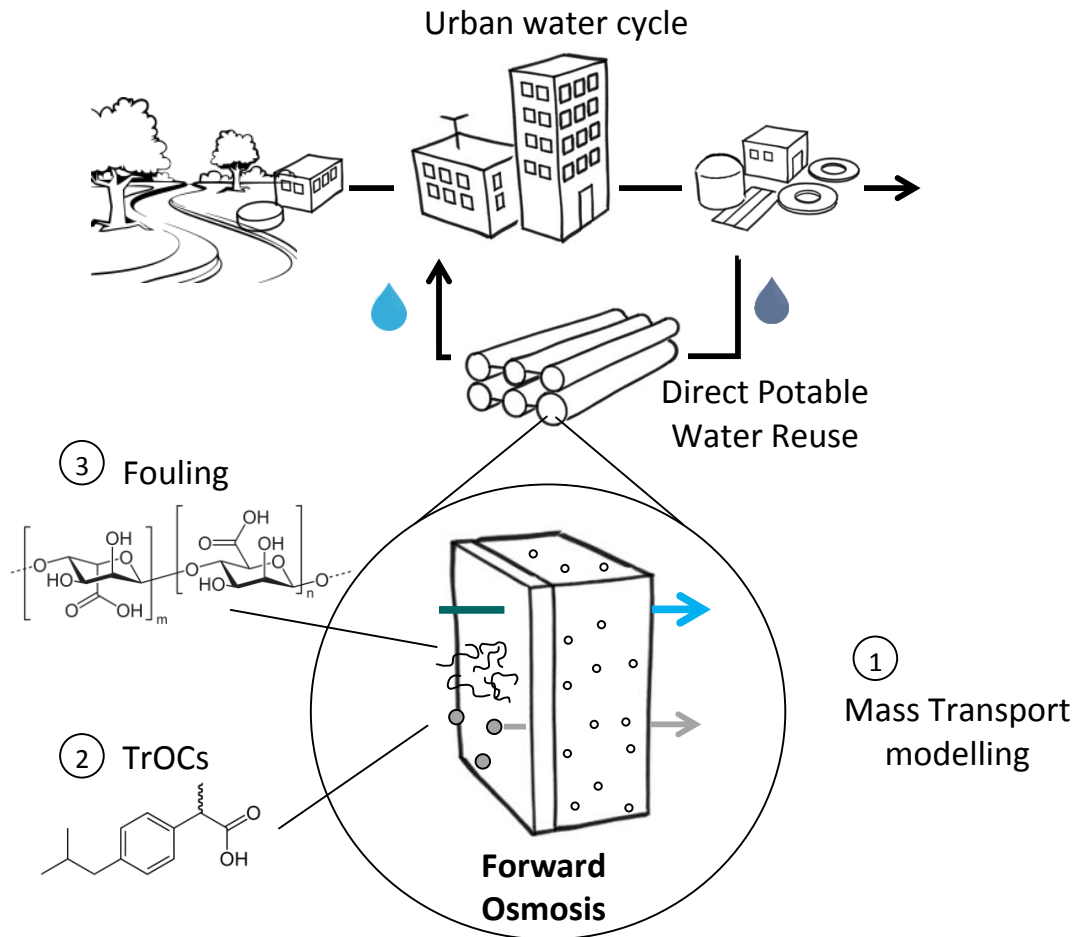


Figure 1.1 A holistic scheme of the thesis, showing how water scarcity motivates water reuse in urban areas, employing FO as a possible solution and the main topics researched in this thesis: 1) mass transport modelling, 2) rejection of trace organic contaminants (TrOCs) and 3) membrane fouling.

There are other ODMPs that employ hydraulic pressure to combine with or counteract the osmotic pressure. Pressure-assisted osmosis (PAO), for example, consists in adding hydraulic pressure to the feed solution to enhance water recovery. In contrast, pressure-retarded osmosis (PRO) uses hydraulic pressure on the draw solution to convert the marginal increase in pressure to power production. Although reverse osmosis (RO) is not an ODMP, hydraulic pressure is applied to the draw solution in excess of the osmotic pressure to drive water in the opposite direction of FO. Out of all these processes, RO is the most extensively used in full-scale water treatment facilities, however practical applications of the FO technology are emerging with pilot-scale demonstration projects worldwide (Awad et al., 2019). Recent

developments in membranes, draw solutions and a further understanding of mass transport through dense membranes have contributed to the increased interest of ODMPs in water treatment. Forward osmosis in particular has gained a lot of attention in the last decade leading to an exponential increase in publications and reviews (Shaffer et al., 2015).

1.3 FO in the context of Water Reuse

Numerous bench-scale studies have demonstrated FO as a promising technology in treating complex wastewater at a lower energy demand than other treatment processes and with a much lower fouling tendency (Lutchmiah et al., 2014). These advantages are thought to arise from the lack of hydraulic pressure required to operate it. However, the standalone FO process cannot achieve direct potable reuse. In order to abstract pure water from the draw solution and maintain a high osmotic pressure gradient across the membrane, the draw solute needs to be separated from the water and re-concentrated. As a result, the feasibility of many FO applications relies on the efficiency and energy demand of this re-concentration process (Ge et al., 2013). Many draw solution re-concentration processes have been explored, such as membrane distillation (MD), ultrafiltration (UF), nanofiltration (NF) and reverse osmosis (RO). If low-cost waste heat is available, an integrated FO-MD system has great potential in wastewater reclamation (Husnain et al., 2015). On the other hand, operation costs of FO-UF/NF hybrids are more affordable compared to other integrated systems but are inadequate in retaining monovalent ions. Since the most widely employed draw solutes are monovalent inorganic salts, the FO-RO hybrid is often recommended (Chung et al., 2012). Its potential in reclaiming water and ultimately achieving direct potable reuse has not gone unnoticed and lab-scale FO-RO pilots have been designed and tested (Bamaga et al., 2011; Hancock et al., 2013). The additional RO step adversely increases energy demands, but it also offers a multi-barrier operation to ensure reclaimed water is apt for public consumption.

Possible applications of the FO-RO hybrid in water reuse include the treatment and concentration of anaerobic digester centrate (Holloway et al., 2007), the development of the osmotic membrane bioreactor (OMBR) to extract water from activated sludge (Achilli et al., 2009; Cornelissen et al., 2008), and water recovery from raw sewage (Lutchmiah et al., 2011). In these applications, the FO step essentially acts as a pre-treatment prior to RO filtration (Ansari et al., 2016). More recently, the FO-RO hybrid system has been implemented at the pilot-scale with seawater or other readily available brines as the draw solution stream. This configuration enables the simultaneous reclamation of complex wastewater and desalination at a lower energy demand whilst maintaining a high quality of produced water (Cath et al.,

2010; Chekli et al., 2016). As part of the process, the draw solution stream is diluted by FO and passed through an RO step to generate drinking water, whereas the wastewater feed is concentrated to facilitate its further treatment (Klaysom et al., 2013). This integrated concept of water reuse and desalination is an alternative to MF-RO and RO trains, whereby a key advantage is the double barrier through a semi-permeable membrane for the treated secondary effluent.

Although FO has proven to be a promising alternative technology for wastewater treatment, further research and conceptual proofs are needed to turn ideas from the laboratory scale into a large-scale treatment process. In addition, mass transport limitations of the FO process and membrane performance still restrict the economic feasibility of many applications (Chung et al., 2012).

1.4 Challenges in FO membrane innovation

Developing membranes that offer high water permeability, high rejection of feed contaminants and lower fouling tendency is regarded as the ultimate goal in the commercialisation of FO in water treatment. However, considering that the forward osmosis process is not fully understood and the least mature of the membrane processes, improving all these factors is challenging and does not necessarily guarantee better overall treatment efficiency. For example, in polymer-based membranes, attempts to improve water flux are usually accompanied by an undesired increase in the permeability of solutes. This includes the draw solutes and even organic contaminants in wastewater feed streams that fail to be fully retained. In order to compare the performance of conventional and new commercial or lab-fabricated FO membranes, a standard characterisation method is required.

Fouling is a key aspect in membrane processes as it compromises the quantity and quality of product water, increases energy consumption and cleaning costs. The effect of high FO flux operation on fouling behaviour is still not fully understood. Lack of an applied hydraulic pressure in FO was initially considered to be the cause of low fouling propensity and high reversibility. However, operating at higher fluxes with novel membranes has been reported to enhance fouling (Blandin et al., 2016b), and recently the FO process has been identified as being intrinsically more prone to fouling than RO (Siddiqui et al., 2018). Pressure drops in feed channels and resulting pressure-build up in large scale FO modules and elements have previously been neglected as they impacted little in the previously prevailing cellulose acetate membranes with low permeability. However, with a change to thin-film composite membranes

and their changed performance, small hydraulic pressures might significantly alter water and solute fluxes and fouling propensity in the FO process.

2 Literature Review

2.1 Mass Transport in FO

A fundamental understanding of the mechanisms at play in FO membrane separation is important in fine-tuning membrane materials and improving the efficiency of the FO process. In this section, the mechanisms of mass transport in the FO process will be thoroughly explained, together with a general description of modelling water and solute fluxes.

Mass transport through FO membranes can be influenced by many factors including membrane type and structure, composition of the feed and draw solutions, hydrodynamic conditions, and more (Wang et al., 2014). FO membranes are composed of a dense, non-porous and very thin active layer that hinders mass transport and a porous support layer for mechanical strength. Generally, in water treatment, the membrane is oriented with the active layer facing the feed solution to minimize fouling (Mi and Elimelech, 2008). The rate at which water and solutes permeate through the membrane largely depends on the size distribution of the active layer's free volume voids (Kim et al., 2017). For example, organic solutes with molecular sizes larger than the free volume voids are retained very efficiently due to steric hindrance. On the other hand, small inorganic ions such as Na^+ , Mg^{2+} , Cl^- and SO_4^{2-} have effective hydrated radii smaller than the free volume voids, resulting in greater diffusion rates. In addition to the free volume voids, water and solute permeability through the active layer are dictated by the physico-chemical properties of the membrane. Water permeates better through hydrophilic membranes, whereas small inorganic ions have considerably lower permeability than water due a combination of electrostatic mechanisms. These include electrostatic interactions between the charged membrane and the ions, electro-neutrality across the membrane and the effect of Donnan potential (D'Haese et al., 2016).

The draw solution is the driving force for water transport through the membrane. A wide range of draw solutes have been explored in the literature, from inorganic salts to organic solutes, each with their own advantages and drawbacks (Achilli et al., 2010; Ge et al., 2013). Draw solutions are chosen based on their wide availability, low cost, ease of regeneration and the osmotic pressures that they generate. Usually very concentrated draw solutions are employed and, as a result, an unwanted but significant reverse diffusion of draw solute into the feed may occur. This is termed reverse solute flux (RSF) (Cath, 2009). In water treatment, the feed water may contain a myriad of solutes of different sizes that can diffuse through the membrane into the draw solution, including inorganic salts and organic compounds. Transport

of these solutes is denominated as feed solute flux but it is commonly reported in terms of feed solute rejection and less commonly as feed solute passage as they usually permeate to a low extent, analogous to pressure-driven RO. Furthermore, FO is subject to Concentration Polarisation (CP) effects, a phenomenon that arises due to unequal mass transfer rates at the solution-membrane interfaces. CP includes effects that occur externally, termed External Concentration Polarisation (ECP), but can also incur internally in the porous membrane support layer, termed Internal Concentration Polarisation (ICP). Hydrodynamic conditions such as the cross-flow velocity have significant impacts on the degree of CP (Mccutcheon and Elimelech, 2006). This affects the concentration of both the feed solutes and the draw salt and it is further described in the next section.

2.1.1 Modelling mass transport

Attempts to model the water flux (J_w) and both feed and draw solute fluxes (J_s) in FO have led to numerous semi-empirically derived equations. For mass transport across the active layer, equations are derived from the solution-diffusion (S-D) model, whereas for transport across the porous support layer and boundary layers from convective-diffusion theory (Mccutcheon and Elimelech, 2006; Wang et al., 2014). Many of the proposed equations incorporate the effects of concentration polarisation, but attempt to simplify the complex phenomena involved by incorporating assumptions and lumping several aspects into single parameters (Manickam and McCutcheon, 2017). Nagy (2014) introduced a general mass transport model that describes all transport processes and mass transfer resistances in series. These consist in the active and support layers of the membrane and the external feed and draw boundary layers. Knowing the mass transfer parameters in each of the individual transport layers is the basis for determining the draw solute concentration distribution at the distinctive membrane-solution interfaces (Figure 2.1). Accordingly, the effective concentration difference across the active layer and the resultant water flux and solute fluxes can be predicted (Tow and Lienhard, 2016). Due to its comprehensive inclusion of all phenomena occurring from the feed to the draw side, this is the model that will be used throughout the thesis to interpret the results.

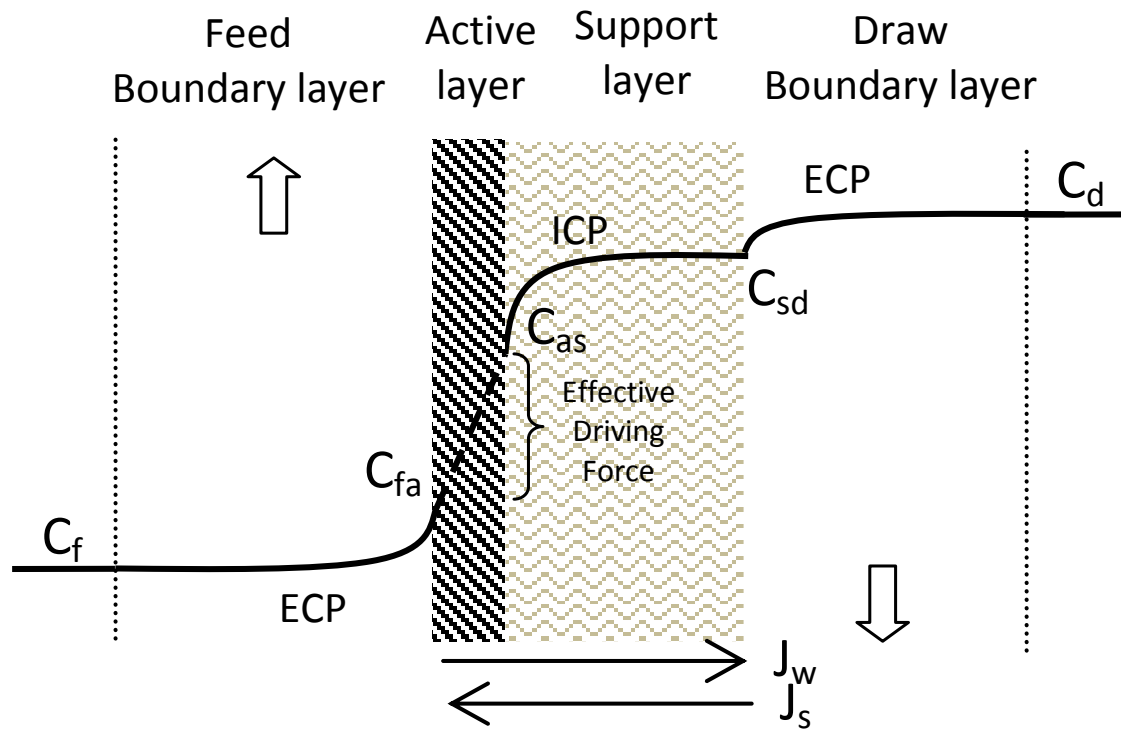


Figure 2.1 Draw solute concentration profile across all the transport layers showing the detrimental effects of ECP and ICP on the effective driving force. On the feed side, ECP is concentrative, whereas on the draw side both ICP and ECP are dilutive. The effective driving force across the active layer determines the water (J_w) and reverse solute fluxes (J_s).

2.1.2 Active layer

The dense active layer generates the greatest resistance to water and solute transport. Hence, the overall flux of water and solutes across the membrane is dictated by the solution and diffusion of these species in the active layer. In the model, the active layer is considered non-porous and homogenous, water and solutes are assumed to be uncoupled and no interactions between water, solutes and the membrane are taken into account. The water flux is defined as a function of the effective osmotic pressure difference across the active layer and the membrane water permeability coefficient (A), as shown in equation (2.1). Whereas, the solute flux is defined as a function of concentration difference across the active layer and the solute permeability coefficient (B), shown in equation (2.2):

$$J_w = A(\pi_{as} - \pi_{fa}) \quad (2.1)$$

$$J_s = B(C_{fa} - C_{as}) \quad (2.2)$$

Here C_{fa} and π_{fa} are the solute concentration and osmotic pressure at the feed solution-active layer interface. C_{as} and π_{as} are the solute concentration and osmotic pressure at the active layer-support layer interface, respectively. Since these concentrations and osmotic pressures cannot be determined experimentally, they have to be derived from the model. The solute flux (equation (2.2)) is valid for feed solute fluxes and RSF. In the case of RSF, the difference in salt concentration across the active layer is negative; therefore the salt flux will result in the opposite direction to the water flux.

It is important to note that both A and B coefficients are intrinsic to the membrane and are considered to be constant regardless of hydrodynamic conditions and osmotic driving force. Nonetheless, a recent study has suggested that water permeability (A) is affected by osmotic dehydration and that the solute permeability coefficient (B) is concentration-dependent (D'Haese et al., 2016). In the same study, electrostatic interactions between the active layer and the solutes were incorporated to expand the S-D model but were found to be of limiting importance.

2.1.3 Boundary Layers

In the feed and draw boundary layers (BL), both convective and diffusive mass transport occur (D'Haese et al., 2016). Since the convective transport of solutes exceeds diffusion, external concentration polarisation (ECP) arises. On the feed side, solutes transported towards the membrane are retained, and the solute is concentrated at the feed solution-active layer interface. Whereas, on the draw side, permeated water dilutes the salt at the support layer-draw solution interface (Figure 2.1). The following equation describes the solute flux in the boundary layers in terms of both convective and diffusive transport:

$$J_s = J_w c - D_b \frac{dc}{dx} \quad (2.3)$$

With J_s being the solute flux, J_w the water flux, c and x are the solute concentration, and the position in the boundary layer, respectively, and D_b the solute diffusivity in the bulk solution. Integrating equation (2.3) and assuming steady-state, the solute fluxes can be derived for the feed and draw boundary layers as follows:

Feed boundary layer

$$J_S = -J_w \frac{C_{fa} - C_f \exp\left(\frac{J_w}{k_f}\right)}{\exp\left(\frac{J_w}{k_f}\right) - 1}$$

(2.4)

Draw boundary layer

$$J_S = -J_w \frac{C_d - C_{sd} \exp\left(\frac{J_w}{k_d}\right)}{\exp\left(\frac{J_w}{k_d}\right) - 1}$$

(2.5)

By re-arranging these equations, solute concentrations at the feed solution-active layer interface (C_{fa}) and support layer- draw solution interface (C_{sd}) can be determined:

$$C_{fa} = C_f \exp\left(\frac{J_w}{k_f}\right) + \frac{J_S}{J_w} (\exp\left(\frac{J_w}{k_f}\right) - 1) \quad (2.6)$$

$$C_{sd} = C_d \exp\left(\frac{-J_w}{k_d}\right) + \frac{J_S}{J_w} (\exp\left(\frac{-J_w}{k_d}\right) - 1) \quad (2.7)$$

With C_f being the concentration of the bulk feed solution and C_d the bulk draw solution concentration. k_f and k_d are the mass transfer coefficients of the feed and draw sides, respectively. The mass transfer coefficients indicate the extent of mixing in the respective flow channels and are calculated from a Sherwood number relation ($k = D_b \cdot Sh/d_H$) which in turn is a function of the Reynold's number (Re), the Schmidt number (Sc) and the hydraulic diameter of the flow channel (d_h). For flow channels without a spacer the relation is adapted from Schock and Miquel (1987), whereas in the presence of a spacer, the relation is adapted from Koutsou et al (2009). The following equations describe the Sherwood relations in laminar flow regime ($Re < 2000$) without (2.8) and with a spacer (2.9):

$$Sh = 1.85(ReSc \frac{d_h}{L})^{0.33} \quad (2.8)$$

$$Sh = 0.2Re^{0.57} Sc^{0.4} \quad (2.9)$$

The hydraulic diameter of the spacer filled draw channel is calculated as follows:

$$d_h = \frac{4\epsilon_s}{\frac{2(w+h)}{wh} + (1-\epsilon_s)S_{VS}} \quad (2.10)$$

With ϵ_s , S_{VS} , w and h being the porosity, spacer volume-specific surface area, channel width and height respectively. The detrimental effects of ECP on water flux can be reduced by increasing the cross-flow velocity (CFV) in the flow channels and introducing turbulence with a

spacer. In both cases, solutes at the interface are swept parallel to the membrane and ECP is reduced.

2.1.4 Support layer

The tortuous and porous structure of the support layer reduces the diffusivity of the draw salt and inhibits convective mixing, giving rise to internal concentration polarisation (ICP). ICP is considered the most significant flux limiting mechanism in FO as it reduces the draw salt concentration and therefore the osmotic pressure at the support layer-active layer interface. To account for the reduced diffusivity and dispersion of salt in the support layer, a structural parameter is defined as a function of support layer length, tortuosity and porosity ($S_s = \delta_s \tau_s / \epsilon_s$). The draw salt flux in the support layer can then be derived from Equation (2.11):

$$J_s = -J_w \frac{C_{sd} - C_{as} \exp\left(\frac{J_w S_s}{D_s}\right)}{\exp\left(\frac{J_w S_s}{D_s}\right) - 1} \quad (2.11)$$

And the concentration of draw salt in the active-support layer interface (C_{as}) can be determined as follows:

$$C_{as} = C_{sd} \exp\left(\frac{J_w S_s}{D_s}\right) + \frac{J_s}{J_w} (\exp\left(\frac{J_w S_s}{D_s}\right) - 1) \quad (2.12)$$

With D_s being the diffusion coefficient of salt in the support layer. Once all the layers are modelled, the osmotic pressures at the active layer interfaces (π_{fa} and π_{as}) can be determined from their respective concentrations (C_{fa} and C_{as}) by applying the van't Hoff law, which is valid at the low solute concentrations used in this study:

$$\pi = jRTC \quad (2.13)$$

With j being the speciation factor of the salt (for NaCl this is 2), R the gas constant, T the temperature and C the concentration.

2.2 FO Membrane development

In the 1990's the development of thin cellulose tri-acetate (CTA) membranes by HTI played a significant role in the rising interest in the FO process. Since then, CTA membranes have been the benchmark for understanding mass transport in FO and for testing the FO process under different feed and draw solution compositions and hydrodynamic conditions. However, analogous to prior developments in RO membranes in the last decade, CTA membranes have

been largely replaced by new generation thin-film composite (TFC) membranes due to their superior water permeability (Alsvik and Hägg, 2013; Klaysom et al., 2013). Furthermore, the possibility to develop and optimize active and support layers separately has enabled the development of TFC membranes targeted at specific applications (Ren and Mccutcheon, 2014).

Many TFC membranes with a range of materials, structures, physico-chemical properties, and performance parameters have been fabricated in industrial and academic laboratories worldwide (Xu et al., 2017). Support layers are fabricated to be ultrathin, highly porous and with a low tortuosity to reduce the structural parameter and ICP (Tirafferri et al., 2011). To meet these requirements, different morphologies have been developed such as finger-like pore structures, macrovoid-free (sponge-like) or with electro-spun fibres. Because the active layer is deposited on the support layer by interfacial polarisation, the support material roughness and the ability to withstand mechanical stress are very important factors. The most widely used TFC membranes are generally composed of a very thin polyamide active layer on top of a polysulphone substrate with an embedded woven or non-woven polyester support (Phillip et al., 2010). Nonetheless, other membrane materials, additives and post-treatment modifications have been used in the active and support layers to increase selectivity, hydrophilicity, stability and surface charge (Xu et al., 2017; Zhou et al., 2014).

Recently, novel TFC membranes with exceptionally high water fluxes have reached the pre-commercialisation stage. The companies that supply these membranes maintain membrane structure and the material undisclosed but provide water and solute flux data. Several lab-scale studies conducted with these membranes have indeed reported enhanced water permeability (Arena et al., 2015; Blandin et al., 2016b; Jang et al., 2018; Nguyen et al., 2015). However, there is a practical limit to developing very high water flux membranes as high water permeability is adversely accompanied by a decreased solute selectivity, in accordance with the permeability-selectivity trade-off theory (Rastgar et al., 2017). On the other hand, strong mechanical resistance and low fouling propensity of these membranes has been reported and their operation in water reuse applications, such as the osmotic membrane bio-reactor, has also been tested (Blandin et al., 2018, 2016a).

2.3 Membrane Characterisation

With the increasing number of FO membranes being developed there is a need to quantitatively evaluate their performance in a standardised way. This would enable direct membrane comparisons regardless of operating conditions, membrane configuration, type and

concentration of draw solution. A number of membrane characterisation techniques have been suggested and summarised in a review by Kim et al. (2017). Currently, the most commonly adapted approach is the measurement of the intrinsic membrane parameters: water permeability coefficient (A), solute permeability coefficient (B) and structural parameter (S_s) using semi-empirical models. These indicators are predicted either with pressurised or non-pressurised tests, often termed RO-FO and FO-only tests, and provide a good basis for comparing membrane performance. Ideally, the membrane structural parameter (S_s) should be determined with direct measurement tools to avoid the inaccuracies of semi-empirical approaches. A few techniques have been proposed and reported in the literature, for example X-ray computed tomography (Manickam and McCutcheon, 2017). Nonetheless, these methods are very expensive, time-consuming and do not yet offer accurate estimates of the S_s value.

The pressurised RO-FO test entails a series of RO experiments to identify the A and B values. Prior to the RO experiments, the membrane is compacted at high hydraulic pressure in order for the membrane to reach equilibrium. Consequently, to determine the structural parameter of the support layer, the membrane is characterised by a single FO test by fitting water and solute fluxes to a S-D model (McCutcheon and Elimelech, 2006). This method was proposed by Cath et al. (2013) as a standard procedure for characterising FO membranes. However, after comparing the values obtained in different laboratories, it was found to be an inappropriate method for FO membranes that are not fabricated to withstand significant hydraulic pressure. The inaccurate and unreliable measurements of the membrane performance parameters were attributed to membrane deformation (Blandin et al., 2013; Kim et al., 2014). A study on the effect of trans-membrane hydraulic pressure on FO membrane performance reported a decline in salt permeability at moderate pressures. Compression of the active layer-support layer interface was given as the most likely cause (Coday et al., 2013). More recently, Kook et al. (2018) investigated whether hydraulic pressure and osmotic pressure are identical in nature. It was suggested that hydraulic pressure is a physical force affecting the structural integrity of the membrane in the macroscopic scale, affecting transport of solute species through defects and membrane compaction. As a result, it was concluded that water and solute permeability are both susceptible to hydraulic pressure and should not be characterised using the RO-FO method.

Due to the fundamental differences in the driving forces in FO and RO processes, Tiraferri et al. (2013) proposed a FO-only characterisation method that evaluates membrane performance under the representative osmotic driving force. It involves a single FO experiment whereby the concentration of the draw solution is incremented step-wise. The intrinsic membrane

parameters (A , B and S_s) are then determined through non-linear regression by fitting the FO transport equations to the experimentally obtained water and solute fluxes. In a similar study, the superior suitability of the non-pressurised and statistical method for characterising FO membranes was confirmed (Lee et al., 2016). Despite offering greater prediction accuracy, a few shortcomings of the method have been identified. According to Kim et al. (2014), the B values obtained by this method only represent the reverse salt flux and do not apply for feed solute fluxes and their equivalent rejections. An extension to Tiraferri's method was proposed by D'Haese et al. (2016) who introduced concentration-dependent draw solute diffusivity during ICP calculation and different model fitting criteria.

Overall, it is very difficult to measure the true membrane performance parameters for their implementation in S-D models. Hydraulic pressure is a source of membrane deformation and leads to deviations in the calculated parameters. Different membrane coupons, operating conditions during characterisation, experimental set-ups and statistical analyses also lead to noticeable inconsistencies. Therefore, unless a more fundamental characterisation method is developed, the FO-only approach is the most appropriate for membranes used in FO conditions. So far, the novel high-flux membranes introduced in the previous section have only been characterised using the FO-RO method (Blandin et al., 2016b; Nguyen et al., 2015). In addition, mass transport through these membranes has not been studied in detail, particularly reverse salt flux. For these membranes to be used in pilot- and large-scale applications, a better understanding of their permeability capacity and potential is required.

2.4 Rejection of Trace Organic Contaminants (TrOCs)

Urban and industrial wastewaters are commonly polluted by organic micro-pollutants such as pharmaceuticals, personal care products and pesticides. These are often termed trace organic contaminants (TrOCs) and have been found to pose a threat to aquatic species in the environment and our drinking water sources, even at low concentrations (Anderson et al., 2006; Schwarzenbach et al., 2006). Given that FO is particularly effective in treating heavily impaired water sources without extensive pre-treatment, studying the rejection of these micro-pollutants by the FO process has become another focal point in FO research. With the advent of the FO-RO hybrid, a closed-loop draw solution configuration can lead to the build-up of TrOCs in the draw solution. This has been reported to influence the product water quality to a greater extent than if only an RO step is used as the treatment process (D'Haese et al., 2013). In this section, the varying mechanisms that dictate the rejection of TrOCs in FO will be explained, followed by a description of the hypothesised role of RSF on TrOCs rejection.

Numerous studies focusing on the rejection of TrOCs by FO membranes have all indicated very high levels of rejection, both in the bench- and pilot-scale (Alturki et al., 2013; Coday et al., 2014; Hancock et al., 2011). The mechanisms responsible for the rejections of organic solutes are very similar to pressurised membrane processes and are usually a combination of steric hindrance, membrane affinity and electrostatic interactions (Bellona et al., 2004). These depend mainly on the nature of the organic compound, the physicochemical properties of the membrane and the feed water characteristics. Charged compounds have generally shown high rejection (above 90%) (Hancock et al., 2011). On the other hand, rejection of uncharged compounds has been found to be more varied and influenced by solute size and hydrophobicity (Kong et al., 2014a). It is important to note that hydrophobic interactions consist in an initial adsorption of solutes onto the membrane, followed by saturation of the membrane's active layer and permeation of the compounds. Therefore, prior studies that did not allow for a steady-state solute permeation to be reached might not have reported reliable conclusions on the influence of hydrophobicity on rejection.

Jin et al. (2012) investigated the rejection of TrOCs by CTA and TFC membranes and concluded that the transport of TrOCs through the benchmark CTA membrane was mainly governed by steric effects, with hydrophobic and electrostatic interactions playing minor roles. For example, TrOCs with a large hydrated radius have consistently shown lower permeability in CTA membranes than neutral TrOCs (D'Haese et al., 2013). On the other hand, TFC membranes have shown better overall rejections due to improved membrane physicochemical properties such as greater negative surface charge, more hydrophobic character and smaller hydrated pore sizes (Xie et al., 2014). Novel TFC membranes that have been studied with regards to rejection of organic contaminants have shown very high rejections of neutral TrOCs by steric hindrance, membrane adsorption of hydrophobic neutral TrOCs, and the highest rejections for negatively charged TrOCs due to electrostatic repulsion with the membrane surface (Jang et al., 2018).

2.4.1 Role of the draw solution on the rejection of TrOCs

Unlike RO in which the solute transport is unidirectional and is mainly affected by the membrane properties and the water flux, in FO the presence of RSF makes solute transport across the active layer more complex. In most TrOCs rejection studies, the effect of RSF on the permeability of the TrOCs through the membrane was not considered. The first extensive investigations on the effect of draw solute on the permeation of TrOCs were conducted by Xie et al (2012a). A higher permeation of TrOCs with $MgSO_4$ and glucose as the draw solute

compared to NaCl was observed. Since MgSO_4 and glucose have significantly lower membrane diffusion coefficients than NaCl, the differences were attributed to a “hindered forward diffusion” of TrOCs by RSF. This hindering effect was also observed in the rejection of boron by FO membranes. Forward boron flux was found to be inversely proportional to RSF by the draw solution (Kim et al., 2012). In contrast, D’Haese (2017) reported a decrease in the permeability of TrOCs through CTA when using MgSO_4 instead of NaCl as the draw solute. He argued that if the fluxes were coupled, large differences would be seen between the permeability of TrOCs in the presence of RSF and in the absence of RSF, a phenomenon that was not observed in his study. More recently, Kim et al. (2017) also reported no direct correlation between the permeability of TrOCs through CTA membranes and RSF, and deduced that the difference in permeability obtained using different draw solutes was due to the different water fluxes generated by the draw solutions.

Nonetheless, a draw solute-dependent rejection was reported for some of the predominantly smaller TrOCs (D’Haese, 2017). Rather than flux coupling, a hypothesis was formed based on the draw solute partitioning into the membrane and modulating the average effective membrane pore size. Partitioning of chloride and sodium ions into the membrane is thought to suppress the pore hydration layers, increasing the average pore size and consequently allowing smaller compounds to pass through (Xie et al., 2014). Sulphate and magnesium ions, on the other hand, have large hydrated radii and partition into the membrane to a lower extent, thus having a lower influence on the average pore size and the permeability of low molecular weight organic compounds. Another hypothesis that was proposed by D’Haese (2017) was an increase in the Lewis basic nature of the membranes when draw solutes partition into it, especially draw solutes containing sulphates. Since most organic compounds are also Lewis basic, the solute-membrane affinity reduces due to decreased polar solute-membrane interactions. These draw solution-induced changes on the physiochemical nature of TFC membranes have not been studied yet.

FO membranes are also known to have a negative surface charge, particularly TFC membranes as they contain a larger proportion of negatively charged functional groups on the surface (Jang et al., 2018; Valladares Linares et al., 2011). Hence, numerous studies have reported a better rejection of anionic compounds due to an electrostatic repulsion by the membrane and a lower rejection of cationic compounds due to an opposite attraction force (Blandin et al., 2016a; Jin et al., 2012). However, D’Haese (2017) reported a consistently higher rejection of cationic TrOCs by CTA membranes. Other trends that he observed were a greater permeation of anionic TrOCs when using a draw solute with a more mobile anion (e.g. MgCl_2), and a

greater permeation of cationic TrOCs when using a draw solute with a more mobile cation (e.g. Na₂SO₄) (D'Haese, 2017). These results were explained mechanistically by Donnan dialysis; to maintain electro-neutrality across the membrane, the rapid migration of draw solute ions to the feed side is balanced by an equivalent migration of same charged TrOCs to the draw side. Kong et al. (2014) also reported an ion exchange mechanism during FO operation with negatively charged organic compounds. Although Donnan dialysis suitably describes the role of RSF on the permeability of charged TrOCs through CTA membranes, the impact of RSF on novel TFC membranes has yet to be explored.

In conclusion, TFC FO membranes have shown high levels of TrOCs rejections, superior to those obtained from conventional CTA membranes. This has been attributed to the modified active layer characteristics that enhance the selectivity of the membranes. However, the role of the draw solution on the transport of TrOCs is still debated and needs to be clarified. This is particularly important for novel membranes which are developed for higher permeability but might suffer from lower draw solute selectivity. With the onset of newer active layer properties that increment the water flux, the altered interactions between the membrane and the feed organic solutes needs to be thoroughly investigated before applying the membranes for water treatment. Furthermore, long-term steady-state rejections of TrOCs need to be studied further in relation to adsorption and degradation during long-term operation

2.5 Fouling propensity in FO

All membrane processes, when applied to wastewater treatment, suffer from membrane fouling. This is the deposition of suspended particles, organic macromolecules, inorganic salts and microorganisms on the membrane surface and within the membrane structure. Besides lowering the water recovery, fouling increases operation costs due to cleaning and replacement of irreversibly fouled membranes. Although FO has often been reported to be less prone to fouling than RO, the impact of fouling on FO process performance has led to numerous studies aimed at identifying the factors and mechanisms that affect and govern fouling behaviour, as well as the best approaches for mitigating fouling (Cornelissen et al., 2008).

The fouling mechanisms in FO are similar to those in pressure-driven membrane processes (Tang et al., 2011). Convective transport of foulants towards the membrane surface increases their concentration at the active layer interface and eventually foulants precipitate to form a cake layer. Initially, the extent of fouling is governed by foulant-membrane interactions and

then, as the layer forms, by foulant-foulant interactions. These are subject to many factors including the feedwater composition (feed solution pH and ionic strength), membrane surface properties (hydrophobicity and charge) and hydrodynamic conditions (initial water flux and cross-flow velocity), all of which are thoroughly summarised in a review by She et al. (2015).

There are other unique and more complex mechanisms in FO that stem from the presence of concentration polarisation and RSF. For example, enhanced fouling due to lowering of adverse CP effects has been reported (Tang et al., 2010). In addition, RSF has also been found to accelerate fouling, particularly divalent cations (Ca^{2+} and Mg^{2+}) that can complex with the carboxylic groups in organic molecules (She et al., 2012). In this section, the unique interplay of FO mechanisms that affect fouling will be explained, the mass transport model will be extended to incorporate the fouling layer and the different fouling behaviours under non-pressurised and pressurised conditions will be evaluated.

2.5.1 Modelling the effects of fouling on solute and water flux

The deposition of foulants on the membrane surface is driven by the convective water flux. As the foulants accumulate and a foulant layer develops, it leads to an increased resistance for water transport and it also introduces more complex concentration polarisation effects. Since the water flux is strongly related to all these factors, the FO process becomes self-regulating. Fouling lowers the water flux and therefore the CP effects. As a consequence, the water flux is spontaneously raised again leading to more fouling. The self-regulating nature of the FO system means that modelling the effects of fouling mechanisms on water and solute flux is challenging. For simplification, alginate gel (an organic macromolecule) will be used as the only model foulant in this study because it is a major component of wastewater and has ideal foulant characteristics.

Tow and Lienhard (2016) extended Nagy's layered transport model to incorporate a foulant cake layer. The new model was successfully applied using foulants with sufficiently large pores, such as alginate (Figure 2.2). Similar to the support layer, the foulant cake layer is also composed of a porous and tortuous structure which hinders the back-diffusion of solutes and inhibits mixing. As a result, the build-up of a cake layer increases the concentration of solutes at the active layer interface and introduces cake-enhanced concentration polarisation (CECP) (Hoek and Elimelech, 2003). A cake structural parameter is defined as a function of cake layer length, tortuosity and porosity ($S_C = \delta_C \tau_C / \epsilon_C$) and implemented in the same way as the support layer to determine solute flux through the cake layer:

$$J_s = -J_w \frac{C_{ca} - C_{fc} \exp\left(\frac{J_w S_c}{D_c}\right)}{\exp\left(\frac{J_w S_c}{D_c}\right) - 1} \quad (2.14)$$

By rearranging equation (2.14), the new concentration of draw solute in the cake-active layer interface (C_{ca}) can be determined as such:

$$C_{ca} = C_{fc} \exp\left(\frac{J_w S_c}{D_c}\right) + \frac{J_s}{J_w} (\exp\left(\frac{J_w S_c}{D_c}\right) - 1) \quad (2.15)$$

With D_c being the diffusion coefficient of salt in the foulant cake layer. Although the CECP effect is significant and reduces the osmotic pressure difference over time, a major contributor to water flux decline is the cake hydraulic resistance. It reduces the effective driving force by introducing a pressure drop. From the capillary model and the Hagen-Poiseuille equation, Tow and Lienhard (2016) derived an equation that best describes the pressure drop in terms of cake structural parameter and pore hydraulic diameter:

$$\Delta P = \frac{32\mu S_c J_w}{D_{h,c}^2} \quad (2.16)$$

Where $D_{h,c}^2$ is the hydraulic diameter of the pores in the cake and μ is the viscosity of the water. In addition to CECP and hydraulic resistance, ICP self-compensation effect is also present during fouling of FO membranes. As the water flux decreases due to fouling, ICP is alleviated and compensates for the reduced water flux by raising it. Lastly, reverse diffusion of draw salt into the feed solution plays a role in exacerbating CECP and reducing the osmotic driving force, this is termed RSF-enhanced CECP. All of these mechanisms work together in altering the water and solute fluxes and consequently the rate of fouling in the FO process. The expression for the overall effective osmotic pressure difference across the active layer, including the effects of ECP, ICP and CECP, is given below:

$$\Delta\pi_m = \frac{\left(\pi_d e^{-J_w\left(\frac{1}{k_d} + \frac{S_s}{D_s}\right)} - \pi_f e^{J_w\left(\frac{1}{k_f} + \frac{S_c}{D_c}\right)}\right)}{1 + \frac{B}{J_w} \left(e^{J_w\left(\frac{1}{k_f} + \frac{S_c}{D_c}\right)} - e^{-J_w\left(\frac{1}{k_d} + \frac{S_s}{D_s}\right)}\right)} \quad (2.17)$$

The resultant water and reverse salt flux can be derived from equations (2.1 and (2.16):

$$J_w = A \left(\pi_{as} - \pi_{ca} - \frac{32\mu S_c J_w}{D_{h,c}^2} \right) \quad (2.18)$$

$$J_s = B(C_{as} - C_{ca}) \quad (2.19)$$

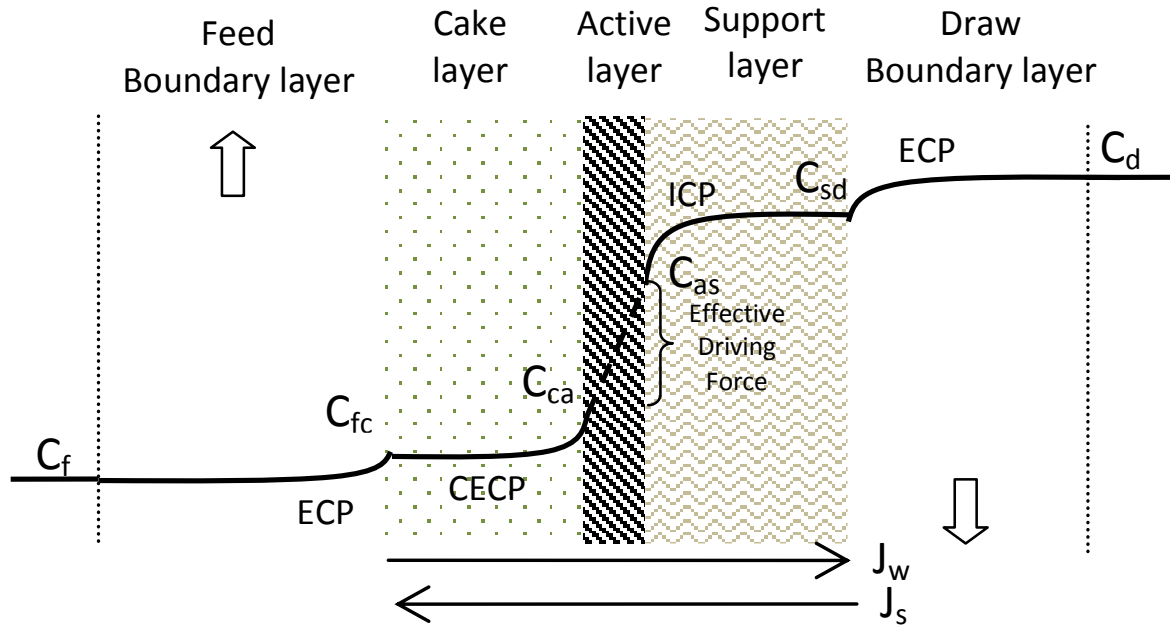


Figure 2.2 Draw solute concentration profile across all the transport layers, including the foulant cake layer, and showing the effects of ECP, ICP and CECP.

2.5.2 Roles of osmotic and hydraulic pressure on fouling

The different driving forces, osmotic pressure in FO and hydraulic pressure in RO and PAO, have been reported to generate a different fouling behaviour between these processes (Blandin et al., 2015; Y. Kim et al., 2014; Kwan et al., 2015; Lay et al., 2010; Lee et al., 2017, 2010; Mi and Elimelech, 2010; Xie et al., 2015). A summary of these studies is listed in Table 2.1. FO has repeatedly shown lower fouling propensity and greater fouling reversibility than PAO and RO. This difference has been mainly attributed to the lack of an applied hydraulic pressure, leading to a looser and less compacted fouling layer, which is easily removed in a cleaning step by simply increasing the cross-shear velocity. The implications of these findings are largely responsible for the surging interest in the FO process, particularly in applications requiring the treatment of very contaminated wastewaters (Linares et al., 2014).

However, contrasting results have been observed. Jang et al. (2016a) found that fouling was more severe in FO and that the water flux could not be recovered as easily. Tow and Lienhard (2016) also concluded from fouling quantification that more foulant mass was being deposited on the membrane in FO. Moreover, the same group reached the conclusion that hydraulic pressure in RO was not responsible for the commonly observed compaction of the fouling layer (Tow and Lienhard, 2017). In this latter study, foulant compaction due to hydraulic pressure and foulant compression due to permeation drag through the cake layer were

thoroughly analysed. Recently, Siddiqui et al. (2018) reaffirmed the notion of greater fouling deposition in the FO process and postulated a few reasons for the inconsistent findings between the different groups. These were mainly attributed to the different experimental methods and fouling quantification techniques used.

In the earlier studies, the extent of fouling was correlated to the water flux decline and, in some cases, fouling reversibility was determined from the recovered water flux after a physical cleaning step. Both of these approaches do not directly measure the thickness and density of the fouling layer and use water flux as an indicator of fouling which is highly susceptible to any changes in the effective driving force. For example, many of the prior studies maintained the driving force in RO (hydraulic pressure) constant, whereas in FO (osmotic pressure) it gradually decreased due to the dilution of the DS. Although the observed water flux in FO was corrected for this dilution, the complex CP mechanisms in FO were not taken into account. As a result, the comparison of the water flux between the two processes was not valid. Other more direct techniques to determine the fouling layer structure have been used, including confocal laser scanning microscopy (Xie et al., 2015), methylene blue dyeing (Tow et al., 2016) or just simply weighing the final foulant mass (Lee et al., 2017). However, the accuracy and applicability of these methods is debatable.

To conclude, fouling in FO is a major challenge that inhibits the efficiency of the process in treating wastewaters and in final water production. In spite of this, FO has been reported to be more resistant to fouling than other pressure-driven membrane processes such as RO and NF. The reasons for this are still unclear, albeit most results point out to the lack of an applied hydraulic pressure. The feasibility of FO as an alternative treatment technology to current membrane processes is believed to hinge on the lower fouling propensity of the FO process. As a result, understanding the complex interplay of FO fouling mechanisms, their impact on the effective driving force and on the fouling behaviour in osmotic and hydraulic pressure processes is crucial in the advancement of FO in water treatment. Furthermore, the fouling propensity of novel high-flux TFC membranes is yet to be investigated.

Table 2.1 Summary of recent fouling studies which compare fouling behaviour in FO, PAO and RO mode. Flux decline rates vary significantly whereas flux recovery is usually greater in FO mode. Comparing all the studies is difficult because different membranes, experimental set-ups, foulants and feed pressures are used.

Membrane	Foulant	Mode	Feed Pressure	Draw Solute	Flux Decline (%)	Flux Recovery (%)	Ref.
HTI CTA	200mg/L Alginate, 0.5mM Ca ²⁺ , 50mM NaCl	FO	-	4M NaCl	55	99	(Mi and Elimelech, 2010)
		RO	28 bar	-	50	72	
CTA	200mg/L Alginate, 1mM Ca ²⁺ , 50mM NaCl	FO	-	5M NaCl	50	87	(Lee et al., 2010)
		RO	31 bar	-	15	0	
HTI CTA	200ppm Silicon Dioxide nanoparticles, 1g/L NaCl	FO	-	1.4M NaCl	18	-	(Lay et al., 2010)
		RO	19.2 bar	-	8	-	
HTI CTA	4.2mM Silica, 115mM NaCl, 19m MgCl ₂	FO	-	4M NaCl	49	98	(Mi and Elimelech, 2013)
		RO	31 bar	-	51	80	
HTI CTA	100mg/L Alginate, 1g/L Silica, 50mM NaCl	FO	-	5M NaCl	7	95	(Y. Kim et al., 2014)
		PAO	18.8	3.5M NaCl	8	92	
HTI TFC	Synthetic wastewater with EPS	FO	-	1.3M NaCl	12	-	(Kwan et al., 2015)
		RO	20.7 bar	-	30	-	
HTI TFC	200mg/L Alginate, 1mM Ca ²⁺	FO	-	2.5M Glucose	15	99	(Xie et al., 2015)
		PAO	5.5 bar	1.5M NaCl	12	58	
		RO	12.5 bar	-	16	2	
HTI CTA	200mg/L Alginate, 200mg/L Humic acid, 1200mg/L Red Sea Salt and 220mg/L CaCl ₂	FO	-	70 g/L RSS	30	92	(Blandin et al., 2015)
		PAO	4 bar	35g/L RSS	42	70	
Dow SW30HR and HTI CTA	200mg/L Alginate, 1mM Ca ²⁺ , 3.5% NaCl	FO	-	24% NaCl	73	-	(Tow and Lienhard, 2016)
		RO	50 bar	-	63	-	
Polymeric TFC	500mg/L Alginate, 1000ppm NaCl	FO	-	4M NaCl	65	80	(Jang et al., 2016)
		RO	28 bar	1.3M NaCl	0	-	
Polyamide TFC	250mg/L Alginate, 1mM Ca ²⁺ , 2g/L NaCl	FO	-	0.6M NaCl	48	96	(Lee et al., 2017)
		PAO	7.5bar	0.6M NaCl	69	70	
		I-PAO	7.5 bar	0.6M NaCl	66	79	
SW30HR and HTI CTA	250mg/L Alginate, 1mM Ca ²⁺ , 29mM NaCl	FO	-	5M NaCl	52	107	(Tow and Lienhard, 2017)
		RO	40 bar	-	39	90	
HTI CTA	200mg/L Alginate, 5mM Ca ²⁺ , 45mM NaCl	FO	-	1.5M NaCl*	50	92	(Siddiqui et al., 2018)
		RO	17.6 bar	-	47	96	

*Draw solution concentration was kept constant

3 Research Objectives

In the literature review a number of topics regarding the FO process were elucidated, from the complex mass transport phenomena through FO membranes to the issues of trace organic contaminants (TrOCs) and fouling associated with treating wastewater with FO. In each of these areas, knowledge gaps have been identified which require further investigation. Since new FO membranes are constantly being developed, the study of state-of-the-art TFC membranes added novelty to the dissertation. The research objectives were divided into three parts representing each one of these research areas: (1) membrane characterisation, (2) transport of TrOCs and (3) fouling propensity. These are listed below with the corresponding approach that will be taken to reach the objectives:

1. a) Compare the mass transfer processes through novel TFC membranes to the conventional membranes and relate their performance to the intrinsic transport and structural parameters

Conventional and novel high-flux membranes were characterised using two different FO-only characterisation methods, based on the general mass transport model in FO. Although both methods employ a single FO experiment to determine water and salt fluxes, the algorithms employed to calculate the intrinsic membrane performance parameters (A, B, S_s) were different.

b) Evaluate the accuracy of the calculated intrinsic parameters, their applicability in further models and as a metric for comparing membrane performance

The two methodologies were compared in terms of reliability, with particular focus on the errors associated with the experimental and the parameter optimisation parts. Then the accuracy and applicability of the parameters were evaluated by comparing with those reported in the literature.

2. a) Investigate the fate and rejection of trace organic contaminants by novel TFC membranes in long-term FO experiments

Possible adsorption or degradation of TrOCs in a bench-scale FO set-up was initially examined. Consequently, the rejection of 18 TrOCs with a wide range of physico-chemical properties by the novel FO membranes was determined and related to the following rejection mechanisms: steric hindrance, hydrophobic and electrostatic interactions.

b) Investigate the role of the draw solution and the reverse salt flux on the transport of TrOCs through FO membranes.

A series of TrOCs permeability experiments through the novel FO membranes were performed with different feed and draw solution conditions, in the presence and absence of a reverse salt flux. The relationship between the physico-chemical properties of the solutes/membranes and the transport of organic solutes enabled to identify the mechanisms involved.

3. a) Improve the current understanding of fouling mechanisms under different osmotic and hydraulic pressure driving forces

Since the evolution of fouling accumulation on the membrane is not properly reflected by the water flux, a different approach was undertaken that calculates the varying contributions of concentration polarisation effects, hydraulic resistance and hydraulic pressure on the driving force. When all these processes were considered, the cake structural parameter could be accurately modelled. Experiments in FO and PAO mode with non-constant and constant osmotic pressure differences were compared in terms of fouling propensity.

b) Determine the fouling propensity of novel TFC membranes and relate it to the membrane characteristics

From the results of all the fouling experiments, the different fouling behaviours of the two novel TFC membranes were analysed.

4 Materials and Methods

This chapter includes a detailed description of the membranes and chemicals used throughout the thesis, the experimental set-up and its supervisory control and data acquisition system employed and the chemical analysis for organic compounds. There is a section on the experimental procedures that were undertaken in each of the independent studies. These consist in the (1) membrane characterisation multi-stage experiments, (2) permeability of TrOCs under different experimental conditions and (3) membrane fouling experiments. Lastly, the detailed experimental design, equations used in the calculations and the data analyses are included later in the respective chapters.

4.1 Membranes

Four commercially-available flat-sheet membranes were used in this thesis. One with cellulose triacetate (CTA) and the other three were TFC membranes with a polyamide active layer. The CTA membrane, manufactured by Hydration Technology Innovations (HTI) had an embedded polyester mesh support for mechanical strength. One of the TFC membranes (TFC-1) was also manufactured by HTI and consisted in a polysulphone support layer embedded in a polyester woven fabric. The other two TFC membranes were manufactured by Porifera Inc. (TFC-2) and Toray chemicals (TFC-3), respectively, and also consisted in a polyamide layer and a polysulphone sub-layer embedded on a woven support.

Table 4.1 Membrane performance parameters and physico-chemical properties for the selected membranes, obtained with the RO-FO characterisation method and further characterisation from literature. Membrane providers of TFC-2 and TFC-3 are kept undisclosed.

Membrane type	A ($\text{L m}^{-2} \text{ h}^{-1} \text{ bar}^{-1}$)	B (10^{-7} m s^{-1})	S (μm)	Surface roughness (nm) ^a	Hydrophobicity ($^\circ$) ^b	Surface charge (mV) ^c	Ref.
CTA HTI	0.46	2.92	454	1.86 \pm 0.18	63 \pm 7	-6.5 \pm 0.3	(Nguyen et al., 2015)
TFC-1 HTI	2.10	0.70	1227	37.40 \pm 3.70	47 \pm 18	-9.0 \pm 1.0	(Blandin et al., 2016b)
TFC-2	2.10	1.20	344	30.80 \pm 3.50	36 \pm 6	-13.7 \pm 1.9	(Blandin et al., 2016b)
TFC-3	5.36	2.63	266	34.20 \pm 2.74		-58.0 \pm 0.0	(Nguyen et al., 2015)
	8.82	2.46	276	50.50 \pm 2.20	40 \pm 2		(Nguyen et al., 2018)

a determined by atomic force microscopy of the active layer

b determined through sessile drop contact angle measurement

c zeta-potential determined by streaming potential analyser

CTA and TFC-1 membranes were only used in the characterisation study as reference membranes, whereas TFC-2 and TFC-3 were used throughout the thesis. All membrane samples were stored at 20°C and soaked in DI water for at least 1 h before use. No pre-compaction was applied. In all experiments the membranes were always oriented with the active layer facing the feed solution. The physico-chemical properties of the membranes were obtained from the literature and are summarised in Table 4.1.

4.2 Chemicals

Three inorganic salts were used as draw solutes, sodium chloride (NaCl, reagent grade) and magnesium chloride (MgCl₂, reagent grade) from Scharlau (Spain) and sodium sulphate (Na₂SO₄, ≥ 99%) from Sigma-Aldrich (USA). As the synthetic foulant, alginic acid sodium salt, also known as alginate, was purchased from Acros Organics (Belgium). Alginate is a naturally-occurring, water-soluble polymer comprised of varying ratios of mannuronic and guluronic acid residues. Alginate can be gently cross-linked by the addition of divalent cations (Lee and Mooney, 2012). Therefore, Calcium chloride (CaCl₂, reagent grade), also obtained from Scharlau (Spain), was used to induce cross-linking and accelerate fouling. A total of 18 trace organic contaminants were obtained from Sigma-Aldrich (USA) at 97% purity and above, as listed in Table 4.2. These were chosen with a range of physico-chemical properties to represent different charge, molecular weight (MW), minimal projected surface area (MPSA) and pH corrected hydrophobicity (LogD). These properties were chosen to probe the main interactions between the organic solutes and the membrane and are discussed in more detail in section 6.3. The physico-chemical values for these properties were acquired from the free web-pages Chemicalize and DrugBank (Table 4.2). A stock solution containing 120 mg/L of all the selected TrOCs was made in methanol (Scharlau, Spain, HPLC grade CH₃OH) to make sure all compounds dissolved entirely. This solution was then diluted to 1 mg/L for low-concentration dosing and stored at 4°C. Out of the 18 TrOCs, 9 were selected for permeability experiments (see section 6.2) and stock solutions of each compound were prepared separately, with acetonitrile (Scharlau, Spain, HPLC grade CH₃CN), at a concentration of 500 mg/L for high-concentration dosing and stored at 4°C. In the latter experiments acetonitrile was used instead of methanol because it was found to dissolve organic compounds better and because it was used as the mobile phase in their HPLC analysis.

Table 4.2 List of the selected organic compounds with the purity and product reference. The physico-chemical properties of the TrOCs are also summarised.

Compound	Purity	Product Reference	Charge (pH 6) ^a	logP ^b	logD (pH 6) ^b	MW (g/mol) ^b	Minimum projection area (Å ²) ^b
Ibuprofen (IBU)	≥98%	I4883-5G	-1.00	3.84	2.67	206.3	35.4
Gemfibrozil (GEM)	≥99%	G9518-5G	-1.00	4.39	2.80	250.3	42.1
Diclofenac (DIC)	≥98%	D6899-5G	-1.00	4.26	2.26	296.1	41.0
Furosemide (FUR)	≥98%	F4381-5G	-1.00	1.75	0.00	330.7	40.9
Indomethacine (IND)	≥98%	I8280-5G	-1.00	3.53	1.34	357.8	51.3
Bezafibrate (BEZ)	≥98%	B7273-5G	-1.00	3.99	1.83	361.9	40.4
Sulfamethoxazole (SFX)	≥98%	S7507-5G	-0.96	0.79	0.60	253.3	46.1
Acetaminophen (ACE)	≥99%	A7085-100G	0.00	0.91	0.91	151.2	21.7
Phenazone (PHE)	≥97.5%	A5882-25G	0.00	1.22	1.22	188.2	32.4
Thiabendazole (THI)	≥99%	T8904-5G	0.00	2.33	2.32	201.3	25.0
Carbamazepine (CBZ)	≥98%	C4024-5G	0.00	2.77	2.77	263.3	40.2
Trimethoprim (TRI)	≥98%	T7883-5G	0.31	1.28	0.27	290.3	51.6
Atenolol (ATE)	≥98%	A7655-5G	1.00	0.43	-2.68	266.4	36.9
Venlafaxine (VEN)	≥98%	V7264-5G	1.00	2.74	-0.07	277.4	55.8
Nadolol (NAD)	≥98%	N1892-5G	1.00	0.87	-2.26	309.5	49.7
Verapamil (VER)	≥99%	V4629-5G	1.00	5.04	1.76	454.6	78.7
Erythromycin (ERY)	≥98%	E5389-5G	1.00	2.60	-0.29	733.9	107.2

^a obtained from DrugBank^b obtained from Chemicalize

4.3 Experimental Set-up

All the experiments in this thesis were performed with a custom-made bench-scale cross-flow membrane cell unit made of polyacrylate. The cell unit had symmetric draw and feed channels (20.5 x 4.5 x 0.15 cm) and an effective membrane area of 92 cm². In some experiments, feed and draw channels were fitted with 1.2 mm thick diamond-mesh spacers. These have the form of non-woven crossed filaments that improve flow distribution and turbulence in analogy to large-scale FO modules (Similar to S#1 in She et al., 2013). They are employed to mitigate fouling and concentration polarisation phenomena (Koutsou et al., 2009). In the experiments employing a feed hydraulic pressure, two layers of permeate RO spacers, commonly used in the permeate channel of RO modules, were fitted in the draw channel as membrane backing (Similar to S#3 in She et al., 2013). In addition to the permeate spacers, small plastic beads were used to fill the entrance pathway of the channels in order to avoid membrane deformation at increased pressure. The cell unit was connected to a feed and a draw reservoir from which feed and draw solutions were re-circulated with a peristaltic pump with a range of speeds from 0.1 to 220 RPM (Watson Marlow, model 530S). The pump heads (Watson Marlow, model 314X) had four rollers to minimise pulsations and were fitted with Marprene tubing (3.2 x 1.6 mm) to provide flow rates ranging from 0.17 to 370 mL/min). By means of rotameters, the flow rate in the circulation system was adjusted to reach a desired channel cross-flow velocity (CFV). For TrOCs rejection and characterisation experiments the CFV was maintained at either 7.6 or 10.0 cm/s to control the effect of external concentration polarisation and pressure drops through the channels, whereas for fouling experiments the CFV ranged from 2 to 6 cm/s to encourage fouling. The membrane cells were operated in both counter-current and parallel-current modes.

The changing volume of the feed solution was recorded by data logging the weight of the feed reservoir with a balance (KERN, model PCB 600-1). Water flux through the membrane was then determined from the permeated volume of water using the following equation:

$$J_w = \frac{(V_{F,f} - V_{F,0})}{A_m t} \quad (4.1)$$

Where J_w is the water flux, $V_{F,f}$ is the final volume of the feed reservoir, $V_{F,0}$ is the initial volume of the feed reservoir, A_m is the effective membrane area, and t is the duration of each stage. Conductivity meters (HACH, model 5396), connected to a Programmable Logic Controller (PLC), were placed in both reservoirs to continuously measure conductivity.

Conductivity was converted to concentration by means of calibration curves. The concentration of draw solute in the feed and draw solutions were then used to measure the reverse salt flux with the following mass balance equation:

$$J_s = \frac{C_{F,f}(V_{F,0} - J_w A_m t) - C_{F,0} V_{F,0}}{A_m t} \quad (4.2)$$

Where J_s is the solute flux, $C_{F,f}$ is the final feed solution concentration of salt, $C_{F,0}$ is the initial feed solution concentration of salt. The experimental setup was equipped with a draw solution re-concentration system which consisted in a pump (Watson Marlow, model 120S D/V 1-200RPM) that re-circulated draw solution through a funnel filled with solid draw salt and back into the draw reservoir (Figure 4.1). If the conductivity of the draw solution decreased below a set-point, the pump was automatically activated by the PLC to restore the original concentration.

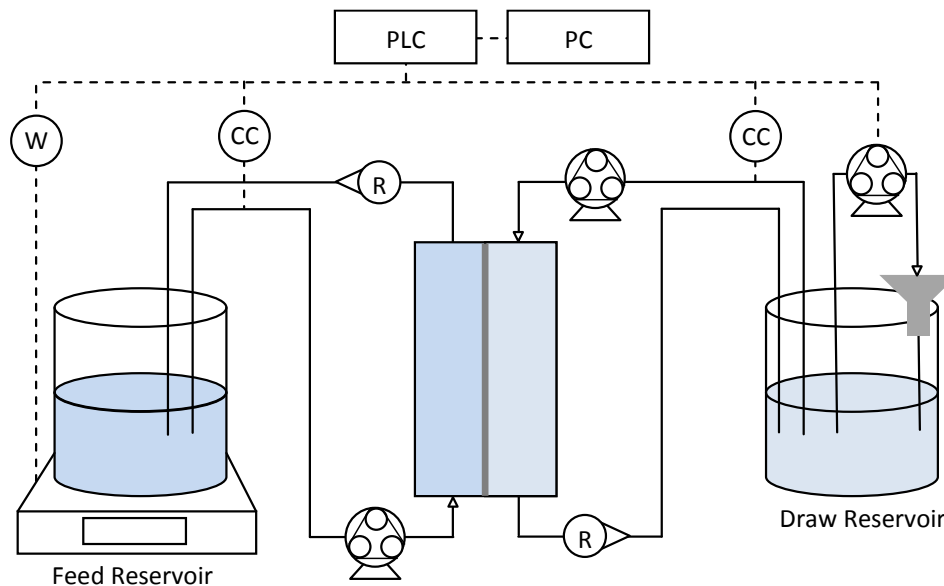


Figure 4.1 Diagram of the experimental set-up, showing the circulation of the feed and draw solutions from the reservoirs, through the membrane cell unit and back into the reservoirs. Conductivity (CC) of both solutions and the weight (W) of the feed solution were monitored via a PLC connected to a PC. The draw re-concentration system used to maintain the draw solution concentration constant is also shown on the right.

4.4 Chemical Analysis

4.4.1 Low-concentration TrOCs analysis

For samples that contained low-concentrations of TrOCs (ng/L- μ g/L range), the analysis was carried out according to the method developed by Gros et al. (2012). This consisted in solid

phase extraction (SPE) followed by ultra-high-performance liquid chromatography coupled to quadrupole linear ion trap tandem mass spectrometry (UPLC-QqLIT).

The SPE technique involved extracting either 25 mL or 200 mL from the samples depending on the expected concentrations. These volumes were then made up in volumetric flasks with either 800 μ L or 5 mL of 0.1M Na₂EDTA to quench metal ions in solution and 250 μ L of 100 ppb surrogate (sulfadimetoxine-d6, sulfadoxine-d3 and ketoprofen-d3) to identify errors in the SPE procedure. Consequently, the solutions were filtered through pre-conditioned Oasis-HLB cartridges, washed twice with HPLC grade water, dried and the cartridges were stored in the freezer at -20°C for 2 weeks. Elution of the organic compounds from the cartridges was done twice with HPLC grade methanol. The samples were then concentrated by evaporating the solvent with a weak stream of nitrogen, transferred to vials and blown to dryness with nitrogen again. Finally, the samples were reconstituted with 1 mL of CH₃OH/Water (10:90 %v,v) solution and stored in the freezer at -20°C for 1 week.

The instrumental analysis was performed by an expert technician. Briefly, a Waters Acquity Ultra-Performance TM liquid chromatography system was used with different columns for compounds analysed under positive (PI) and negative (NI) electrospray ionization. The column specifications, optimised separation conditions, solvents used, gradient elution, and the parameters used in the UPLC instrument coupled to a 5500 QTRAP hybrid triple quadrupole-linear ion trap mass spectrometer are all detailed in (Gros et al., 2012). All data were acquired and processed using Analyst 1.5.1 software (SCIEX, MA, USA). Due to the high salt content of the samples, matrix effects were evaluated by peak suppression or enhancement. Calibration curves were generated with the internal standard to correct for the matrix effects. Established concentration points of the calibration curves ranged from 0.1 to 25 μ g/L. In addition, recoveries of the TrOCs were determined by spiking the blanks with known concentrations of TrOCs. All of recoveries were higher than 50%.

4.4.2 High-concentration TrOCs analysis

For samples that contained high-concentrations of TrOCs (μ g/L-mg/L range), a new analytical method was developed. An HPLC-UV (Agilent 1200) instrument fitted with a C18 column (Microsorb-MV 100-5 250 x 4.6 mm) and working temperature of 30°C was used to determine the concentrations of the TrOCs in the samples. This instrument required no extensive pre-treatment of the samples which were injected directly with a volume of 100 μ L. In order to obtain a good separation of the compound elution peaks, the selected TrOCs were divided into

three groups based on their retention time and physico-chemical properties (Table 4.3). Each group was analysed with a different isocratic elution method which consisted in a specific mobile phase mixture and an eluent flow rate of 1 mL/min. Less hydrophobic compounds were analysed with a higher aqueous to organic (H₂O:CH₃CN) mobile phase mixture whereas more hydrophobic compounds with a lower H₂O:CH₃CN ratio. This ensured no overlapping of elution peaks and decreased interactions between oppositely charged compounds. The peaks were quantified by calculating the peak area and the concentration of each compound was then obtained from a calibration curve. Established concentration points of the calibration curves ranged from 0.1 to 2 mg/L. The lower limit of quantification for all TrOCs was approximately 20 µg/L.

Table 4.3 A list of the three groups of TrOCs that were analysed independently by HPLC-UV with the corresponding retention times and mobile phase mixtures. These were chosen based on retention times, polarity and charge.

Group of TrOCs	Retention time (min)	Mobile phase mixture
ATE	4.15	65% H ₂ O, 20% NH ₄ HCO ₂ (pH=3 with formic acid), 15% CH ₃ CN
ACE	4.70	
NAD	8.85	
TRI	4.02	45% H ₂ O, 20% NH ₄ HCO ₂ (pH=3 with formic acid), 35% CH ₃ CN
SFX	5.86	
FUR	9.22	
CBZ	4.18	30% H ₂ O, 20% NH ₄ HCO ₂ (pH=3 with formic acid), 50% CH ₃ CN
BEZ	7.23	
IND	14.16	

4.4.3 SEM Characterisation

The membrane surfaces and cross sections were characterized with a Hitachi S4100 (FESEM) scanning electron microscope. To obtain cross sections, membrane samples were frozen in liquid nitrogen and fractured manually. All samples were dried in vacuum at room temperature (~24 °C) for 24 h, and sputter coated with a thin layer of carbon. The cross sections were then imaged at an accelerating voltage of 15 keV (Wang et al., 2012).

4.5 Characterisation experiments

As part of the membrane characterisation methods, FO experiments were performed at increasing DS concentrations to yield the input parameters for the computed algorithms. The bench-scale membrane cell unit was operated with a cross-flow velocity of 25 cm/s, using diamond-type spacers in both feed and draw channels. Feed and draw solution temperatures were kept at approximately around 20°C and the pressure build-up in feed and draw sides was

maintained below 20 mbar. The FO membrane cell unit was flushed for at least 1h with DI water prior to each experiment to remove air bubbles in the unit and to ensure complete wetting of the new membrane sample. Once the weight and conductivity measurements stabilised, NaCl was added to obtain the desired concentration of draw solution and start the first stage. Each stage lasted 15 minutes in order to obtain reliable average values of feed (C_f) and draw (C_d) solution concentrations. A stable water flux (J_w) and reverse salt flux (J_s) were also obtained for each stage. This procedure was repeated for three more stages in which a higher concentration of NaCl draw solution was employed every time. The selected draw solution concentrations were chosen to obtain an appropriate range of water fluxes and reverse salt fluxes. This enabled the use of the assumptions made in the S-D models used for the characterisation methods (section 2.1). The same procedure was implemented for the CTA and the three TFC membranes.

4.6 Long-term operation TrOCs rejection experiments

To investigate the adsorption of TrOCs onto the membrane and the apparatus of the FO system, and the degradation of TrOCs over time in aqueous solution, a long-term experiment was initially performed. This consisted in re-circulating the feed and draw solutions for 76 hours through the system. Both feed and draw solutions were initially made up of milli-Q water, thus exerting no osmotic pressure difference and resulting in zero permeate water flux. Consequently, they were both spiked with 1 $\mu\text{g/L}$ of TrOCs at the start of the experiment to avoid a concentration gradient from feed to draw and diffusion through the membrane (Table 4.4). A total of 16 samples, 8 from the FS and 8 from the DS, were taken approximately every 12 hours by collecting 100 mL from both reservoirs at the same time. The samples were filtered through a 0.45 μm PVDF filter and analysed by low-concentration TrOCs analysis. After the experiment, milli-Q water was re-circulated overnight to wash out any residual TrOCs from the system.

The rejections of TrOCs by TFC-2 and TFC-3 were tested by re-circulating the feed and the draw solutions for 46 hours with the respective membrane samples in the membrane cell unit. The feed solution was made up of 5L of milli-Q water spiked with 1 $\mu\text{g/L}$ of TrOCs. The NaCl draw solution concentration was kept at 160 mM and 24 mM for the TFC-2 and TFC-3 membrane, respectively. These concentrations were chosen to maintain the water flux at around 10 $\text{L m}^{-2} \text{h}^{-1}$. During the experiment, 10 samples (5 from the FS and 5 from the DS) were taken approximately every 12 hours by collecting 100 mL from feed reservoir and 200mL from the

draw reservoir. All the samples were filtered through a 0.45 μm PVDF filter and stored in the freezer for low-concentration TrOCs analysis.

Table 4.4 Starting conditions for the long-term fate of TrOCs in the FO system and the membrane rejection experiments.

Starting Parameters	Fate of TrOCs	Rejection of TrOCs	
		TFC-2	TFC-3
CFV (cm/s)	10.1	10.1	10.1
$C_{F,0}^{\text{TrOCs}}$ ($\mu\text{g/L}$)	1.0	1.0	1.0
$C_{D,0}^{\text{TrOCs}}$ ($\mu\text{g/L}$)	1.0	0.0	0.0
$C_{F,0}$ (mM)	0.0	0.0	0.0
$C_{D,0}$ (mM)	0.0	160	24
$V_{F,0}$ (L)	1.0	5.0	5.0
$V_{D,0}$ (L)	1.0	1.0	1.0

4.7 TrOCs permeability experiments

The effect of the draw solution on the transport of TrOCs was investigated by a series of TrOCs permeability experiments. These included diffusion experiments without a draw solution and at increasing ionic strength, followed by an ordinary FO experiment. Before any permeability experiments, membrane saturation was achieved exposing the pristine coupons to the 9 organic compounds for 24h by spiking the feed and draw solutions with 1 mg/L of the mix of all 9 TrOCs. Then, prior to each individual experiment, the system was washed for 1h with DI water to remove any residual TrOCs from the system tubing and the membrane. Samples of the feed and draw solutions, taken after the washing procedure, repeatedly showed insignificant concentrations of TrOCs, certifying that the washing protocol was effective.

4.7.1 Diffusion experiments

The first part consisted in determining the diffusion of TrOCs through the two novel TFC membranes in the absence of a draw solute. These experiments were carried out to identify the solute-membrane interactions that are involved in the diffusive transport of the organic solutes. In order to analyse the samples efficiently, the selected TrOCs were spiked in the feed solution in three different groups at a concentration of 1 mg/L. Therefore for each experiment, three 24h runs were carried out, each with a different group of TrOCs and with 1 L of DI water in both feed and draw compartments. A total of three samples were taken for each run, two

from the feed solution (at time 0 and time 24h) and one from the draw solution (at time 24h). The draw solution was sampled only at the end because initial concentrations of TrOCs in the draw solution were expected to be insignificant. All samples were frozen and subsequently analysed by HPLC-UV. The absence of a water flux and reverse salt flux during these tests was confirmed by the negligible change in feed solution weight and conductivity.

The diffusion experiments in DI water were complemented with diffusion experiments at higher ionic strengths, also in the absence of water and reverse salt fluxes. These were aimed at determining the impact of the draw salt on the solute-membrane interactions involved in the diffusive transport of TrOCs. Higher membrane ionic strengths were achieved by increasing the concentration of NaCl in both feed and draw solutions initially to 0.1M and then to 0.5M. Additionally, 0.5M MgCl₂ was also tested since the Mg²⁺ ion has a double positive charge, a higher ionic strength and a larger hydrated size, therefore affecting membrane surface charge and diffusivity to a greater extent. Since the salt concentrations were maintained equal on both the feed and the draw solutions, no osmotic pressure difference developed and the water flux and reverse solute flux were kept at a minimum. These experiments were performed in a similar way to the D-DI Water experiments. They were all carried out in three runs, each with a different group of TrOCs in the feed solution and lasting 24h.

4.7.2 FO experiments

The final set of experiments determined the permeability of TrOCs through the two TFC membranes during FO operation in the presence of a forward water flux and reverse salt flux. By comparing the permeability of TrOCs during FO operation to the diffusion experiments, the effect of both water and reverse salt fluxes on the transport of TrOCs could be analysed. In order to maintain a transmembrane water flux of approximately 10 L m⁻² h⁻¹ throughout the experiments, the draw solution was made up of 0.1M NaCl and 0.07M NaCl for TFC-1 and TFC-2, respectively. These concentrations were determined experimentally. In both cases the feed solution consisted of 3 L DI water, spiked with each of the three groups of TrOCs and re-circulated for 24h. To avoid dilution of the draw solution by the permeation of water and maintain the same osmotic driving force, the automatic re-concentration system was employed.

Table 4.5 Starting conditions for the diffusion experiments with DI water, the diffusion experiments at higher ionic strength and for the FO experiments

Starting Parameters	Diffusion	Diffusion (higher Ionic Strength)		FO mode	
		NaCl	MgCl ₂	TFC-2	TFC-3
CFV (cm/s)	7.6	7.6	7.6	7.6	7.6
$C_{F,0}^{TrOCs}$ (mg/L)	1.0	1.0	1.0	1.0	1.0
$C_{F,0}$ (M)	0.0	0.1-0.5	0.1-0.5	0.1	0.07
$C_{D,0}$ (M)	0.0	0.1-0.5	0.1-0.5	0.0	0.0
$V_{F,0}$ (L)	1.0	1.0	1.0	3.0	3.0
$V_{D,0}$ (L)	1.0	1.0	1.0	1.0	1.0

4.8 Fouling experiments

4.8.1 Effect of constant osmotic pressure

A series of fouling experiments were initially performed with the TFC-2 and TFC-3 membranes to understand the effects of constant DS concentration on membrane fouling (Table 4.6). The feed and draw channels were fitted with diamond-type FO spacers to reproduce the conditions in large-scale FO modules. Throughout this study, a cross-flow velocity of 7.6 cm/s was maintained. A baseline test was run prior to every fouling test, in which no foulant was added to the feed solution. Consequently, using the same draw solution concentration and operating conditions as the baseline test, 200 mg/L of Sodium Alginate and 1mM of CaCl₂ was added to the feed solution to initiate the fouling deposition. In the draw solution, NaCl was added to establish an initial water flux of approximately 20 L m⁻² h⁻¹. The water flux and change in draw solution concentration were monitored for 8 hours until the end of the experiment. Baseline and fouling tests were done in experiments with decreasing DS concentration and experiments at constant DS concentration. The surface mass density of the final deposited alginate cake layer was measured by carefully peeling-off the thin layer, air-drying for 48 hours and weighing the dried film.

4.8.2 Effect of hydraulic pressure

For this study the membrane cell unit geometry was changed to allow for the alginate cake layer to deposit only on the membrane. The feed channel thickness was decreased to 0.08cm and used without a spacer; whereas the draw channel was fitted with two RO permeate spacers to avoid membrane deformation at applied hydraulic pressures. Due to the different

channel geometry, the cross-flow velocity was unable to be maintained constant; however, it did not deviate significantly from 3.5 cm/s. Such a low CFV was employed to accelerate fouling. Similar to the fouling experiments described in 4.8.1, prior to every fouling test, a baseline test was performed. Then, 200 mg/L of sodium alginate and 1mM CaCl₂ were added to the feed solution to initiate fouling. All the experiments were initially performed in FO mode without an applied hydraulic pressure and then in PAO mode with 1 bar in the feed solution. In the draw solution, NaCl was adjusted to establish an initial water flux of 20 L m⁻² h⁻¹. Again, the water flux decline and changing reverse draw solute flux were monitored for 8 hours. The alginate cake layer that formed at the end of each fouling experiment was extracted from the membrane by peeling it from the surface. Consequently, this thin layer was air-dried for 24 hours and weighed.

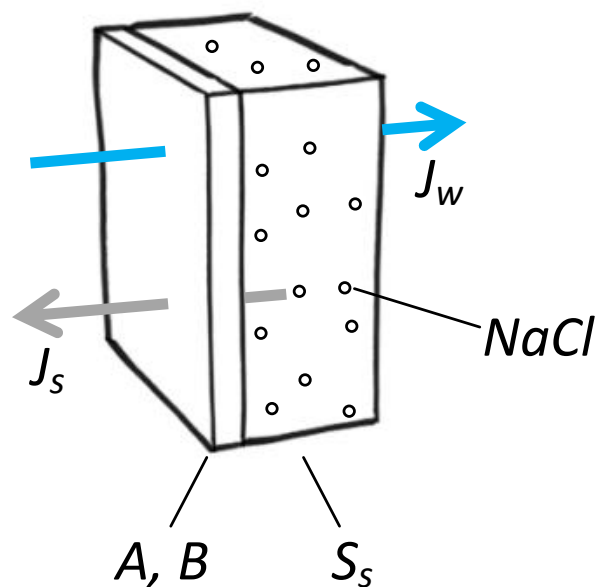
Table 4.6 Starting conditions for the fouling experiments designed to determine the effect of a constant osmotic pressure as driving force and the fouling experiments designed to determine the effect of hydraulic pressure as driving force.

Starting Parameters	NaCl				Na ₂ SO ₄					
	TFC-2		TFC-3		TFC-2		TFC-3			
	FO*	FO	FO	PAO	FO	PAO	FO	PAO		
CFV (cm/s)	7.60	7.60	3.87	5.07	2.07	2.07	5.85	5.85	3.29	6.21
C _{F,0} ^{Alginate} (mg/L)	200	200	200	200	200	200	200	200	200	200
C _{F,0} ^{CaCl₂} (mM)	1.0	1.0	1.0	1.0	1.0	1.0	1.0	1.0	1.0	1.0
C _{D,0} (M)	1.1	0.6	1.2	0.8	0.7	0.5	1.0	-	0.6	0.3
V _{F,0} (L)	3.0	3.0	2.5	2.5	2.5	2.5	2.5	2.5	2.5	2.5
V _{D,0} (L)	1.0	1.0	1.0	1.0	1.0	1.0	1.0	1.0	1.0	1.0

* Non-constant DS Concentration

5 FO-only characterisation of novel TFC membranes

In this chapter, the selected CTA and TFC membranes were characterised by two FO-only characterisation methods that use similar experimental conditions but distinct mass transport models and algorithms to calculate the membrane performance parameters A , B and S_s . Unlike the conventional approaches that require at least two separate independent experiments in RO and FO mode (Cath et al., 2013; Wong et al., 2012), these new methodologies avoid pressurization and the associated membrane deformation by using only a single FO experiment, thus reproducing real FO conditions. The FO-only characterisation methods used in this study were initially contrasted and evaluated in terms of reliability and accuracy. Then the permeability and structural parameters that were determined for the four selected membranes were compared and used to explain the differences in mass transport through novel TFC membranes.



5.1 Experimental Design and Evaluation

5.1.1 Characterisation experiments

The FO-only characterisation methods proposed by Tiraferri et al. (2013) and D’Haese et al. (2016) are fundamentally very similar. A number of experimentally obtained parameters are fitted to the FO mass-transport model and the unknown A , B and S_s parameters are then estimated from an iteration algorithm. The differences between the two methods are the assumptions used and the algorithms implemented which are discussed in the next section. Nonetheless, the experimental part was identical for both methods. This consisted in multi-stage FO experiments with an increasing DS concentration in each stage. In order to maintain the DS concentration constant, the DS re-concentrating system was operated. At the end of each experiment a number of parameters were obtained, these included the draw solution concentrations ($C_{d,i}^{EXP}$), feed solution concentrations ($C_{f,i}^{EXP}$), water fluxes ($J_{w,i}^{EXP}$) and reverse salt fluxes ($J_{s,i}^{EXP}$) for all the stages in the experiment. These were used as input parameters in both characterisation methods. According to the solution-diffusion model it is assumed that the J_w/J_s ratio is constant as it only depends on the intrinsic membrane active layer characteristics A and B . Hence, the coefficient of variation of the J_w/J_s ratio (CV) was used as a control parameter for data quality in each experiment.

5.1.2 Model implementation

The model implementation part was different between the two characterisation methods. In Tiraferri’s method (CM1), the effect of ECP was assumed to be negligible. Therefore the exponential terms $\exp(J_w/k_f)$ and $\exp(J_w/k_d)$, that represent the deviation of concentration due to ECP in the feed and draw side respectively, were omitted from equations (2.4) and (2.5) in the model. In addition, the diffusion coefficient for the DS solution within the support layer was assumed to be constant and set equal to the bulk diffusion coefficient of aqueous NaCl solution ($D_s = D_b = 5.33 \times 10^{-6} \text{ m}^2/\text{h}$). Using initial estimates of A , B and S_s , the calculated concentrations at the membrane interfaces ($C_{fa,i}^{CALC}$, $C_{sd,i}^{CALC}$, $C_{as,i}^{CALC}$) and in turn the calculated water ($J_{w,i}^{CALC}$) and reverse salt fluxes ($J_{s,i}^{CALC}$) were derived from the input parameters using equations 2.1, 2.2 and 2.6-2.8. To convert concentrations to osmotic pressures, the van’t Hoff equation was employed (equation (2.13)). At high concentrations of NaCl solutions this equation is not valid. However, the concentrations of NaCl at the membrane interfaces employed here are low enough and do not deviate from the ideality assumption. Consequently, the membrane’s performance parameters were approximated by minimising in an iterative process the sum of squares of the relative offsets between the experimental and

calculated water and salt fluxes (equation (5.1)). During the optimisation, the error minimisation was subjected to a non-linear equality constraint.

$$error = \sum_{i=1}^n \left(\frac{J_{w,i}^{EXP} - J_{w,i}^{CALC}}{J_w^{-EXP,n}} \right)^2 + \sum_{i=1}^n \left(\frac{J_{s,i}^{EXP} - J_{s,i}^{CALC}}{J_s^{-EXP,n}} \right)^2 \quad (5.1)$$

In D'Haese's method (CM2), feed and draw side ECP is included in the model, therefore the mass transfer coefficients (k_f , k_d) are derived from equations (2.8) and (2.10) and from the experimental hydrodynamic conditions used, such as the CFV and spacer geometry. The concentrations at the boundary layers ($C_{fa,i}^{CALC}$ and $C_{sd,i}^{CALC}$) are calculated from equations (2.6) and (2.7). In addition, a concentration-dependent draw solute diffusivity is introduced. Since the draw salt concentration inside the support layer is diminished by the ICP effect, the diffusivity of salt at the active-support layer interface ($D_{s,i}$) is corrected. This is done using the comprehensive compilation of experimentally obtained diffusion coefficients of electrolytes at varying concentrations, sourced from Lobo (1993). Instead of optimising all three performance parameters, in this method only S_s is estimated. Therefore a value of S_s is initially assumed and the concentration at the active-support layer interface ($C_{as,i}^{CALC}$) is calculated from equation (2.12). Then the membrane permeability coefficients for each stage (A_i and B_i) are calculated by rearranging equations (2.1) and (2.2), and their relative errors are minimised using the following equation:

$$error = \frac{1}{n} \sum_{i=1}^n \left(\frac{\sqrt{(A_i - \bar{A})^2}}{\bar{A}} + \frac{\sqrt{(B_i - \bar{B})^2}}{\bar{B}} \right) \quad (5.2)$$

Both minimization algorithms used in the two characterisation methods were implemented using the Solver tool (Microsoft Excel) which employs a generalised reduced gradient method with forward differencing. The sequence of steps used in modelling the membrane performance parameters by CM1 and CM2 is shown in Figure 5.1. In order to determine the goodness of the fit, a coefficient of determination for the water flux and reverse salt flux was calculated as such:

$$R_w^2 = 1 - \frac{\sum_{i=1}^n (J_{w,i}^{EXP} - J_{w,i}^{CALC})^2}{\sum_{i=1}^n (J_{w,i}^{EXP} - J_{w,i}^{-EXP,n})^2} \quad (5.3)$$

In this study, the selected membranes were not characterised by the conventional RO-FO methodology. Instead, membrane performance parameters obtained by the RO-FO method

were extracted from the literature, where available. Previous studies have concluded that although both methodologies are able to yield consistent membrane performance parameters, there is poor agreement between them, and that the values derived from the FO-only method provide a better prediction of water and salt fluxes (Kim et al., 2017).

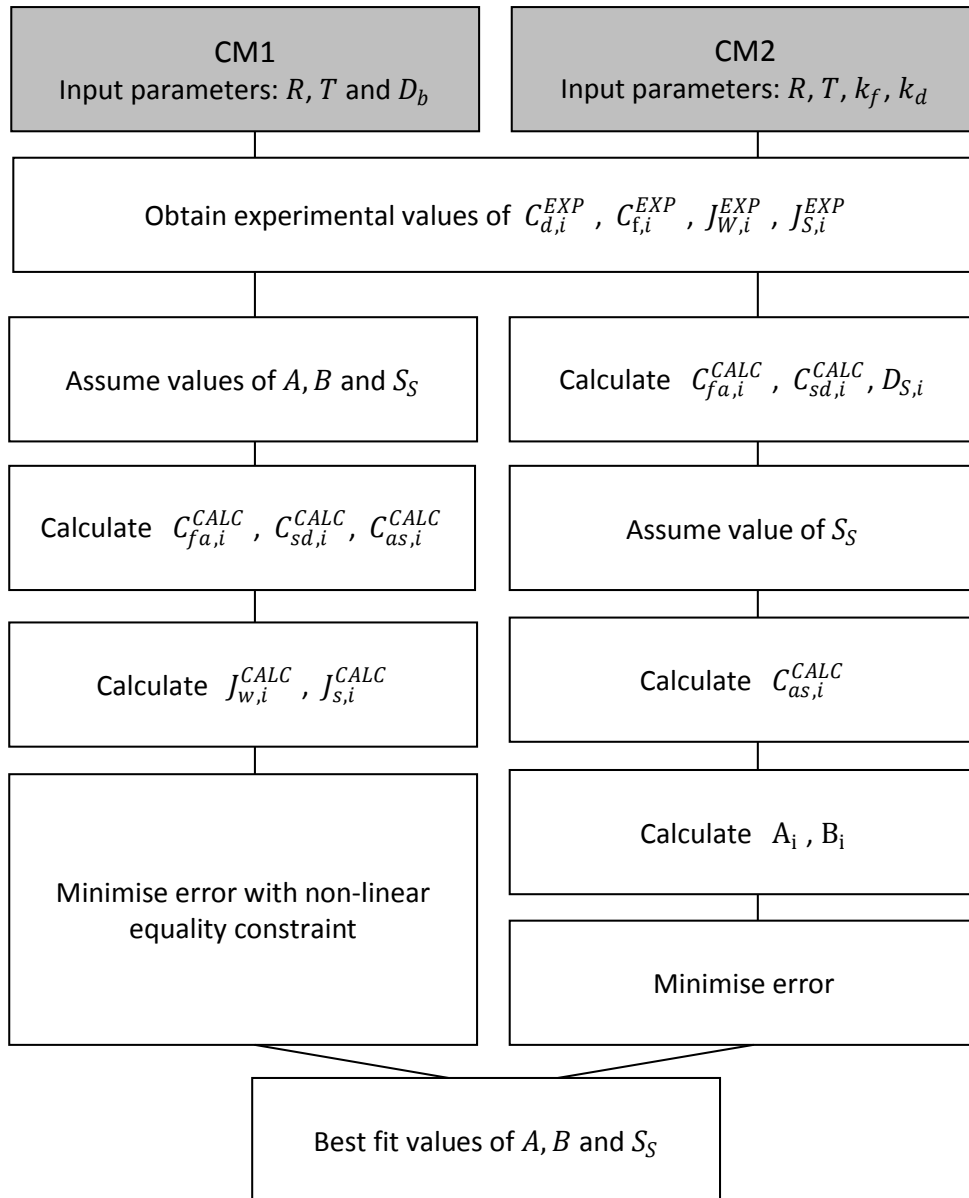


Figure 5.1 Flowchart of the optimisation procedure for the characterisation methods. Additional input parameters for CM2 include the mass transfer coefficients and concentration-dependent diffusivity.

5.2 Results and Discussion

5.2.1 Characterisation experiments

The experimentally obtained water and draw salt fluxes from the multi-stage characterisation experiments are shown in graphs A and B in Figure 5.2 as a function of draw solution concentration. The higher water fluxes of the TFC membranes compared to the conventional CTA membrane demonstrate the improvements in water permeability in recent years. Particularly the TFC-3 membrane shows exceptionally high water fluxes. Nonetheless, despite the high water permeability of TFC-3, draw solute retention was lower with a significantly higher RSF. As a result, membrane performance is often determined by the J_w/J_s ratio to take into account both water and reverse salt fluxes. TFC-2 has the highest ratio, indicating that a greater volume of water permeates through the membrane per mole of salt that leaks into the feed solution. Maintaining a low RSF is essential in some applications in which the quality of the feed stream can be compromised by a high salt content, i.e. osmotic membrane bioreactor (Blandin et al., 2018).

The assumption that the J_w/J_s ratio remains constant is the basis of the solution-diffusion model and any deviations need to be properly analysed. From graph C in Figure 5.2, it seems that CTA and TFC-1 membranes have relatively constant J_w/J_s ratios throughout the experimental stages. In contrast, the J_w/J_s ratios of TFC-2 and TFC-3 showed a tendency to decrease as a function of DS concentration until a stabilised value was reached at high DS concentrations. A similar trend was observed by D'Haese et al. (2016) when using a greater range of DS concentrations and more types of draw salt. A possible reason for the non-constant ratio observed was attributed to experimental errors and error propagation, these are explained further below. Another explanation that was given for the trend was the presence of concentration-dependent mechanisms that affect the J_w/J_s ratio and that are not included in the current model. For example, a higher salt permeability coefficient (B) would be expected at high DS concentrations if the electrical double layer is compressed by counter-ion charge screening. In the case of NaCl as the draw solute, compression of the electrical double layer would strongly reduce electrostatic repulsion between the membrane and the salt ions, hence facilitating the transport of salt. This would result in a higher RSF and a decreased J_w/J_s ratio at increasing DS concentration, thus potentially explaining the observed trend herein.

According to Tiraferri et al. (2013), a coefficient of variation of the J_w/J_s ratio (CV) within 10% is recommended to assure that the experimental data is reliable for further data treatment. As shown in graph D of Figure 5.2, CTA, TFC-1 and TFC-2 had an average CV value below 10%.

TFC-3 was the exception with a CV value of 12.2%. Nonetheless, all TFC membranes were accompanied with relatively large errors. This can either be due to the higher permeability of TFC membranes which makes them more prone to experimental water and salt flux-related errors, or because the salt permeability coefficients (B) of TFC membranes are more dependent on DS concentration changes.

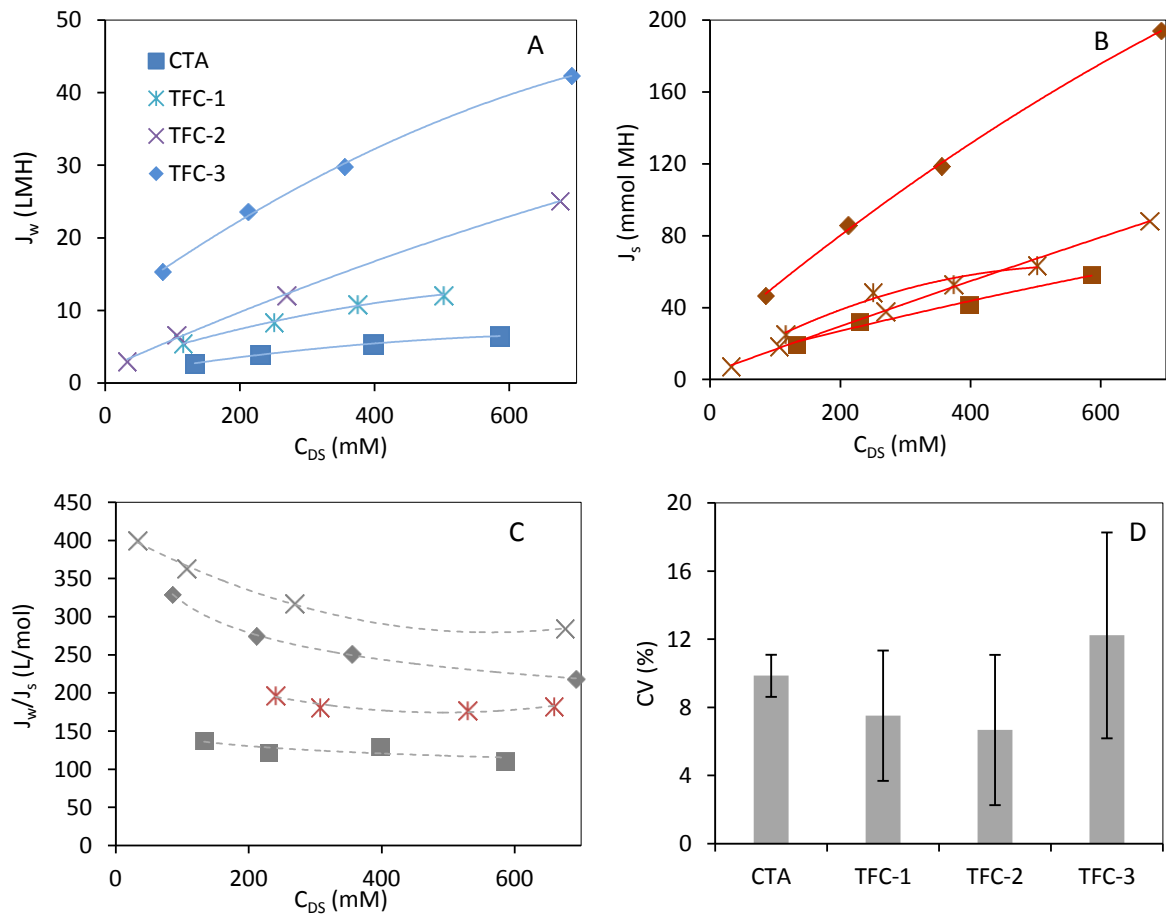


Figure 5.2 Graphs A, B and C illustrate water fluxes, reverse salt fluxes and the ratio of water to reverse salt flux (J_w/J_s) for the four selected membranes for a range of DS concentrations. These were taken from a single characterisation experiment for each of the membranes and are not averaged values. Graph D shows the averaged coefficient of variation (CV) as a percentage for the four membranes.

Regarding the experimental errors, it is worth noting that in calculating the RSF there were a number of possible sources of error. The mass balance equation (4.2) relies on the precision of the conductivity meters in measuring the conductivity of the feed solution. Since each stage lasted only 15 minutes, the transfer of NaCl mass into the FS during the initial stages at low DS concentration often resulted in small changes in conductivity. In the same mass balance equation, accurate feed volumes were required in the calculation of RSF, including the volume of water in the feed reservoir and the volume in the feed circulation. Poor measurements of

conductivity and total feed volumes might have yielded inaccurate values of J_s . For example a 10% error in the measurement of feed conductivity was found to increase the CV value almost three-fold. Despite the significant errors on the calculated CV values, the membrane performance parameters were calculated for all four membranes.

5.2.2 Assessing model accuracy

A second control for the reliability of the calculated parameters are the coefficients of determination for both water (R_w^2) and salt fluxes (R_s^2). These coefficients indicate the goodness of the fit between modelled and experimental fluxes. According to Tiraferri et al., (2013) coefficients higher than 0.95 are recommended to ascertain that membrane parameters are accurately predicted, whereas results with coefficients below 0.90, should be omitted. R_w^2 and R_s^2 coefficients were calculated for both methods and are listed in Table 5.1.

Table 5.1 Coefficients of the determination of water and reverse salt fluxes for the selected membranes obtained from the two different characterisation methods

Membrane Type	CV (%)	R_w^2		R_s^2	
		CM1	CM2	CM1	CM2
CTA	9.9 ±1.2	0.98 ±0.02	0.95 ±0.06	0.98 ±0.00	0.98 ±0.02
TFC-1	7.5 ±3.8	0.99 ±0.00	0.98 ±0.00	0.97 ±0.01	0.97 ±0.01
TFC-2	6.7 ±4.4	0.99 ±0.01	0.98 ±0.01	0.98 ±0.03	0.96 ±0.04
TFC-3	12.2 ±6.0	0.94 ±0.04	0.91 ±0.09	0.96 ±0.03	0.91 ±0.08

The coefficients of determination for CTA, TFC-1 and TFC-2 were all above 0.95 indicating that the calculated parameters are at most 10% off from their true value. Again, results for TFC-3 were the least reliable. However, since the R^2 values of TFC-3 were superior to 0.90, the results were not discarded. It is interesting to note that although CM2 applies a more complete model that includes ECP and concentration-dependent draw solute diffusivity, the characterisation method yielded slightly lower R^2 values. The accuracy of the membrane parameters determined by the two FO-only methods can also be interpreted by plotting the calculated fluxes and the experimental fluxes side by side. As shown in Figure 5.3, CM1 yields membrane parameters that provide a better fit. On the other hand, CM2 slightly overestimates the membrane performance parameters, especially the water permeability coefficient (A) for the two novel TFC membranes. This suggests that, although CM2 implements a more comprehensive model, the error minimisation algorithm used is less effective in determining membrane performance parameters accurately.

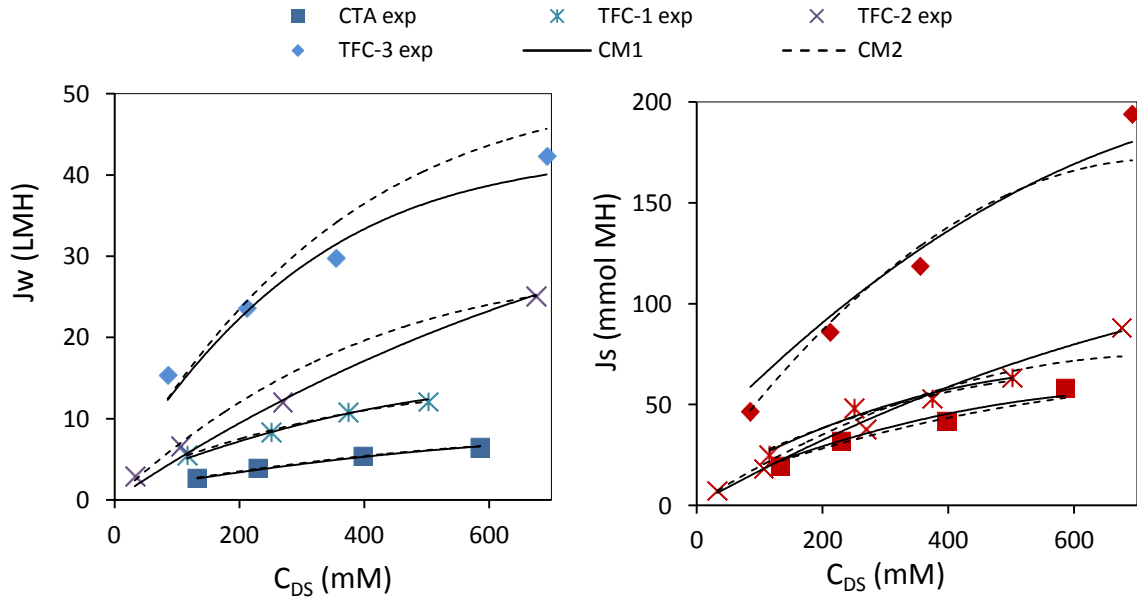


Figure 5.3 Fitting of modelled water and reverse salt fluxes to the experimental fluxes obtained. The better fit of the CM1 method compared to the CM2 method is clearly seen, particularly for the water flux.

5.2.3 Membrane Performance parameters

Table 5.2 summarises the calculated average membrane performance parameters obtained by the two FO-only methodologies used in this study (CM1 and CM2). Also listed in the table are the performance parameters of the selected membranes obtained by other authors applying FO-only and also RO-FO characterisation methods. An initial comparison between the parameters obtained in this study for the selected membranes confirms the predicted trend; the lowest calculated permeability coefficients (A, B) correspond to the CTA membrane and the highest to TFC-3. As expected, novel TFC membranes show great improvements in water permeability at a cost of a lower salt retention. Nonetheless, their J_w/J_s ratios are still higher than conventional membranes making them more attractive in applications which prioritise water production over reverse salt leakage. TFC-2 and TFC-3 also have significantly lower structural parameters (S_s).

In order to understand how these membrane parameters relate to the overall water and salt fluxes, the concentration polarisation effects in each of the transport layers and the effective driving force were modelled in a similar way to a recent study (Bui et al., 2015). The contribution of each CP component to the overall driving force was modelled using CM1 for the four different stages, as shown in Figure 5.4. The effect of the feed side ECP on the driving force was almost negligible because DI water was used as the feed solution. Whereas the effect of the draw side ECP was clearly noticeable and increased as higher DS concentrations

were employed, especially for TFC-2 and TFC-3 due to the higher water fluxes obtained. Out of all the membranes tested, CTA and TFC-1 suffered from the greatest impact of ICP on the driving force. This is attributed to the greater structural parameter (S_s), proportional to a thicker, less porous and more tortuous support layer, which inhibits mixing of the draw salt. Despite the fact that TFC-2 and TFC-3 showed insignificant ICP effects at low DS concentrations, this changed at higher DS concentrations with ICP becoming very pronounced, again due to the higher water fluxes achieved. The impact of a greater ICP effect is reflected on the effective driving force and the resultant water and reverse salt fluxes, which do not increase proportionally with DS concentration, but rather reach a plateau at very high DS concentrations (Figure 5.2A and B).

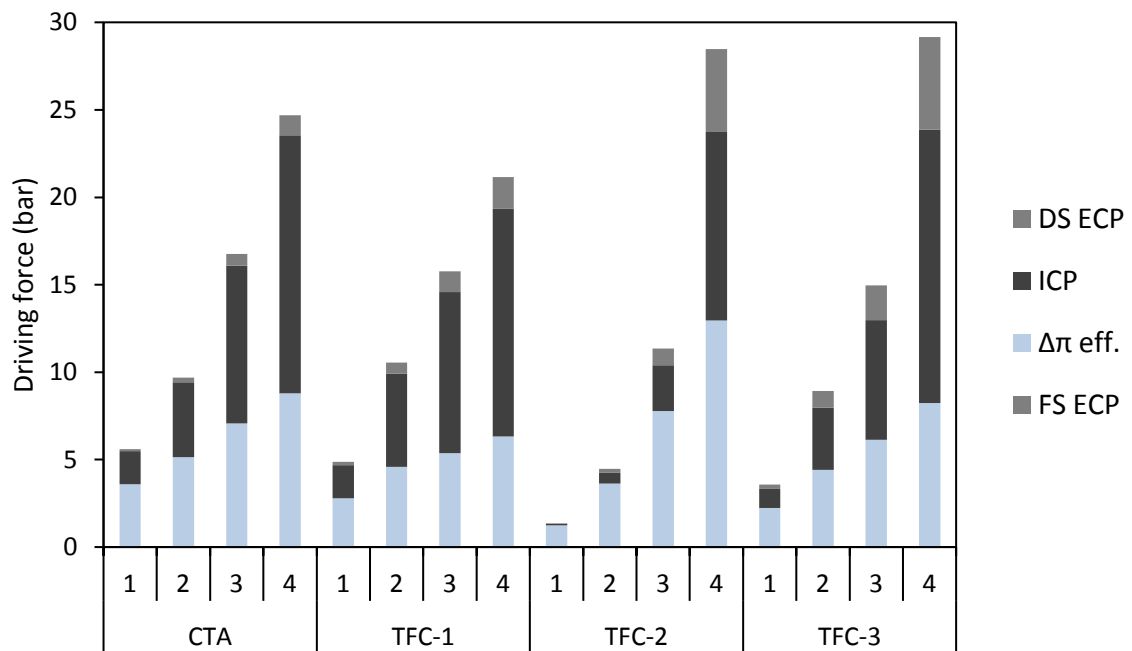


Figure 5.4 Impact of the different concentration polarisation effects on the overall driving force and the resulting effective driving for the four selected membranes at increasing DS concentrations. The numbers represent the stages, with stage 4 having the highest DS concentration. The CP effects and effective driving force were modelled using CM1.

To identify which of the membrane parameters has a stronger influence on the water and reverse salt flux, a range of structural parameters, water permeability and salt permeability coefficients were modelled using CM1. These results are illustrated in Figure 5.5. From the results, the water permeability coefficient (A) is the most important determinant of the water flux. It explains why the effective driving force increased in similar magnitude for all the membranes (Figure 5.4) but the water fluxes were much higher for the novel TFC membranes. On the other hand, the salt permeability coefficient (B) has a negligible impact on the water flux but had the greatest influence on the reverse salt flux. To a lower extent, the water flux

and reverse salt flux are also influenced by the structural parameter through the ICP effect. An increasing S_s value lowers the effective driving force and both water flux and reverse salt flux, accordingly.

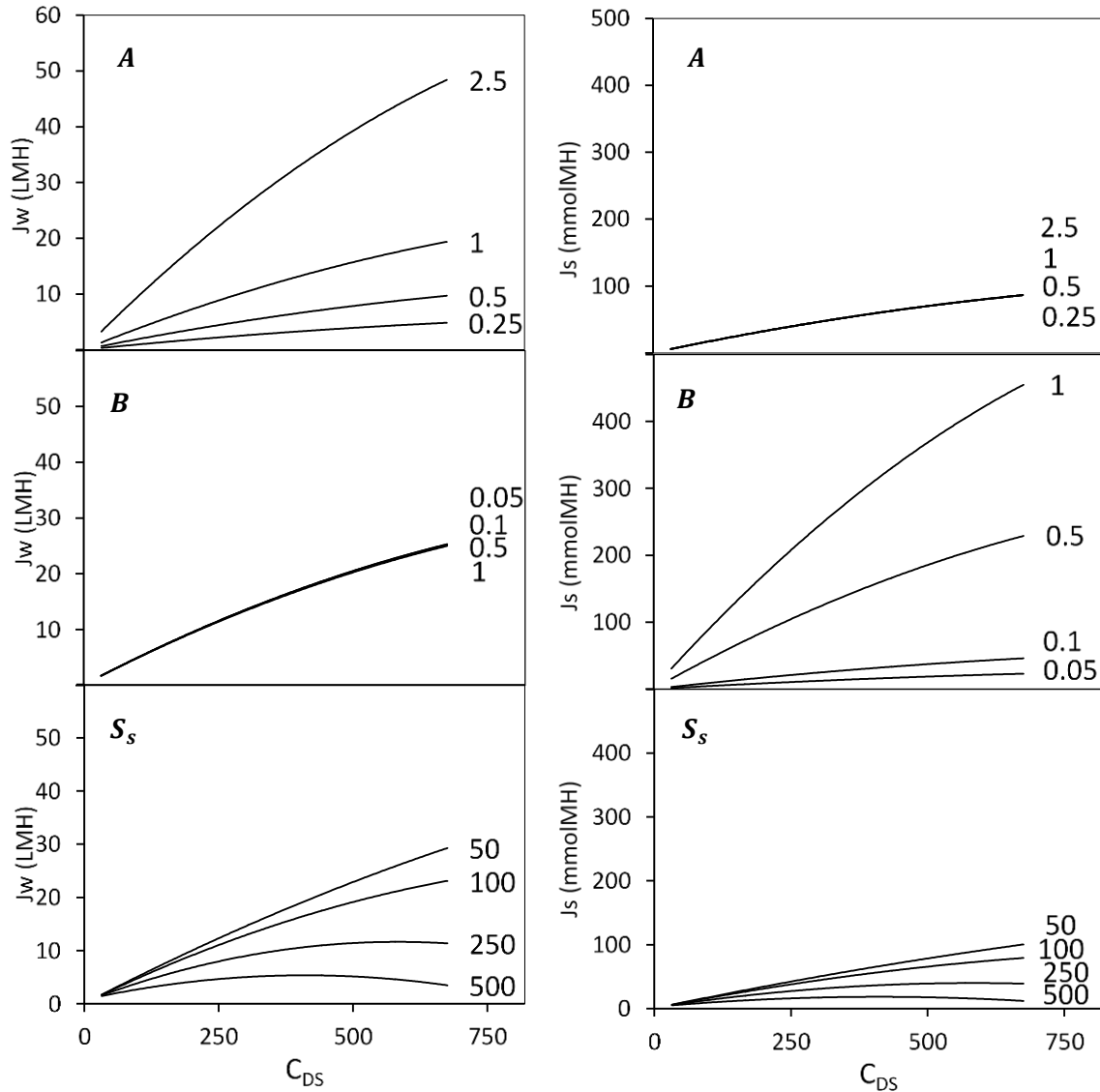


Figure 5.5 Modelled water and reverse salt fluxes for a varying range of A , B and S_s values. CM1 was used to model these fluxes for the TFC-2 membrane only. When changing one parameter, the other parameters were kept constant at the values obtained from the characterisation of TFC-2: $A = 1.30 \text{ Lm}^{-2}\text{h}^{-1}\text{bar}^{-1}$, $B = 0.19 \text{ Lm}^{-2}\text{h}^{-1}$, $S = 81 \text{ }\mu\text{m}$.

Many prior studies have characterised the widely-used CTA membrane and it has become the benchmark for comparing characterisation methods. The most relevant studies, shown in Table 5.2, have reported membrane performance parameters that vary significantly between them (Cath et al., 2013). As previously mentioned, differences between parameters obtained by FO-only and RO-FO characterisation methods can be attributed to the distinct driving forces

(osmotic pressure vs. hydraulic pressure). However, there seems to be a great disparity between the parameters obtained by the FO-only methods too. This variability most probably arises from the different experimental set-ups used and the different batches of membrane samples tested. Hence, a direct comparison between the calculated parameters and those obtained from literature is futile. The same applies to the TFC membranes, even though fewer characterisation studies have been performed on them.

Despite the difficulty in comparing the parameters obtained in this study with literature, the calculated parameters are within the range expected for the respective membranes. It is interesting to note that the errors related to some of the calculated parameters were relatively large, particularly for TFC membranes. For example, the structural parameter of TFC-1 averaged $650 \mu\text{m}$ with an error of $\pm 234 \mu\text{m}$, and the salt permeability of TFC-2 averaged $0.70 \text{ Lm}^{-2}\text{h}^{-1}$ with an error of $\pm 0.40 \text{ Lm}^{-2}\text{h}^{-1}$. Such a large variability in the parameters does not originate from experimental errors or the use of an inadequate model because both CV and R^2 values are acceptable. It is rather due to the irregularity of membrane coupons. TFC membranes are known to be more vulnerable to defects due to the fragility of the active layer (Xu et al., 2017). Therefore loss of TFC membrane integrity could be the cause of large variability in the calculated performance parameters.

The two novel TFC membranes (TFC-2 and TFC-3) are structurally very similar as exposed by SEM images of their cross-sections (Figure 5.6). In addition, from the SEM images a greater thickness was determined for TFC-3 ($73.2 \mu\text{m}$) compared to TFC-2 ($54.8 \mu\text{m}$). If the porosity and tortuosity of both membranes is similar, these results agree with the characterisation results, in which TFC-3 showed a slightly greater structural parameter. Since the structural parameter only describes the support layer of the membrane, the differences in permeability coefficients observed are due to the composition and chemistry of the active layer. It is likely that TFC-3 contains a larger proportion of free volume voids, and together with a greater negative surface charge, it explains the greater permeability. A study on the pore size distribution of FO membranes has reported a lower free volume radius for TFC-3 compared with the conventional CTA membrane (S. J. Kim et al., 2017). A similar investigation on the active layer pore size distribution of the selected membranes using positron annihilation lifetime spectroscopy (PALS) would enable a better understanding of their separation performance.

Table 5.2 Summary of the membrane performance parameters obtained from the two FO-only characterisation methods (CM1 and CM2) used herein for the selected membranes. Also listed are the parameters reported from other FO-only and RO-FO methods in the literature on the same membranes.

Membrane Type	Characterisation Method	A ($L m^{-2} h^{-1} bar^{-1}$)		B ($L m^{-2} h^{-1}$)		S_s (μm)		Ref.
CTA	FO-only	0.51	± 0.05	0.26	± 0.05	635	± 70	CM1
	FO-only	0.64	± 0.16	0.26	± 0.01	616	± 240	CM2
	FO-only	1.34	± 0.25	1.36	± 0.37	498	± 37	(Tiraferrri et al., 2013)
	FO-only	0.41	± 0.04	0.16	± 0.00	333	-	(D'Haese et al., 2016)
	RO-FO	1.50	± 0.18	0.10	± 0.01	370	± 20	(Tiraferrri et al., 2013)
	RO-FO	0.55	-	0.48	-	463	-	(Coday et al., 2013)
	RO-FO	0.70	-	1.50	-	663	-	(Blandin et al., 2016a)
	RO-FO	0.62	± 0.03	0.70	± 0.20	443	± 43	(S Manickam and McCutcheon, 2012) (Nguyen et al., 2015)
TFC-1	FO-only	1.82	± 0.36	0.48	± 0.11	659	± 234	CM1
	FO-only	2.32	± 0.54	0.52	± 0.14	657	± 251	CM2
	FO-only	2.67	± 0.36	1.47	± 0.17	639	-	(D'Haese et al., 2016)
	RO-FO	1.30	-	0.30	-	1227	-	(Blandin et al., 2016a)
	RO-FO	1.63	-	0.83	-	690	-	(Coday et al., 2013)
TFC-2	FO-only	1.55	± 0.70	0.71	± 0.41	123	± 50	CM1
	FO-only	1.80	± 0.72	0.72	± 0.38	106	± 63	CM2
	RO-FO	2.10	-	1.20	-	344	± 4	(Blandin et al., 2016a)
TFC-3	FO-only	5.34	± 1.72	0.81	± 0.33	180	± 85	CM1
	FO-only	6.35	± 1.75	0.92	± 0.33	201	± 55	CM2
	RO-FO	5.36	-	2.63	-	266	-	(Nguyen et al., 2015)
	RO-FO	8.82	-	2.46	-	276	-	(Nguyen et al., 2018)

To conclude, novel TFC membranes have shown excellent water permeability at the expense of a lower salt retention, due to a more permeable pore structure of the active layer. Despite this, their overall selectivity was higher than the conventional FO membranes, demonstrating their superiority in treating wastewater. Two FO-only methodologies were successfully implemented in characterising the selected membranes. Although the experimental part of the FO-only methods presented issues associated with a non-constant J_w/J_s ratio, the algorithms employed in estimating the membrane performance parameters were found to be effective, especially for CM1. A likely reason for the non-constant J_w/J_s ratio is that mass transport model employed either lacks relevant variables or some of the existing variables are concentration-dependent. The lower support layer structural parameter of the novel TFC membranes resulted in a lower ICP effect, but with increasing water fluxes, ICP grew exponentially impeding excessively high water fluxes to be reached. Overall, it was found to be

very difficult to obtain the *real* membrane performance parameters, because of the variation in membrane coupons and the operating conditions used in the experimental part. Unless FO membranes are characterised under similar conditions, draw salts and experimental set-ups, the parameters obtained by these methods do not serve as an appropriate metric for comparing membrane performance.

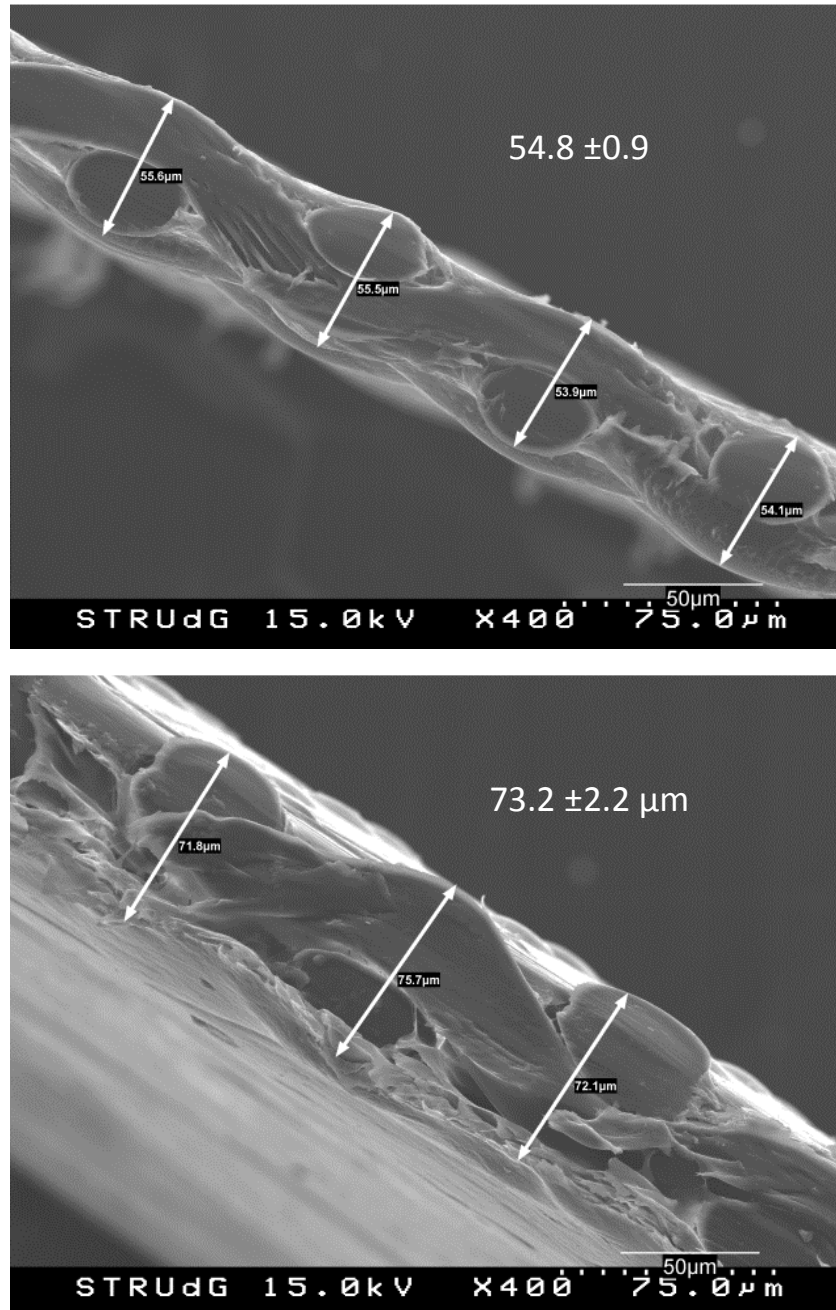
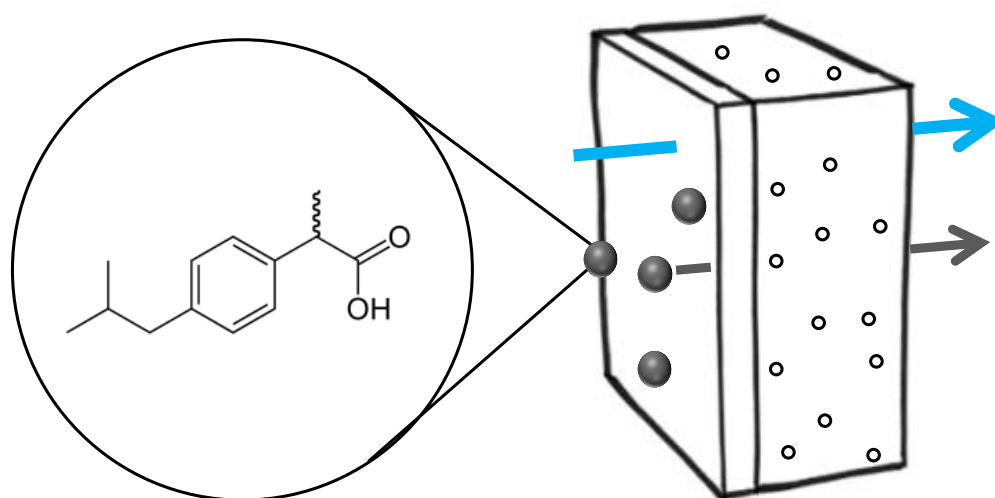


Figure 5.6 SEM images of the cross-section of TFC-2 (top) and TFC-3 (bottom) showing the average thickness of the membranes and the woven structure of the support layer.

6 Transport of trace organic contaminants through novel TFC membranes

In this chapter, the transport of several organic compounds through two novel TFC membranes was investigated to evaluate their potential in removing TrOCs from contaminated feed waters and to better understand the mechanisms of rejection. Firstly, the fate of TrOCs in a bench-scale FO system was probed by carrying out long-term experiments. These were followed by ordinary rejection experiments in FO mode which allowed for an initial comparison between the selectivity of the two membranes. Finally, the role of the draw solution and the mechanisms involved in the rejection of organic compounds were further explored with a series of TrOCs permeability experiments. Throughout the chapter, the relationship between the physicochemical properties of the solutes and membrane, and the transport of organic solutes enabled to identify these mechanisms.



This chapter was published as:

Marc Sauchelli, Giuseppe Pellegrino, Arnout D'Haese, Ignasi Rodriguez-Roda, Wolfgang Gernjak. 2018 Transport of trace organic compounds through novel forward osmosis membranes: Role of membrane properties and the draw solution. *Water Research*: 141, 65-73.

6.1 Experimental Design and Evaluation

6.1.1 Fate and rejection of TrOCs in FO

Adsorption of organic compounds onto the membrane and the consequentially incomplete mass balance is the greatest limitation of studying the rejection of TrOCs in FO as it can lead to an overestimation of the rejection (Kimura et al., 2003). Membrane adsorption, which has been reported to occur through hydrophobic interactions and hydrogen bonding (Heo et al., 2013; Nghiem et al., 2004), is considered the first step in the transport of these compounds. In the early stages of an experiment the apparent rejection might seem very high, but the real rejection can only be determined after membrane saturation has been reached and steady-state permeation of the compounds is established. Therefore, long-term operation experiments were initially performed to investigate the fate of TrOCs in the FO system and to determine if adsorption and degradation were occurring. This was examined by monitoring the concentration of the TrOCs in the feed and draw solutions for approximately three days. Afterwards, sufficiently-long FO rejection experiments were carried out for both TFC membranes to allow for the accurate determination of rejection. All samples were analysed with the low-concentration TrOCs analytical method (section 4.4.1). Consequently, the rejection percentages of TrOCs by TFC-2 and TFC-3 at the different stages of the experiment were determined from the concentrations using the following mass balance equation:

$$R = \left(1 - \frac{C_P^{\text{TrOCs}}}{C_F^{\text{TrOCs}}}\right) 100\% = \left(\frac{C_{D,t}^{\text{TrOCs}} V_{D,t} - C_{D,i}^{\text{TrOCs}} V_{D,i}}{V_P} \frac{C_{F,t}^{\text{TrOCs}} + C_{F,i}^{\text{TrOCs}}}{2}\right) 100\% \quad (6.1)$$

Where C_P^{TrOCs} , C_F^{TrOCs} and C_D^{TrOCs} are the concentrations of TrOCs in the permeate, the feed solution and the draw solution, respectively. V_D and V_P are the volumes of the draw solution and the permeate. Subscripts i and t denote the initial stage and different time intervals during the experiment, respectively. By sampling early on during the experiment and then at longer time intervals, possible adsorption of compounds to the membrane could be observed with a decrease in rejection. The overall rejection for each TrOC by the membranes was then calculated from the average of all the rejection percentages obtained at the different stages, allowing for an accurate determination of steady-state rejection. In addition, when calculating the overall rejection, the mass of TrOCs taken out of the draw solution from each sample was also included in the mass balance.

6.1.2 Effect of DS on permeability of TrOCs

In assessing the role of the DS on the transport of TrOCs, three changes were made from the previously described rejection experiments: a) higher concentrations of TrOCs were used to minimize experimental and analytical errors, b) 9 out of the 18 TrOCs were selected to probe specific compound-membrane interactions and c) instead of evaluating the rejection, the permeability of the TrOCs was used as the parameter for comparison as it includes both diffusive and convective transport (Kim et al., 2007). The reasons of these three changes are explained in more detail in the following sections because they're based on the outcome of the rejection experiments. As previously mentioned, determining the rejection of TrOCs once the membrane is saturated with the target compounds is highly recommended. The same applies to the determination of TrOCs permeability coefficients (Plakas and Karabelas, 2012). Therefore an initial membrane saturation experiment was also performed in this case to reach steady-state permeation of TrOCs.

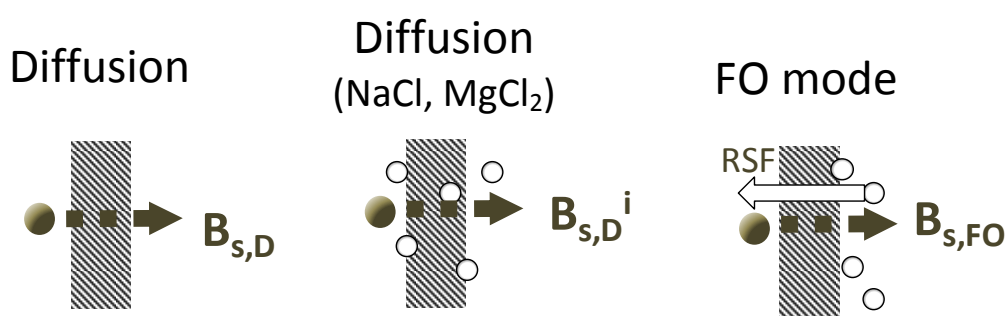


Figure 6.1 Schematic illustrations of the different permeability experiments; on the left the diffusion experiment without any salt and only DI water, in the middle the diffusion at increasing ionic strength (*i* stands for the different concentrations of NaCl or MgCl₂, either 0.1M or 0.5M) and on the right the normal FO experiment with added NaCl in the draw solution only.

The series of TrOCs permeability experiments that were performed included the diffusion experiments without a draw solution and DI water in feed and draw solutions, diffusion experiments at increasing ionic strength using NaCl and MgCl₂ as the feed and draw solutions, separately and at different concentrations, followed by ordinary FO experiments (Figure 6.1). All samples were analysed with the high-concentration TrOCs analytical method described in section 4.4.2. To calculate the membrane permeability coefficient of the TrOCs from the concentrations obtained in the diffusion experiments ($B_{s,D}$), the following pseudo-steady state derivation of Fick's first law of diffusion was applied, as described by Kim et al (2007):

$$B_{s,D} = \left(\frac{V_F V_D}{V_F + V_D} \right) \frac{1}{A_m t} \ln \left(\frac{C_{F,i}^{TrOCs} - C_{D,i}^{TrOCs}}{C_{F,t}^{TrOCs} - C_{D,t}^{TrOCs}} \right) \quad (6.2)$$

On the other hand, the membrane permeability coefficients of the TrOCs from the FO experiments ($B_{s,FO}$) were calculated with the following expression, adapted from the solution-diffusion model (Wijmans and Baker, 1995):

$$B_{s,FO} = \frac{J_w C_{P,t}^{TrOCs}}{C_{F,t}^{TrOCs} - C_{P,t}^{TrOCs}} \quad (6.3)$$

Where $C_{P,t}^{TrOCs}$ is the permeate concentration of TrOCs at time t which can be obtained with the following mass transfer equation:

$$C_{P,t}^{TrOCs} = \left[\frac{(V_{D,t} C_{D,t}^{TrOCs}) - (V_{D,i} C_{D,i}^{TrOCs})}{J_w A_m t} \right] \quad (6.4)$$

The difference between the equations used in the diffusion experiments (equation (6.2)) and the FO experiments (equation (6.3)) is the inclusion of convective transport in the FO experiments due to the presence of a water flux. Nonetheless, both equations result in accurate determinations of the permeability coefficients as suggested by D'Haese (2017).

6.1.3 Determining solute-membrane interactions

In order to identify the solute-membrane interactions and therefore the mechanisms that dictate the transport of TrOCs through the two membranes, relationships between the permeability coefficients and the properties of the selected TrOCs, e.g. molecular weight (MW), minimal projected surface area (MPSA), hydrophobicity (logD), and electrical charge, were determined by means of the Pearson (r) and Spearman's rank (ρ) correlations. Whilst the Pearson coefficient is used to identify linear correlations, the Spearman's rank identifies monotonic linear or non-linear relationships. A relationship was considered confirmed when the correlations reached values $> |0.75|$.

6.2 Results and Discussion

6.2.1 Fate of TrOCs in system set-up

The initial experiments, designed to probe the fate of TrOCs in a bench-scale FO system, lasted approximately three days. All the TrOCs were re-circulated in the feed and draw solution at equal concentrations of 1 $\mu\text{g/L}$ and no salts were used, therefore no water or reverse salt flux

developed. Samples were taken approximately every 10 hours. From the results, the concentrations of erythromycin, ranitidine and verapamil were persistently lower than the rest of the TrOCs. This suggested large sample preparation errors during SPE or an inadequate analytical methodology for the aforementioned compounds. The other compounds were found at the expected concentrations. As can be seen in Figure 6.2A, some of the organic compounds, such as carbamazepine, ibuprofen and furosemide, had concentrations that remained relatively constant at 1 µg/L for the duration of the experiment. In contrast, a decreasing concentration was observed for other compounds, such as phenazone, diclofenac and gemfibrozil. Whilst diclofenac and gemfibrozil are hydrophobic with LogP values above 4, phenazone has a much lower logP value of 1.22. Therefore, besides adsorption of hydrophobic compounds to the membrane and the system parts, some TrOCs were likely to be degrading over time.

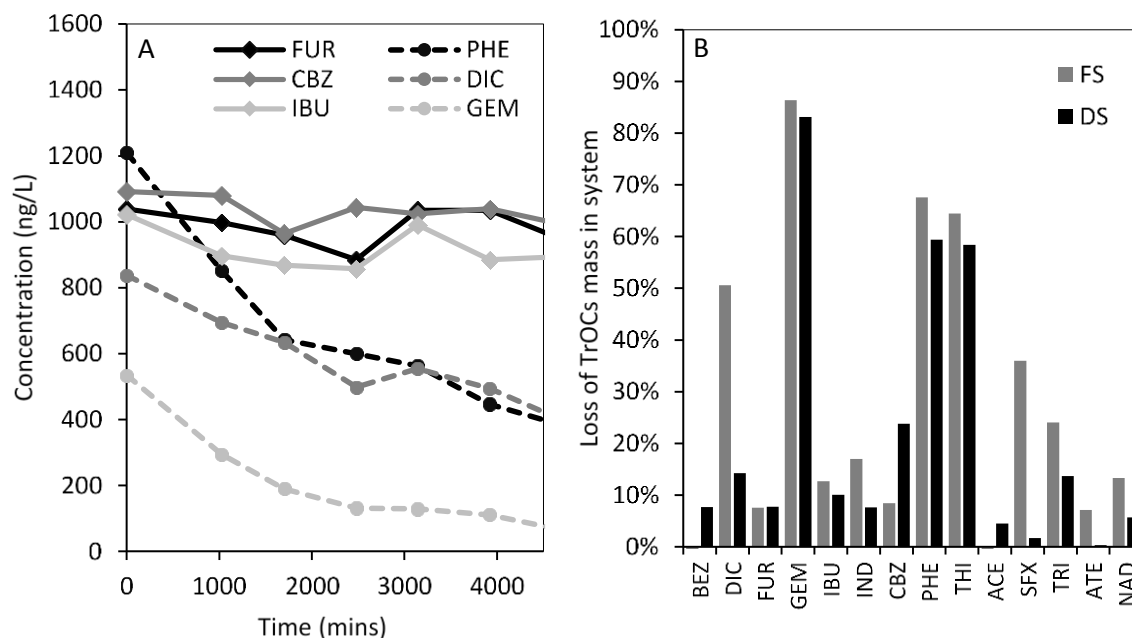


Figure 6.2 Graph A shows the changing concentration of six TrOCs in the feed solution as a function of experimental duration. Only six TrOCs are shown for clarity, some adsorb or degrade in the FO system and therefore decrease in concentration. Graph B depicts the loss of mass for most of the selected TrOCs in the FS and DS at the end of the long-term experiment.

The loss of TrOCs mass in the feed and the draw solution were calculated as percentages as shown in Figure 6.2B. Gemfibrozil, diclofenac, phenazone and thiabendazole were the most vulnerable to adsorption and possibly degradation, consequently, specific attention was paid to these compounds in the next sections. These results also confirm that experiments shorter than three days can be carried out with most of the selected TrOCs without the risk of degradation. It is important to note that relatively large errors were observed in the

concentrations of many compounds, probably due to the deficient sample preparation or analytical method employed. Using such low concentrations of TrOCs makes the results highly dependent on the sensitivity of the analytical instrument and expertise in SPE. In order to obtain more reliable results, spiking at higher concentration of TrOCs is recommended.

6.2.2 Rejection of TrOCs by novel TFC membranes

The TFC membrane rejection experiments lasted for approximately 40 hours, starting with 1 µg/L of TrOCs in the feed solution and an appropriate draw solution concentration to maintain a water flux of approximately 10 L m⁻² h⁻¹. To monitor the changing concentrations of TrOCs in the feed and draw solutions, samples were collected after three hours and then in intervals of 10 hours, summing up to a total of 5 samples. An increasing concentration of organic compounds in the draw solution suggested that the compounds were permeating through the membranes. Similarly, the concentration of TrOCs in the feed solution also increased due to a reduction in volume over time. At each sampling interval, the rejection of TrOCs was calculated using equation (6.1), and the rejection percentages are shown in Figure 6.3. As the experiment progressed, the rejection of the majority of TrOCs by both membranes increased. This suggested that the membranes were already saturated with the TrOCs, non-steady state adsorption of compounds to the membrane occurred at the start of the experiment and it was not affecting the calculation of the rejection.

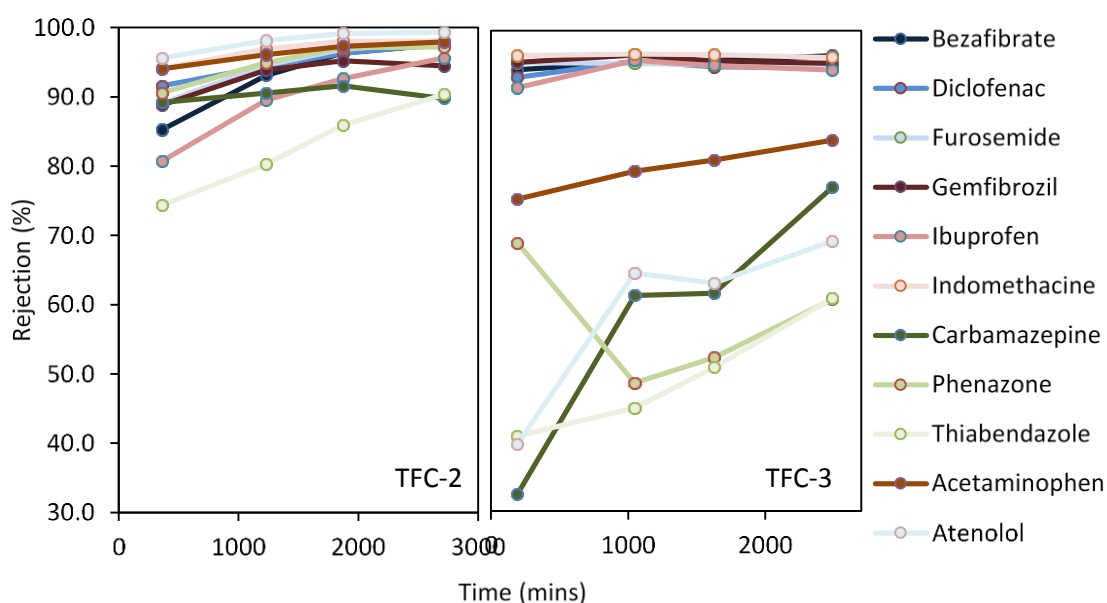


Figure 6.3 Rejection percentages of the selected TrOCs at the different sampling intervals; after 3 hours and then in 10 hour intervals. Besides the rejection of phenazone by TFC-3, the rejection of all the other compounds increased as the experiment progressed.

The average rejection values for the selected TrOCs by the novel TFC membranes are shown in Figure 6.4. Results indicate very high removal of all TrOCs by TFC-2, with rejection percentages above 85%. Thiabendazole had the lowest rejection, probably due to its faster degradability, as detected in the prior long-term experiments. Despite the great removal efficiency of TFC-2, the Pearson and Spearman coefficients indicated no correlation between the rejection of the compounds and their charge, hydrophobicity, molecular weight or minimal projected surface area (Table 6.1). Most likely a combination of steric hindrance and hydrophobic and electrostatic interactions were involved in the rejection. Similarly high removal percentages of organic solutes were reported in a recent study (Blandin et al., 2016a). Significantly higher rejections were observed for TFC-2 compared to HTI's CTA and TFC membranes. This improvement was attributed to smaller membrane pore sizes and a more negative surface charge which electrostatically repelled charged solutes and hydrated the membrane pores, further reducing the pore sizes. In the same study, the higher rejections were also hypothesised to be a consequence of a higher water flux and the influence of RSF.

The rejection percentages of TrOCs by TFC-3 were more varied. Negatively charged compounds were all rejected above 94%. In contrast, the rejection of some neutral and positively charged compounds was much lower. The high negative surface charge of the TFC-3 membrane (-58 mV) may have led to strong electrostatic repulsion of negatively charged compounds. On the other hand, electrostatic attraction of positively charged compounds could explain their lower rejection. In the case of neutral compounds, the membrane surface charge had no effect on rejection; however, pore sizes of the active layer could strongly influence the transport of the neutral TrOCs. There was a lower than expected correlation between rejection and compound charge (-0.68) and no correlation was found for solute size, hydrophobicity and minimal projected surface area. A recent study with the same membrane as TFC-3 found that neutral TrOCs with a higher molecular weight and more hydrophobicity were rejected to a greater extent (Jang et al., 2018). Size exclusion and membrane adsorption were the proposed mechanisms for the rejection of neutral TrOCs. On the other hand, the rejection of charged compounds was found to be mainly dictated by electrostatic interactions. Negatively charged TrOCs were very well rejected by electrostatic repulsion, whilst positively charged compounds were attracted to the membrane surface resulting in a greater concentration gradient and consequently lower rejection. Adsorption of charged compounds to the membrane did not occur due to the stronger electrostatic interactions.

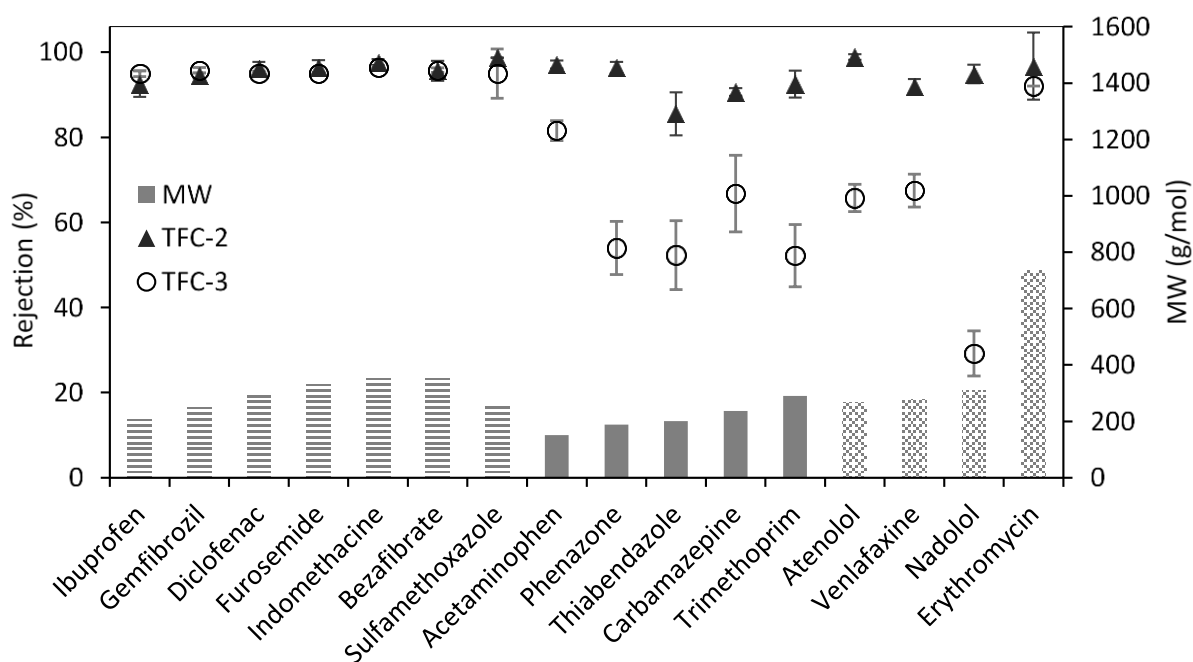


Figure 6.4 Rejection percentages of the 16 TrOCs for TFC-2 and TFC-3 membranes are shown by the triangle and circle symbols, respectively. Ranitidine and Verapamil were omitted due to their poor analysis by HPLC. The MW of the compounds is shown by the bar charts below. The first 7 TrOCs on the left are negatively charged, the 6 in the middle are neutral and the 4 on the right are positively charged.

Table 6.1 Pearson and Spearman's rank correlations between the rejection of the TrOCs by TFC-2 and TFC-3 membranes and their physico-chemical parameters.

Membrane	MW		MPSA		LogD		Charge	
	R	ρ	r	ρ	r	ρ	r	ρ
TFC-2	-0.15	0.06	-0.30	-0.09	-0.49	-0.51	-0.35	-0.11
TFC-3	0.24	0.30	0.14	0.15	0.48	0.50	-0.68	-0.57

r: Pearson correlation coefficient

ρ : Spearman's rank correlation coefficient

To conclude, TFC-2 rejected TrOCs better than TFC-3, particularly the positively charged and neutral compounds. This could be explained by TFC-2 having an active layer with a lower proportion of free volume voids, making steric hindrance the dominant rejection mechanism and explaining why most compounds are rejected equally well. This hypothesis agrees with the fact that TFC-2 also shows lower water and salt permeability. In contrast, the larger average pore free volume of TFC-3 allowed for electrostatic interactions between the membrane and the compounds to have bigger roles in the rejection of TrOCs. However, it needs to be stated that the higher water flux of TFC-3 might have resulted in higher observed rejections. This is because a higher permeate volume (V_p) in equation (6.1) results in a higher rejection. Instead

of the rejection, the permeability of the TrOCs through the TFC membranes would be a more appropriate measure of comparison.

6.2.3 Effect of DS on permeability of TrOCs

In these experiments; a) higher concentrations of TrOCs were spiked in the feed solution. This was done to improve the accuracy in determining the concentration of TrOCs and therefore provide stronger evidence for the ensuing transport mechanisms. It involved developing a new analytical method adapted to the HPLC-UV instrument which is described fully in section 4.4.2. In order to quantify peaks accurately, obtain a good separation of peaks and therefore achieve a time and cost efficient analytical method, fewer TrOCs were selected. Hence, b) nine out of the 18 TrOCs were selected to represent a range of physico-chemical properties and to probe the membrane-solute interactions. The elution peaks of these nine TrOCs were all easy to quantify and did not overlap. In addition, the compounds that were the most vulnerable to adsorption and possible degradation, namely gemfibrozil, diclofenac, phenazone and thiabendazole, were also omitted from the permeability tests. Lastly, c) as described in the previous section, permeability coefficients were chosen as the measure of comparison. In the absence of a water flux, the permeability describes the diffusive transport of solutes, whilst in the presence of a water flux the permeability describes both diffusive and convective transport of solutes.

6.2.3.1 Diffusion tests with DI water ($B_{s,D}$)

The initial diffusion tests were carried out with DI water in the feed and draw solution and the resulting permeability coefficients for TFC-2 and TFC-3 are summarised in Table 6.2. The Pearson and Spearman's rank correlations between the physico-chemical properties of the TrOCs and the permeability coefficients are given in Table 6.3. Unlike the rejection study in the previous section, the Pearson coefficient for the TFC-2 membrane revealed a negative linear correlation between the dimensional parameters of the TrOCs (MW and MPSA) and their permeability, suggesting that solute size and membrane molecular weight cut-off (MWCO) are strong determinants of solute transport through TFC-2. This relationship can be seen in Figure 6.5 which shows a plot of the permeability coefficients against the MW of the selected TrOCs. These results also agree with previous studies on TFC membranes which have identified the average hydrated pore size as a dominant transport limiting parameter (Blandin et al., 2016a; Xie et al., 2014). On the other hand, no relationship was found between the permeability of the TrOCs and their charge or hydrophobicity.

In contrast, the TFC-3 membrane followed a strong charge-based trend that overshadowed steric effects, as indicated by the strong relationship between permeability and charge (r of 0.91 and ρ of 0.97). Negatively charged compounds resulted in very low permeability coefficients ($0.3\text{-}0.6\cdot 10^{-8}$ m/s), whereas positively charged compounds, although significantly bulkier than the neutral compounds, permeated to a much greater extent ($114\text{-}179\cdot 10^{-8}$ m/s). These observations can be clearly seen in Figure 6.5 and agree with the TrOCs rejection study above. In other words, the strong electrostatic effects observed for TFC-3 are caused by the high negative membrane surface charge which generates an electrostatic repulsion towards anionic compounds and an opposite electrostatic attraction towards cationic compounds, previously reported as “charge concentration polarisation” (Verliefde et al., 2008). Neutral compounds, on the other hand, were not affected by these electrostatic interactions and their permeability was mainly governed by steric hindrance and hydrophobic affinity to the membrane. For example, acetaminophen’s small molecular size and low LogD value resulted in a higher permeability coefficient compared to other neutral and charged compounds. Again, this is in line with the previous study on the rejection of organic solutes by the TFC-2 membrane (Jang et al., 2018).

Table 6.2 TrOCs permeability coefficients for all the diffusion and FO experiments and for both novel TFC membranes.

TrOCs	Permeability Coefficients (B , 10^{-8} m/s)											
	TFC-2					TFC-3						
	Diffusion				FO	Diffusion				FO		
	DI	0.1 NaCl	0.5 NaCl	0.5 MgCl ₂	DI	0.1 NaCl	0.5 NaCl	0.5 MgCl ₂	DI	0.1 NaCl	0.5 NaCl	0.5 MgCl ₂
BEZ	1.4	5.1	0.3	1.4	14.1	0.6	13.0	1.9	2.7	0.1		
FUR	7.1	2.4	0.4	5.7	4.6	0.5	11.5	2.4	15.6	0.2		
IND	0.0	0.5	4.1	4.9	4.3	0.3	1.2	4.7	9.6	0.1		
SFX	1.6	0.8	1.1	11.1	3.6	16.4	15.6	6.7	23.8	9.7		
ACE	92.1	37.8	36.1	14.0	35.8	35.9	70.9	82.1	74.4	80.4		
CBZ	5.8	4.2	8.2	5.8	13.6	8.3	5.3	9.3	7.5	5.4		
TRI	5.9	8.6	3.3	17.6	14.6	169.0	26.7	5.8	21.6	125.0		
ATE	14.5	0.1	3.3	0.0	0.3	179.0	29.1	10.6	7.0	264.0		
NAD	8.2	9.2	2.2	15.0	0.3	114.0	20.1	5.9	2.9	58.0		

Table 6.3 Pearson and Spearman's rank correlations between solute physico-chemical properties and the permeability coefficients of the TrOCs for both TFC-2 and TFC-3 membranes. The feed and draw solution compositions are also shown. The physico-chemical properties include: MW (Molecular weight), MPSA (Minimal projected surface area), LogD (Hydrophobicity) and charge.

Membrane	FS and DS	Experiment	MW		MPSA		LogD		Charge	
			r	ρ	r	ρ	r	ρ	r	ρ
TFC-2	DI Water	B _{s,D}	-0.80	-0.53	-0.78	-0.17	0.01	-0.62	0.13	0.52
	0.1M NaCl	B _{s,D} 0.1Na	-0.72	-0.20	-0.82	-0.52	0.10	0.13	0.15	0.27
	0.5M NaCl	B _{s,D} 0.5Na	-0.82	-0.65	-0.83	-0.40	0.19	0.22	0.08	0.27
	0.5M MgCl ₂	B _{s,D} 0.5Mg	-0.37	-0.38	-0.25	-0.38	-0.09	-0.10	0.44	0.32
	0.1M NaCl*	B _{s,FO}	-0.65	-0.18	-0.70	-0.07	0.49	0.55	-	-
TFC-3	DI Water	B _{s,D}	-0.13	-0.48	0.30	0.08	-0.74	-0.60	0.91	0.97
	0.1M NaCl	B _{s,D} 0.1Na	-0.77	-0.48	-0.61	-0.07	-0.21	-0.53	0.36	0.78
	0.5M NaCl	B _{s,D} 0.5Na	-0.82	-0.92	-0.81	-0.37	0.09	-0.15	0.10	0.63
	0.5M MgCl ₂	B _{s,D} 0.5Mg	-0.78	-0.57	-0.64	0.15	0.16	0.02	0.01	-
	0.07M NaCl*	B _{s,FO}	-0.28	-0.62	0.17	0.15	-0.72	-0.63	0.68	0.88

r Pearson correlation coefficient

ρ Spearman's rank correlation coefficient

* Only in the draw solution

6.2.3.2 Diffusion tests at increasing ionic strength ($B_{s,D}^i$ $i = 0.1$ NaCl, 0.5 NaCl or 0.5 MgCl₂)

After the diffusion experiments with DI Water, the permeability coefficients of TrOCs were determined at increasing ionic strength (at concentrations of 0.1M NaCl, 0.5M NaCl and 0.5M MgCl₂ in both feed and draw solutions) to investigate solute-membrane interactions under these changed conditions. The results are summarised in Table 6.2 and the Pearson and Spearman's rank correlations in Table 6.3. For CTA membranes it has been reported that an increase in membrane ionic strength encourages the permeation of smaller TrOCs due to deswelling of the membrane; a reduction of the membrane pore hydration layer (Nghiem et al., 2006). However, the opposite was observed for the TFC-2 membrane when concentrations were increased to 0.5M NaCl. The permeability of the majority of TrOCs reduced (Figure 6.5), and according to the r and ρ coefficients, size became a stronger determinant for their transport. It has been previously shown that for composite membranes used in RO and NF

filtration processes, increasing the membrane ionic strength “shrinks” the membrane pores resulting in a lower permeability of organic compounds (Bellona et al., 2004; Braghetta et al., 1997). Hence, this lowering of the average pore sizes at increased ionic strength could partly explain the reduced permeability of some of the TrOCs through the TFC-2 membrane. With a concentration of 0.5M MgCl₂, the lower partitioning of Mg²⁺ ions into the membrane, due to a larger hydrated radius, was expected to have a weaker “shrinking” effect. Therefore, the TrOCs permeability coefficients when using 0.5M MgCl₂ were expected to lie between those obtained from the diffusion tests without DS and with 0.5M NaCl DS. Whereas this was the case for negatively charged compounds, the permeability of positively charged TrOCs and sulfamethoxazole did not follow these trends.

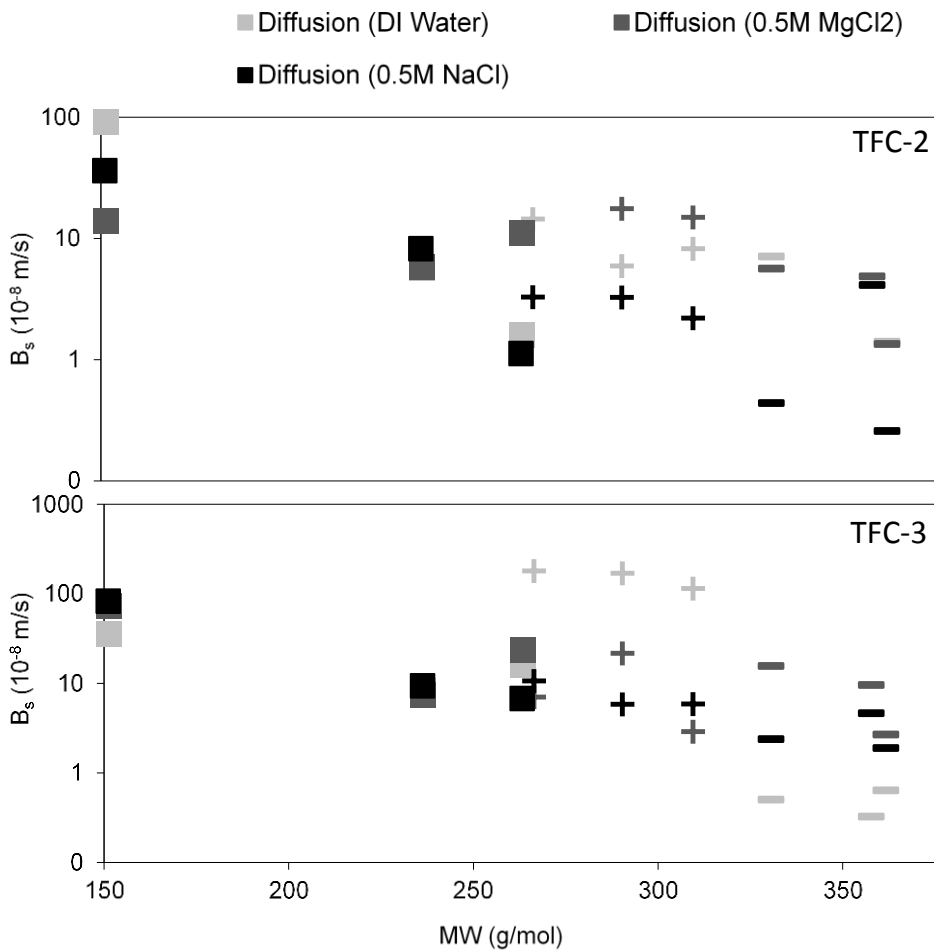


Figure 6.5 Permeability of TrOCs through TFC-2 and TFC-3 as a function of molecular weight for the diffusion tests without salt and with 0.5M NaCl and 0.5M MgCl₂ ionic strength. Positive, negative and neutral compounds are marked with a positive sign, negative sign and a square, respectively.

As described in the previous section, the diffusion of TrOCs through the TFC-3 membrane was strongly influenced by electrostatic interactions with the membrane surface. The importance of these electrostatic interactions on the transport of TrOCs through TFC-3 seemed to diminish at increasing membrane ionic strength. As shown in Figure 6.5, permeability of negatively charged compounds increased, whereas the permeability of positive compounds decreased. It has been found that partitioning of salts into composite membranes “shields” and thus reduces the effective membrane surface charge significantly (Nghiem et al., 2006). Hence, it explains the reduced electrostatic repulsion of negatively charged compounds and reduced electrostatic attraction of positive compounds when increasing ionic strength. In addition, the Pearson’s coefficients demonstrated a stronger correlation between solute size and permeability, suggesting that steric hindrance becomes the more dominant transport limiting mechanism (Table 6.3). Compared to 0.5M NaCl ionic strength, using 0.5M MgCl₂ led to an even greater permeability of negatively charged TrOCs and a lower permeability of positively charged TrOCs (except trimethoprim). It is known that the double charge of Mg²⁺ ions “shields” the membrane negative surface charge to a greater extent (Childress and Elimelech, 1996), resulting in a further weakening of electrostatic interactions between the membrane and the charged solutes. Neutral compounds, on the other hand, had similar permeability coefficients to when 0.5M NaCl was used because the membrane surface charge does not affect their transport.

6.2.3.3 Permeability tests with FO conditions ($B_{s,FO}$)

The final set of experiments consisted in determining the permeability coefficients of the selected TrOCs in the presence of a water flux and a reverse salt flux. Using a draw solution of 0.1M and 0.07M NaCl for TFC-2 and TFC-3, respectively, enabled to generate a similar water flux across both membranes. The results from these experiments were used to draw conclusions on the effect of both water and reverse salt flux on the permeability of TrOCs.

In comparison to the diffusion test with 0.1M NaCl, the permeability of most TrOCs through TFC-2 increased during FO operation (Table 6.2), and according to the correlations in Table 6.3, the importance of solute size on transport reduced. Despite using high cross-flow velocities (7.6 cm/s) to avoid external solute concentration polarisation, the indiscriminate increase in permeability of most compounds observed for TFC-3 could be attributed to this convective transport induced by the water flux (Figure 6.6). The presence of significant solute concentration polarisation means that the effect of RSF on solute transport could not be isolated. Considering that RSF for TFC-2 at a draw solution concentration of 0.1M was only 29 mmol/ m²h, complementary experiments at higher cross-flow velocities and higher RSF would

clarify the effect of RSF on forward TrOCs diffusion. Hindered forward transport of solutes by RSF would be marked by a reduction in permeability of all TrOCs, particularly neutral compounds, whereas, Donnan dialysis would be confirmed by an increase in permeability of anionic solutes due to a favourable exchange with chloride anions and an opposite effect for cationic compounds.

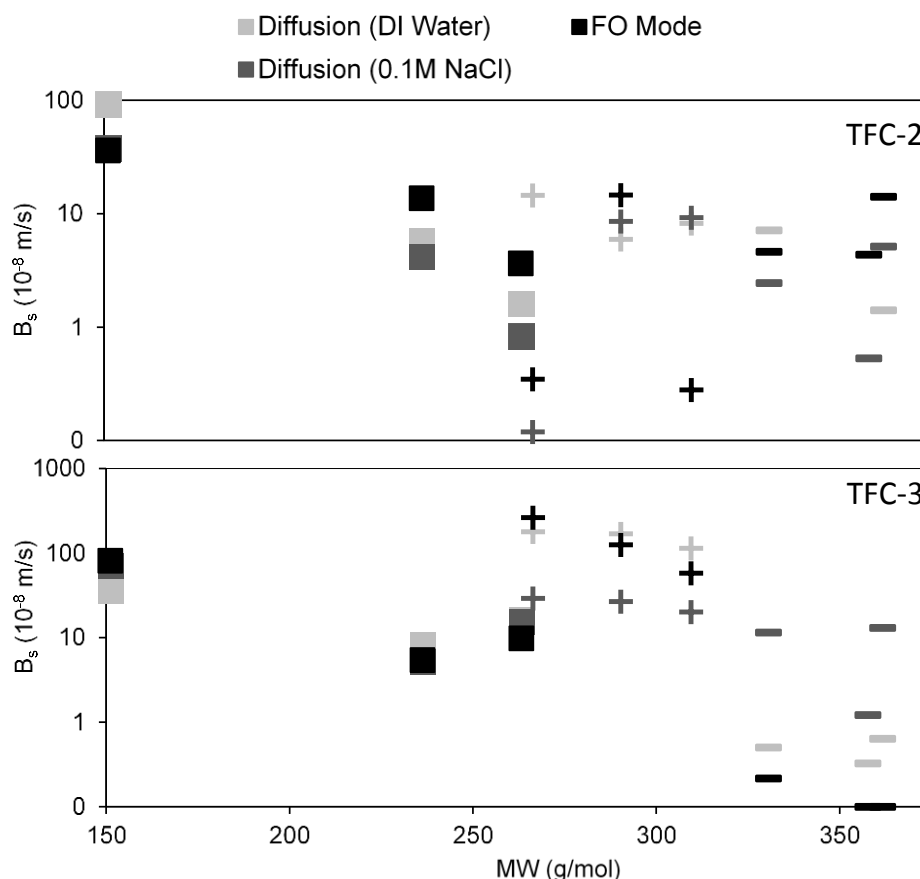


Figure 6.6 Permeability coefficients of TrOCs through TFC-2 and TFC-3 as a function of molecular weight obtained for the diffusion tests without salt, at 0.1M NaCl ionic strength the FO tests. Positive, negative and neutral compounds are marked with a positive sign, negative sign and a square, respectively.

Unlike with the TFC-2 membrane, the permeability of TrOCs during the FO experiments with TFC-3 (average J_w of $12 \text{ L m}^{-2} \text{ h}^{-1}$ and a RSF of $50 \text{ mmol m}^{-2} \text{ h}^{-1}$) were not affected by the convective transport of the water flux. As can be seen in Figure 6.6, the permeability coefficients of neutral compounds were similar to those obtained during the diffusion test with 0.1M NaCl whilst the permeability of positively charged TrOCs increased and the permeability of negatively charged TrOCs decreased. It is clear that electrostatic interactions between the negatively charged membrane and the charged solutes were predominant again in the FO experiments, an observation that is further supported by the Pearson and Spearman's rank

correlations (Table 6.3). Considering that during the FO experiment the maximum NaCl concentration that established in the feed side due to RSF was approximately 0.005M NaCl, the “shielding” effect of the draw solute on the membrane surface charge was likely to be much weaker than in the diffusion experiments. This suggests that RSF could have an impact on the permeability of TrOCs by “shielding” the TFC-3 membrane surface charge only when a high concentration of draw solution is employed (for example >0.5M). All of these mechanisms are illustrated in Figure 6.7.

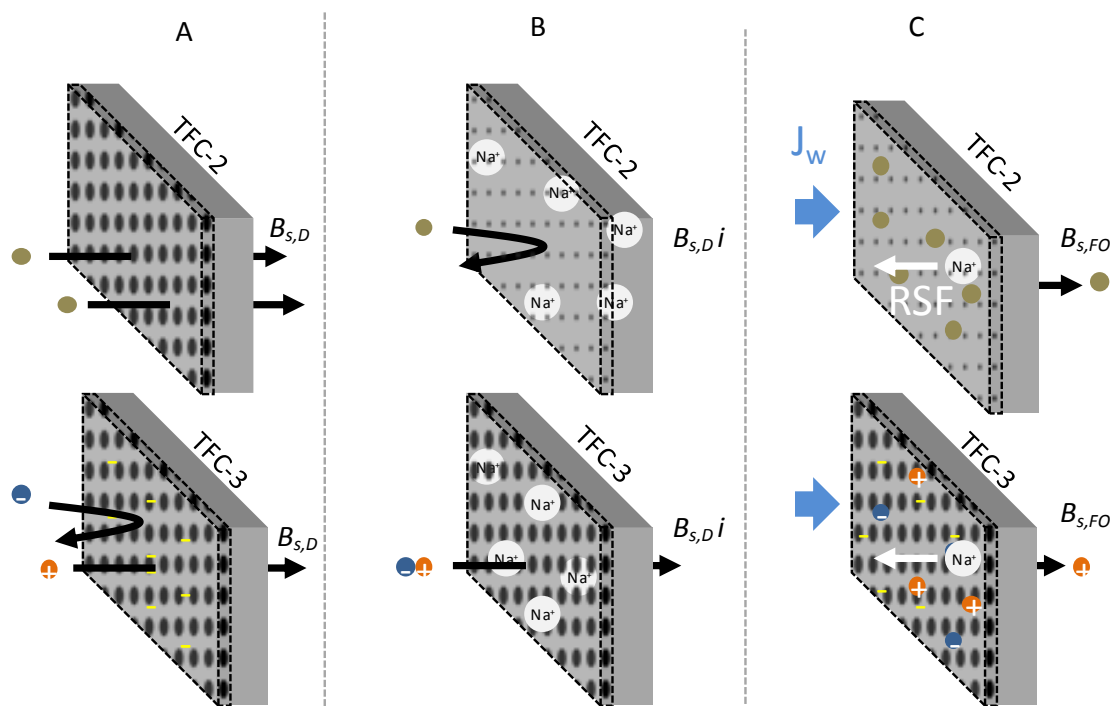


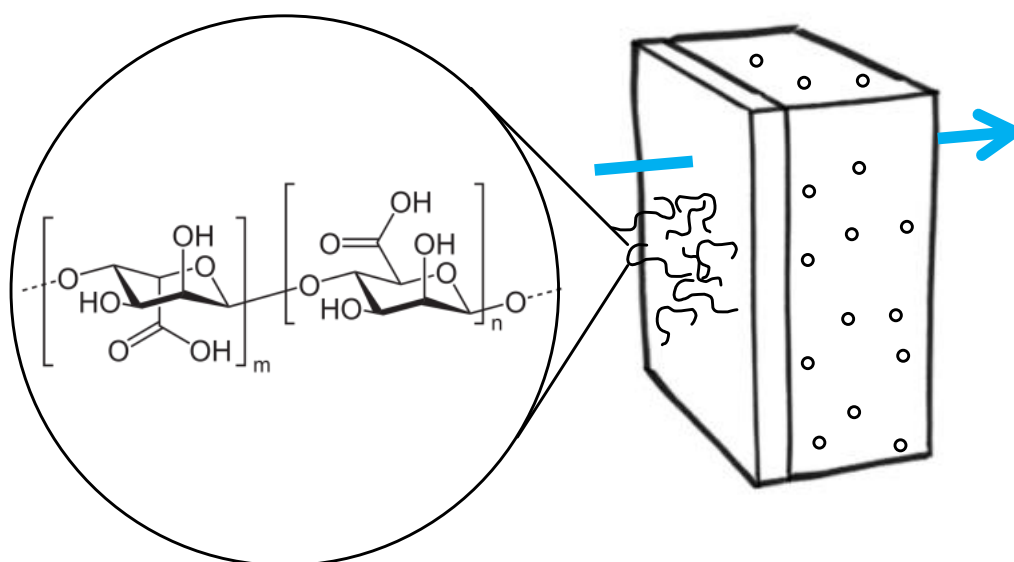
Figure 6.7 Graphical summary of the solute-membrane interactions for TFC-2 and TFC-3 in the different scenarios tested in this study. A) Diffusion tests with DI water: sterics dominated TrOCs transport through TFC-2 whereas electrostatic attraction/repulsion interactions were strongly present in TFC-3. B) At higher membrane ionic strength, a reduction of membrane pore sizes and shielding of membrane surface charges were observed for TFC-2 and TFC-3, respectively. C) In the FO experiments, convective transport of solutes towards the membrane facilitated the permeability of TrOCs whereas reverse salt flux had little impact on their transport.

To summarise, long-term operation experiments proved that only few of the selected TrOCs could not be tested due to their poor analysis, degradability and/or adsorption to the system set-up. The ability of both TFC-2 and TFC-3 membranes to reject organic compounds was generally very high, although the strong negative surface charge and the larger active layer free volume of TFC-3 resulted in significantly lower rejections of small neutral compounds, as well as positively charged compounds. The proposed mechanism for the hindered transport of TrOCs through TFC-2 is steric hindrance and an increase in membrane ionic strength was found

to have a pore shrinking effect therefore enhancing the steric mechanism. On the other hand, electrostatic interactions prevailed between TFC-3 and the charged solutes, but upon higher membrane ionic strengths these interactions were masked. Finally, reverse salt flux did not seem to have a significant and direct impact on solute transport as it may only become important at very high draw salt concentrations.

7 Fouling propensity of novel TFC membranes with different driving forces

In this chapter, the fouling propensity of the two novel TFC membranes was investigated under different driving forces and draw solutions to improve the current understanding of FO fouling mechanisms and their role during the fouling process. The driving forces tested were a constant osmotic pressure difference using two different draw solutions to represent FO mode, and an applied hydraulic pressure in the feed to replicate PAO conditions. Modelling the water flux decline and the effects of CP allowed for an estimation of the CP moduli, the effective driving forces and the foulant cake layer structure. This was related to the final deposited foulant mass to draw conclusions on the different fouling behaviours observed in the various scenarios.



This chapter will be published as:

Marc Sauchelli, Arnout D'Haese, Ignasi Rodriguez-Roda, Wolfgang Gernjak. Alginate fouling of novel TFC membranes and the impact of different driving forces. *In preparation*

7.1 Experimental Design and Evaluation

7.1.1 Effect of constant osmotic pressure on fouling

One of the possible reasons for the different fouling behaviours observed between osmotically-driven and pressure-driven processes, identified by Siddiqui et al. (2018), was that most bench-scale FO fouling experiments have been carried out with a non-constant osmotic pressure difference. In other words, the DS concentration during FO experiments was not maintained constant leading to a gradual dilution of the DS and concentration of the FS. To account for these changes, the experimental fouling flux was corrected with a baseline flux under non-fouling conditions. However, this method failed to include the effects of concentration polarisation. In more recent studies, the DS concentration has been kept constant to reproduce the conditions of large-scale applications, and significant differences in FO fouling propensity have been reported (Siddiqui et al., 2018; Zheng et al., 2018). Therefore, to explore the mechanistic differences between a non-constant and constant osmotic pressure driving force on membrane fouling, a series of FO fouling experiments were performed with the TFC-2 and TFC-3 membranes with non-constant and constant DS concentrations. Baseline tests were also performed a priori to compare the water flux decline between non-fouling and fouling experiments (as illustrated in Figure 7.1). The study of a single model foulant such as alginate is advantageous because the foulant-membrane interactions can be more easily understood. In addition, the study focuses on alginate due to its extensive use in literature and its similarity to extracellular polymeric substances (EPS) which constitute a large part of bio-fouling.

7.1.2 Effect of feed hydraulic pressure on fouling

Most of the previous studies, aimed at determining the effect of hydraulic pressure on fouling, have compared the fouling behaviour between FO and RO processes (Kwan et al., 2015; Lay et al., 2010; Lee et al., 2010; Mi and Elimelech, 2013, 2010; Siddiqui et al., 2018; Tow and Lienhard, 2016). However, in RO mode a high hydraulic pressure is used to drive the water flux which has also been found to impact membrane integrity (Coday et al., 2013). As an alternative, some studies have compared FO fouling to PAO mode, which synergises an osmotic pressure with an applied hydraulic pressure on the feed side to enhance the permeation flux (Blandin et al., 2015; Y. Kim et al., 2014; Lee et al., 2017; Xie et al., 2015). In PAO mode, the applied hydraulic pressure that is employed is usually relatively low, thus allowing for a fairer analysis of the impact of hydraulic pressure on fouling. In this part, a series of FO and PAO experiments were performed with and without an applied hydraulic pressure of

1 bar in the feed solution. To allow for fair comparison, experimental conditions were chosen to obtain similar initial water fluxes. Then, from the water flux decline, the cake structural parameter was modelled and compared to the amount of foulant that accumulated with both driving forces. All the complex concentration polarization effects and fouling mechanisms were considered; including external concentration polarization (ECP), cake-enhanced concentration polarisation (CECP), internal concentration polarization (ICP), the ICP self-compensation effect, and hydraulic resistance. In addition, the amount of fouling was also related to the structure and physicochemical properties of the active layer, as well as the rate of reverse solute flux (RSF). When considering all these mechanisms, a conclusion on the different fouling propensity of FO and PAO processes was made.

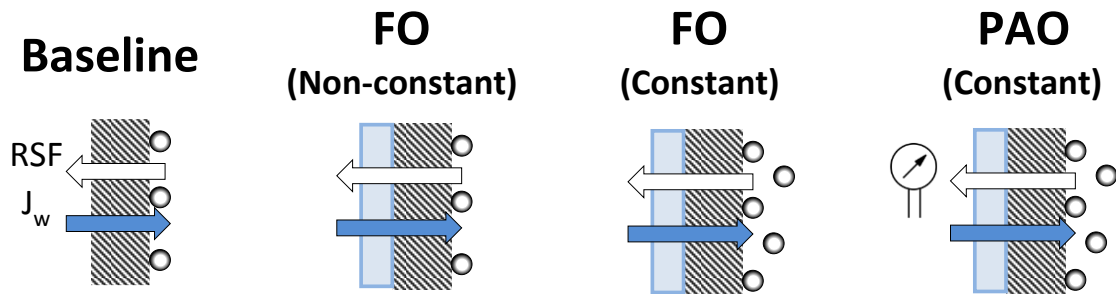


Figure 7.1 Schematic illustrations of the different fouling experiments. From left to right: baseline test without added alginate, fouling with a non-constant osmotic pressure difference, fouling with a constant osmotic pressure difference and PAO mode with a constant osmotic pressure and an applied hydraulic pressure in the feed.

7.2 Modelling cake structural parameter

The water flux decline is not only dependent on fouling but also on the effective driving force, and therefore it is not an appropriate metric for determining the fouling accumulation. Another way to measure fouling is using the osmotic-resistance filtration model which estimates fouling accumulation based on the additional hydraulic resistance imposed by the foulant deposition (She et al., 2015). However, this approach does not reveal any aspect of the cake layer structure. On the other hand, quantifying fouling by calculating the cake structural parameter has been proposed as an alternative and has been recommended by Tow and Lienhard (2016). This method takes all fouling mechanisms into account, and can be used with a range of membranes, processes and feed compositions. Since alginate gels are highly hydrated it is assumed that the porosity is very high and that tortuosity of the gels is close to unity (Karabelas and Sioutopoulos, 2015). As a result, the structural parameter is representative of the cake thickness, and the evolution of S_c can give an approximate

indication of foulant accumulation. Hence, the cake structural parameter (S_c) was calculated for each experiment at different time intervals using Nagy's extended transport model (Nagy et al., 2018; Tow and Lienhard, 2016).

The calculation of the cake structural parameter consists in fitting already determined parameters and experimentally obtained parameters at different stages of the experiment to the mass-transport equations, and then estimating the resulting S_c value at each stage from an iteration algorithm. The membrane performance parameters (A, B, S_s), obtained experimentally in chapter 5, and the mass transfer coefficients for both feed and draw sides (k_f and k_d) were used as inputs. The average alginate pore hydraulic diameter ($D_{h,c}$) is another parameter that describes the structure of the alginate foulant cake and determines the hydraulic resistance to water flux. Previous characterisations of the pore size have led to a range of values depending on the measurement technique, the variation in molecular weight of the alginate cross-linked polymer and the complexation with Ca^{2+} ions. However, the usual range of pore hydraulic diameters has been found to be between 5 and 20 nm depending on the sodium to calcium ratio of the feed solution (Simpliciano et al., 2013). This range of pore sizes was derived from a linear interpolation of pore diameters estimated from experimental measurements at different NaCl concentrations for alginate cakes formed in feed solutions containing 1mM CaCl_2 (Tow and Lienhard, 2016). For the feed solutions used in this study which have a maximum $\text{Na}^+:\text{Ca}^{2+}$ ratio of 15, the equivalent pore diameter from the calculated range corresponds to approximately 5nm, therefore this value is assumed constant and used in the model herein.

At the end of each experiment a number of parameters are obtained, these include the bulk draw solution concentrations ($C_{d,i}^{EXP}$), the bulk feed solution concentrations ($C_{f,i}^{EXP}$), water fluxes ($J_{w,i}^{EXP}$) and reverse salt fluxes ($J_{s,i}^{EXP}$) at different time intervals. From these, the concentrations at the membrane and cake layer interfaces ($C_{fc,i}^{CALC}$, $C_{sd,i}^{CALC}$, $C_{as,i}^{CALC}$) are calculated using equations (2.6),(2.7) and (2.12). Similar to the CM2 model, a concentration-dependent draw solute diffusivity was used in calculating the concentration at the active-support layer interface (D_s). The cake structural parameters were then assumed for each time interval which in turn allowed for the calculation of the draw solute diffusivity values in the cake layer (D_c) and the concentrations at the cake layer- active layer interface ($C_{ca,i}^{CALC}$). Calculated water ($J_{w,i}^{CALC}$) and reverse salt fluxes ($J_{s,i}^{CALC}$) were derived from equations (2.18 and (2.19, using van't Hoff law to calculate the osmotic pressures. Consequently, the cake structural parameters were optimised by minimising in an iterative process the sum of squares

of the offsets between the experimental and calculated water and salt fluxes (equation (7.1)). The sequence of steps used in modelling the cake structural parameter is shown in Figure 7.2.

$$error = \sum_{i=1}^n (J_{w,i}^{EXP} - J_{w,i}^{CALC})^2 + \sum_{i=1}^n (J_{s,i}^{EXP} - J_{s,i}^{CALC})^2 \quad (7.1)$$

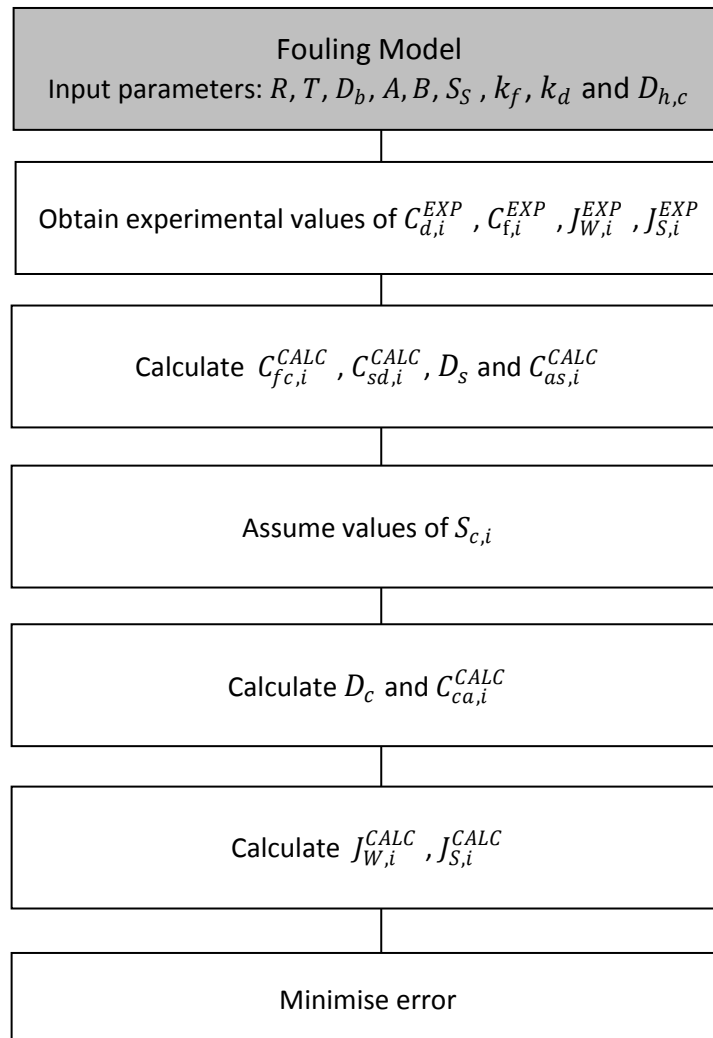


Figure 7.2 Flowchart of the optimisation procedure for the modelling of the cake structural parameter.

7.3 Results and Discussion

7.3.1 Effect of constant osmotic pressure as driving force

The water flux profiles of the fouling experiments with non-constant and constant draw solution concentration are illustrated in Figure 7.3 for the two novel TFC membranes. In the same figure, the water fluxes of baseline tests without added alginate foulant are also shown for comparison. The water flux decline was measured as a percentage function of the

normalized flux ($1 - J_{w,f}/J_{w,0}$). In addition to the cake structural parameter, weighing the alginate layer that formed on the surface of the membrane (once fully dried) provided another indication of the degree of fouling. The values of water flux decline (%), alginate surface density (g/m^2) and cake structural parameter (μm) are all summarised in Table 7.1 for both TFC membranes and for non-constant and constant DS concentrations.

One of the first things that can be noticed from Figure 7.3 is that for TFC-2, the baseline and fouling tests with non-constant DS concentration had almost identical water flux profiles. This indicates that very little fouling accumulated, and from the low alginate mass density that was measured at the end of the experiment ($7.2 \text{ g}/\text{m}^2$), this seemed to be the case. In contrast, for TFC-3, fouling at non-constant DS concentration did lead to a greater water flux decline than the baseline test, as expected. The low fouling observed for TFC-2 could be due to the smoother and more hydrophilic surface of the TFC-2 membrane which discourages fouling on the active layer (see the physico-chemical properties of TFC-2 in Table 4.1). Polyamide TFC membranes with a lower surface roughness and more hydrophilic character have indeed been reported to be less prone to fouling (Gu et al., 2013; Mazlan et al., 2016).

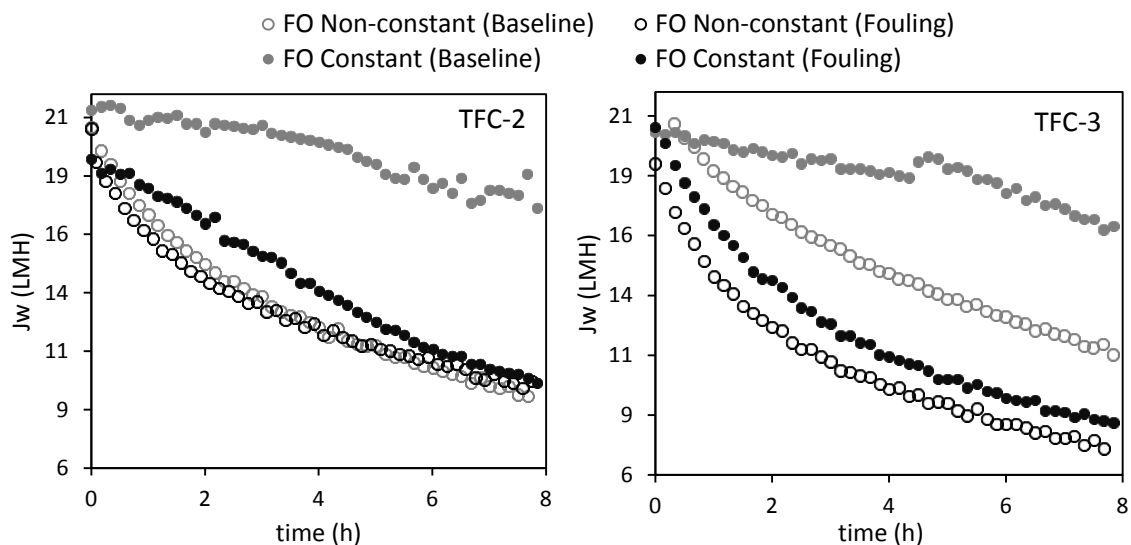


Figure 7.3 Water flux profiles for the baseline and fouling tests, with non-constant and constant DS concentrations and for TFC-2 and TFC-3.

By maintaining the DS concentration constant, the osmotic pressure difference across the membrane was expected to be constant as well. This was confirmed by the relatively stable water fluxes obtained for the baseline tests with constant DS concentration (Figure 7.3). A slight decline in water flux was observed for these baseline tests, 20% for TFC-2 and 22% for TFC-3, and this was attributed to CaCl_2 concentrating in the feed solution and RSF increasing

the NaCl concentration in the feed solution over time. Both leading to a higher feed ECP effect and a loss of osmotic pressure difference across the membrane. Fouling experiments with constant DS concentration showed the expected water flux decline rates, indicating that fouling accumulation was occurring. In addition, the water fluxes decreased exponentially, almost reaching the critical fluxes of the respective membranes. This is the flux at which no more fouling accumulation occurs as fouling removal by cross-flow shear forces equals fouling deposition (Nguyen et al., 2018). For TFC-3, this critical flux was reported to be $\pm 8 \text{ L m}^{-2} \text{ h}^{-1}$ when a combination of alginate and gypsum (Ca^{2+}) are used as synthetic foulants.

Table 7.1 Results of the water flux decline, final alginate surface density and the final calculated cake structural parameter for both TFC membranes and for experiments with non-constant and constant DS concentrations

Membrane	Experiment	Water flux decline (%)	Alginate surface density (g/m^2)	Sc (μm)
TFC-2	FO Non-constant (Baseline)	57	-	-
	FO Non-constant (Fouling)	52 ± 6	7.2 ± 0.6	25
	FO Constant (Baseline)	20	-	-
	FO Constant (Fouling)	48 ± 11	24.7 ± 6.1	847
TFC-3	FO Non-constant (Baseline)	47	-	-
	FO Non-constant (Fouling)	63 ± 5	13.7 ± 2.4	117
	FO Constant (Baseline)	22	-	-
	FO Constant (Fouling)	61 ± 2	21.7 ± 1.1	339

When comparing the fouling experiments with non-constant and constant DS concentration, an interesting observation was made. Although the driving force was different in both cases, the water flux decline between the two fouling experiments was similar. For TFC-2, a water flux decline of 52% and 48% were observed for experiments without and with constant DS concentration, respectively. The corresponding percentages for TFC-3 were even more comparable, 63% and 61%. However, despite the similar water fluxes, fouling experiments at constant DS concentration resulted in a greater cake structural parameter and a heavier alginate layer, indicating more fouling accumulation. Particularly in the case of TFC-2, a constant driving force seemed to really exacerbate fouling, with almost a four-fold increase in alginate mass density from 7.2 to 24.7 g/m^2 . These findings demonstrate first of all that water flux alone is not an appropriate indicator of fouling propensity. As correctly stated by Siddiqui et al. (2018), temporal changes in flux do not reflect the fouling deposition. Secondly, these findings expose the complex nature of FO fouling compared to other membrane filtration processes. In pressure-driven processes the extent of fouling is proportional to the amount of

permeated water, which convectively transports foulants towards the membrane surface (Tang et al., 2011). However, in FO this does not seem to be the case. The complex interplay of CP effects, RSF and effective osmotic pressure difference seems to generate different fouling propensity at similar water fluxes with different osmotic driving forces.

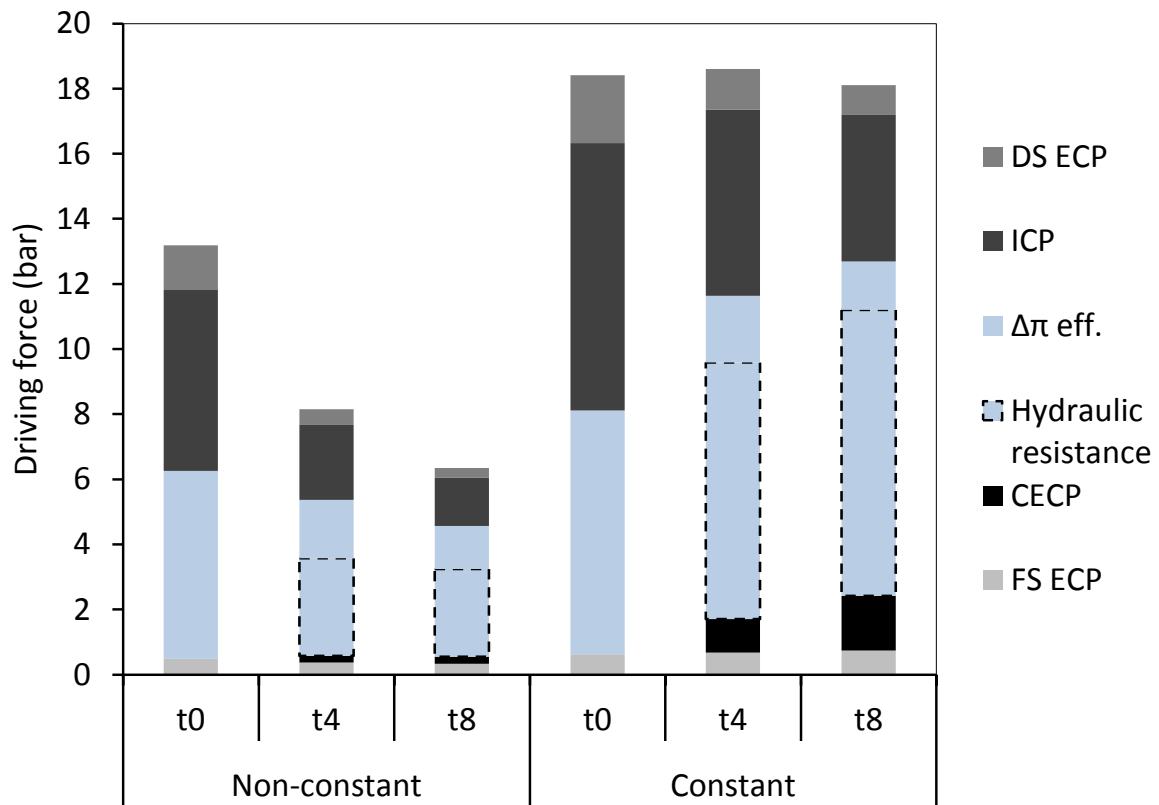


Figure 7.4 Contribution of the different concentration polarisation effects and hydraulic resistance on the overall driving force. The components were calculated for the TFC-3 membrane at three different stages of the experiment, at the beginning, after 4 hours and at the end after 8 hours. The experiments compared are FO fouling with non-constant and constant DS concentrations.

Another way to visualize the processes involved in FO fouling is by modelling the different concentration polarisation effects in each of the transport layers and comparing their impact on the driving force. The magnitude of each CP component was derived from the model and correspond to the osmotic pressure drops in each of the transport layers. In Figure 7.4 the CP components are shown for TFC-3 at three different stages of the experiment, with and without constant DS concentration. For non-constant and constant DS concentration experiments, the effects of both FS and DS ECP on the overall driving force were minimal. On the other hand, the influence of ICP was more pronounced, particularly for experiments with constant DS concentration due to a constantly higher bulk osmotic pressure difference. However, as the experiment progressed, the effect of ICP was offset by the water flux decline, and as the cake

layer evolved, CECP increased only marginally due to the low salt content of the FS. Lastly, hydraulic resistance has an indirect impact on the driving force and is therefore shown in Figure 7.4 in a distinct format. The resultant water flux is a function of the effective osmotic pressure difference ($\Delta\pi_{eff}$) and the hydraulic resistance. Thus, considering that the CP effects had a minor impact on the effective osmotic driving force, it can be concluded that hydraulic resistance was the dominant mechanism in reducing the resultant water flux.

A comparison between the non-constant and constant fouling experiments in terms of the calculated effective driving forces and final foulant mass yields the following hypotheses. a) At constant DS concentration, a higher effective osmotic pressure difference across the active layer ($\Delta\pi_{eff}$) is sustained throughout the experiment. Since alginate gels are mainly composed of water (96% to 99%), outflow of water from the alginate gel in close proximity the membrane active layer might lead to filling-up of the loose network of pores with more alginate molecules. This is analogous to a denser and heterogeneous cake layer, as reported by Tow and Lienhard V (2017) in a similar study. The denser cake layer generates a greater hydraulic resistance agreeing with the results obtained herein. b) Another explanation could be a higher RSF at constant DS concentration. Since a higher effective concentration difference is sustained across the active layer, the greater reverse diffusion of NaCl might enhance the deposition of foulant. The reverse salt fluxes for the non-constant and constant DS concentration experiments for TFC-3 were 111 and 203 $\text{mmol m}^{-2} \text{h}^{-1}$, respectively. Such a large difference could have a significant impact on fouling propensity. This is further explored in section 7.3.3.

7.3.2 Effect of hydraulic pressure as driving force

The water flux profiles of the FO fouling experiments at constant DS concentration and that of PAO fouling experiments at 1 bar of applied feed hydraulic pressure are shown in Figure 7.5. Baseline tests without any added alginate are also included in the figure. In addition, the calculated cake structural parameter and obtained final alginate surface density for these experiments are summarised in Table 7.2. In PAO mode, the draw solution concentration was adjusted so that, together with the 1 bar of hydraulic pressure, an initial water flux of approximately $20 \text{ L m}^{-2} \text{h}^{-1}$ was established, allowing for a direct comparison with the results from the FO tests. A non-negligible water flux decline was observed for FO and PAO baseline tests due to the concentration of CaCl_2 and NaCl (from reverse salt flux) in the feed solution. However, the water flux decline was different between the two modes. For the TFC-2, the

water flux decline was 20% and 26% for FO and PAO mode, respectively. And for TFC-3, the corresponding values were 22% and 12%. This is because the baseline tests in FO mode began at a slightly higher initial water flux as seen in Figure 7.5. Despite this inconsistency, the water flux declines followed the same trend.

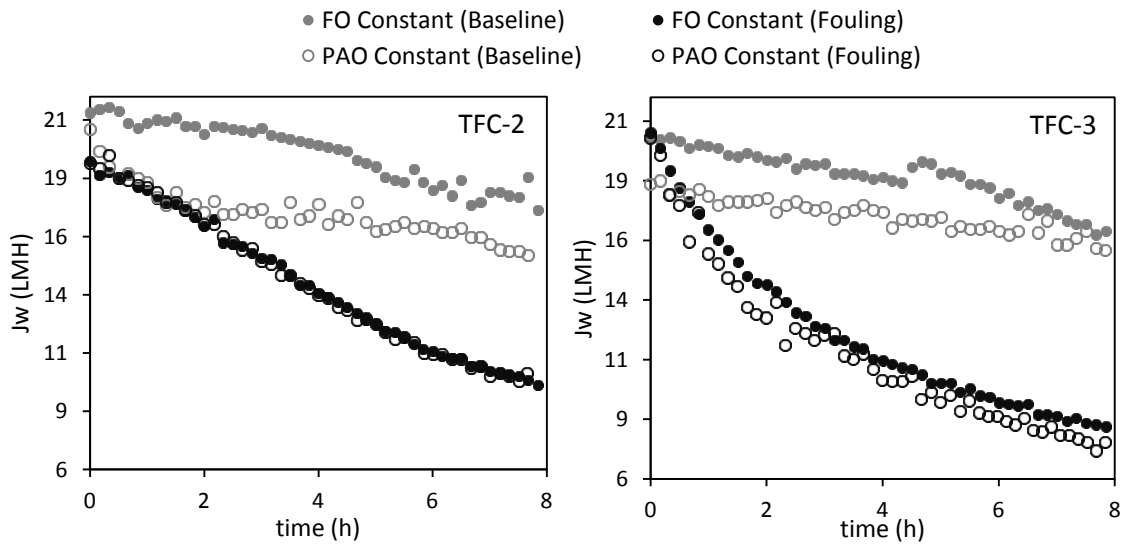


Figure 7.5 Water flux profiles for the baseline and fouling tests, with constant DS concentrations, in FO and PAO experiments and for TFC-2 and TFC-3.

From Figure 7.5, a similar observation to the previous section was made. Although the driving force was different between FO and PAO tests, the water flux decline was very similar. For TFC-2, a water flux decline of 48% and 50% was obtained for FO and PAO modes, respectively. And for TFC-3, the corresponding values were 61% and 63%. The difference with the previous section is that, in this case, the surface density of the final alginate layer formed on the membrane did not agree with the calculated cake structural parameter. From the alginate surface density it seemed that more foulant had deposited in PAO mode, especially for TFC-2 in which 29 g/m² had deposited compared to 24.7 g/m² in FO mode. In contrast, the calculated cake structural parameter suggested the contrary. The S_c values were 200 μm and 80 μm lower in PAO mode compared to FO mode for TFC-2 and TFC-3, respectively, indicating a thinner fouling layer accumulated in PAO mode. Similar observations were reported by Blandin et al. (2015); in PAO operation a much more uniform thin, and dense (i.e. potentially compacted) foulant cake layer formed.

In order to interpret these results, a few explanations were proposed. The first relates to the possible compaction of alginate gel under applied hydraulic pressure and the inaccuracy of the current model used in quantifying the compacted cake structural parameter. Many previous studies have associated a denser and more compacted fouling cake layer to the application of

hydraulic pressure. However, the compaction process is not fully understood, in part because alginate gels are thought to be almost incompressible and mainly because compaction has often been reported to be flux-induced by the hydrodynamic drag force. Although alginate polymers are themselves incompressible, it has been found that water can be forced out of its gel matrix (Tow and Lienhard V, 2017). Furthermore, compaction of the cake with an applied hydraulic pressure has been reported to be induced not only by permeate drag force but also by the transmembrane pressure which compresses foulants hydrostatically (Xie et al., 2015). Both these mechanisms may work simultaneously leading to an irreversible compaction of the alginate gel. According to Tow and Lienhard (2016), compaction of the alginate gel should result in a decrease in cake structural parameter. Since PAO mode shows a decreased cake structural parameter and a greater surface density of alginate, irreversible compaction of the fouling layer could well explain the observations.

Table 7.2 Water flux decline, final alginate surface density and the final calculated cake structural parameter for both TFC membranes and for FO mode and PAO mode experiments

Membrane	Experiment	Water flux decline (%)	Alginate surface density (g/m ²)	Sc (μm)
TFC-2	FO Constant (Baseline)	20	-	-
	FO Constant (Fouling)	48 ± 11	24.7 ± 6.1	847
	PAO Constant (Baseline)	26	-	-
	PAO Constant (Fouling)	50 ± 2	29.2 ± 5.9	623
TFC-3	FO Constant (Baseline)	22	-	-
	FO Constant (Fouling)	61 ± 2	21.7 ± 1.1	339
	PAO Constant (Baseline)	12	-	-
	PAO Constant (Fouling)	63 ± 0	22.0 ± 0.7	256

One of the assumptions used in the model for calculating S_c is that the average hydraulic diameter of the alginate pores remains constant (Nagy et al., 2018). However, compaction of the alginate layer by water flowing out from its pores is analogous to a reduced pore size which causes an overall increase in hydraulic resistance (Tow and Lienhard V, 2017). Compaction has also been found to reduce cake thickness and the cake structural parameter, with no changes in porosity and tortuosity. Direct measurement of alginate gel pore sizes in-situ is difficult, but in order to accurately calculate the cake structural parameter, it should be included in the model (Karabelas and Sioutopoulos, 2015). In order to determine the effect of lower pore sizes on the calculated cake structural parameter, a decreasing pore hydraulic diameter from 5 to 3 nm was introduced in the model and the S_c values re-calculated. The

results are illustrated in Figure 7.6 which shows the evolution of the cake structural parameter for a constant and a decreasing alginate gel pore size. The results revealed that the cake structural parameter is highly sensitive to small changes in D_h , especially if D_h is low and the water flux decline is largely due to hydraulic resistance. More importantly, a significantly lower cake structural parameter was calculated at decreasing pore sizes, resulting in a lower CECP effect. Hence, a model that includes the changing pore sizes of the alginate gel due to compaction would result in lower and more accurate S_c values, analogous to a thinner and denser alginate gel layer.

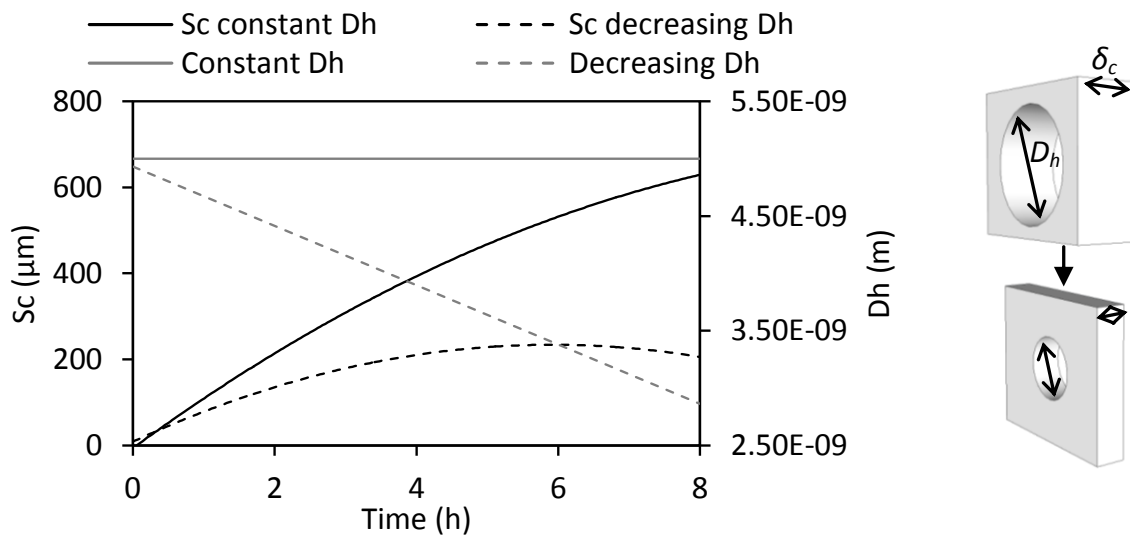


Figure 7.6 Modelled cake structural parameter and pore hydraulic diameter as a function of time for a case in which the pore size remains constant (as assumed in the model) and for a decreasing pore size that is expected during compaction of the alginate gel. This plot was generated using the model. On the right, an illustration of how the pore size (D_h) and the alginate layer thickness (δ_c) would decrease if compaction occurred.

A second possible explanation for the low cake structural parameter emerged from analysing the CP components of the driving force and questioning whether the response of FO membranes to hydraulic pressure is equivalent to osmotic pressure. The proportional contribution of the CP effects, hydraulic resistance and hydraulic pressure on the driving force is shown in Figure 7.7. In PAO mode, the lower bulk osmotic pressure difference resulted in a lower ICP effect as expected. However, if more fouling did accumulate or if compaction did occur, a greater hydraulic resistance component would be observed. As can be seen from the PAO mode bar charts, the 1 bar of applied hydraulic pressure seems to have a minor contribution to the overall driving force. Kook et al. (2018) reported that FO membranes have a greater response to hydraulic pressure as it facilitates water transport through defects and membrane deformation. Therefore, it is likely that the contribution to the driving force from 1 bar of hydraulic pressure is not equivalent to 1 bar of osmotic pressure, but rather much

higher. Consequently, in modelling the cake structural parameter, the exact contribution of hydraulic pressure to the overall driving force needs to be included. To illustrate this idea, the modelled CP components for a scenario in which 5 bars of *real* hydraulic pressure are applied, are shown in Figure 7.7. An increasing contribution of hydraulic pressure on the driving force results in an increase in the cake structural parameter and a more pronounced hydraulic resistance, analogous to a thicker or denser cake layer.

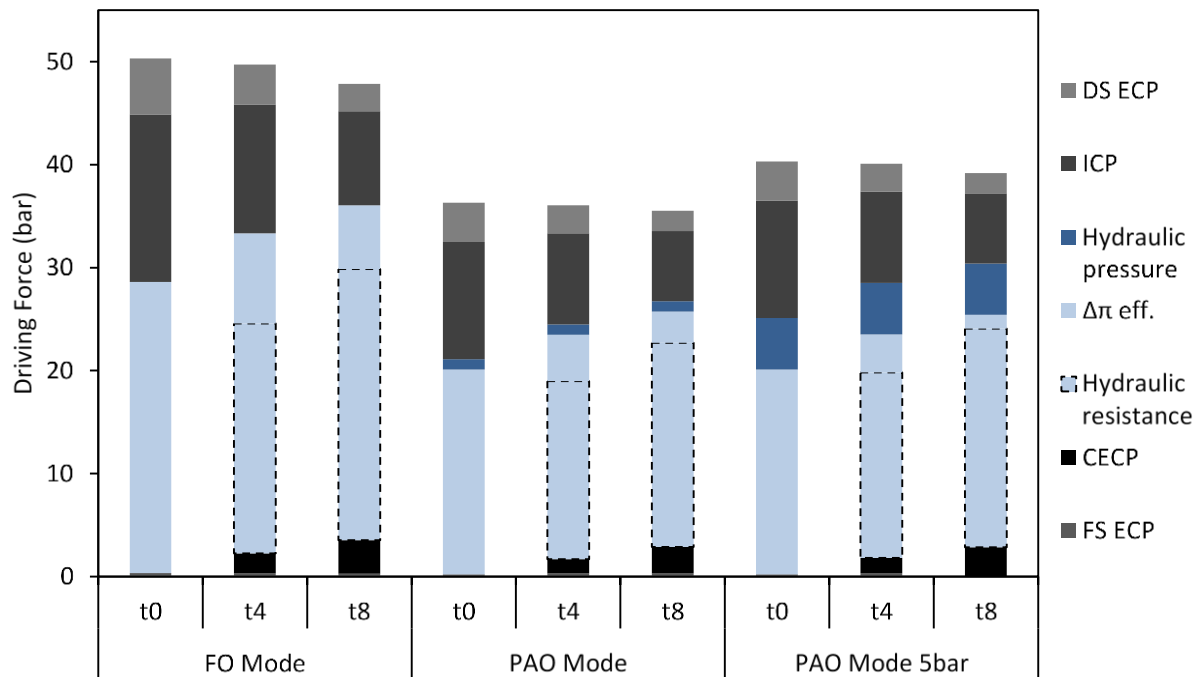


Figure 7.7 Contribution of the different concentration polarisation effects, hydraulic resistance and hydraulic pressure on the overall driving force. Again, these components were calculated for the TFC-3 membrane at three different stages of the experiment, at the beginning, after 4 hours and at the end after 8 hours. The experiments compared are FO mode with constant DS concentration, PAO mode with 1 bar of hydraulic pressure and PAO mode if the real hydraulic pressure is 5 bar.

Furthermore, in modelling the cake structural parameter, the same water and solute permeability coefficients and support layer structural parameter (A, B, S_s) were used in both FO and PAO mode. Although the intrinsic membrane performance parameters obtained in the FO-only membrane characterisation chapter are accurate in FO mode, it is possible that they do not represent accurately the FO membranes under 1 bar of applied hydraulic pressure. As a result, membrane performance parameters obtained under the specific conditions used in this section might have provided a better basis to modelling the fouling cake structural parameter.

7.3.3 Effect of draw salt reverse flux

Since PAO experiments were performed with a lower DS concentration than FO experiments, there were some doubts whether it was the applied hydraulic pressure in the feed or the lower RSF that led to different cake layer structures. She et al. (2012) reported more severe fouling at higher DS concentrations and attributed this partly to RSF. Accumulation of draw salt in the FS due to RSF can change the feedwater chemistry and thus the membrane fouling behaviour. Boo et al. (2011) found that colloidal fouling hindered the back-diffusion of salts which accumulated within the cake layer favouring particle destabilisation and aggregation. More fouling was also reported for a DS with divalent cations (e.g., Ca^{2+} and/or Mg^{2+}), and this was due to the strong interaction between the carboxylic acid groups (COO^-) of the alginate foulant in the FS and the specific cations (Zhang et al., 2013). In addition, faster reverse diffusion of calcium ions was detected when the counter-ions also had greater diffusion rates. For example, more severe fouling was detected with $\text{Ca}(\text{NO}_3)_2$ compared to CaCl_2 because of the faster reverse diffusion of NO_3^- ions.

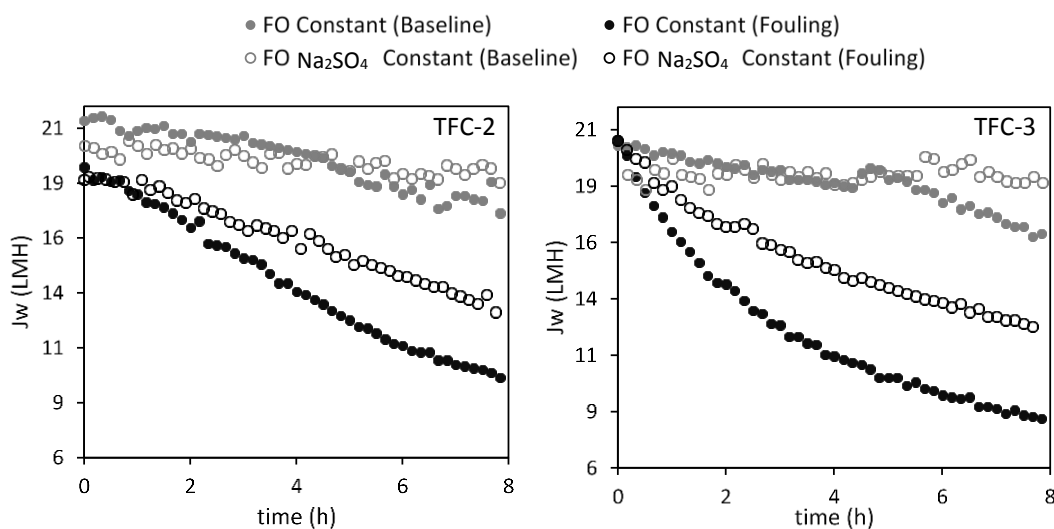


Figure 7.8 Water flux profiles for the baseline and fouling tests, with constant DS concentrations, in FO experiments with NaCl and Na_2SO_4 as draw salts and for TFC-2 and TFC-3.

Therefore, to test the role of RSF on fouling propensity, sodium sulphate (Na_2SO_4) was chosen as the draw solute for comparison due to its lower reverse salt permeability (Heo et al., 2016). The larger hydration radius of SO_4^{2-} hinders its diffusivity through the support layer and its permeability through the active layer. To allow for fair comparison, lower concentrations of Na_2SO_4 were chosen to obtain similar initial water fluxes as the NaCl experiments. In Figure 7.8, the water flux profiles of the fouling and baseline experiments with constant Na_2SO_4 as the draw solution are compared to constant NaCl as the draw solution. The corresponding values

of calculated cake structural parameter and alginate surface density are summarised in Table 7.3.

Table 7.3 Water flux decline, final alginate surface density and the final calculated cake structural parameter for both TFC membranes and for experiments with NaCl as the DS and experiments with Na₂SO₄ as the DS.

Membrane	Experiment	Water flux decline (%)	Alginate surface density (g/m ²)	Sc (μm)
TFC-2	FO Constant (Baseline)	20	-	-
	FO Constant (Fouling)	48 ± 11	24.7 ± 6.1	847
	FO Constant Na ₂ SO ₄ (Baseline)	6	-	-
	FO Constant Na ₂ SO ₄ (Fouling)	32 ± 4	10.5 ± 1.1	274
TFC-3	FO Constant (Baseline)	22	-	-
	FO Constant (Fouling)	61 ± 2	21.7 ± 1.1	339
	FO Constant Na ₂ SO ₄ (Baseline)	2	-	-
	FO Constant Na ₂ SO ₄ (Fouling)	39 ± 0	14.6 ± 0.7	261
	PAO Constant (Baseline)	12	-	-
	PAO Constant (Fouling)	63 ± 0	22.0 ± 0.7	256
	PAO Constant Na ₂ SO ₄ (Baseline)	4	-	-
	PAO Constant Na ₂ SO ₄ (Fouling)	51 ± 0	13.0 ± 1.4	104

Using sodium sulphate as the draw solution led to a lower water flux decline, less deposited alginate weight and a lower cake structural parameter than sodium chloride. The average reverse salt fluxes for experiments with NaCl and Na₂SO₄ as the draw solutions for TFC-3 were calculated to be 203 and 16 mmol m⁻² h⁻¹, respectively. This confirms that Na₂SO₄ has a much lower permeability through the membranes and suggests that a lower RSF leads to lower fouling accumulation. When Na₂SO₄ was used as the DS, a lower concentration of Na⁺ accumulated in the FS. From previous studies on alginate gels, it has been found that calcium and sodium ions independently alter the alginate gel properties and that a lower Na⁺:Ca²⁺ ratio decreases the pore sizes (Simpliciano et al., 2013). An ion exchange reaction between sodium and calcium ions has also been found to change the alginate properties (Smidsrod, 1965). A reduction in pore sizes results in a lower modelled cake structural parameter which agrees with the experiments in this study. In other words, favourable interactions between the alginate gel and sodium ions encourages fouling when a high RSF of Na⁺ is present. Although Na⁺ ions do not have any complexation effect, they increase the local ionic strength, shielding negative charges and serving as fouling promoters for charged foulants such as alginate (She et al., 2015; Xie et al., 2013).

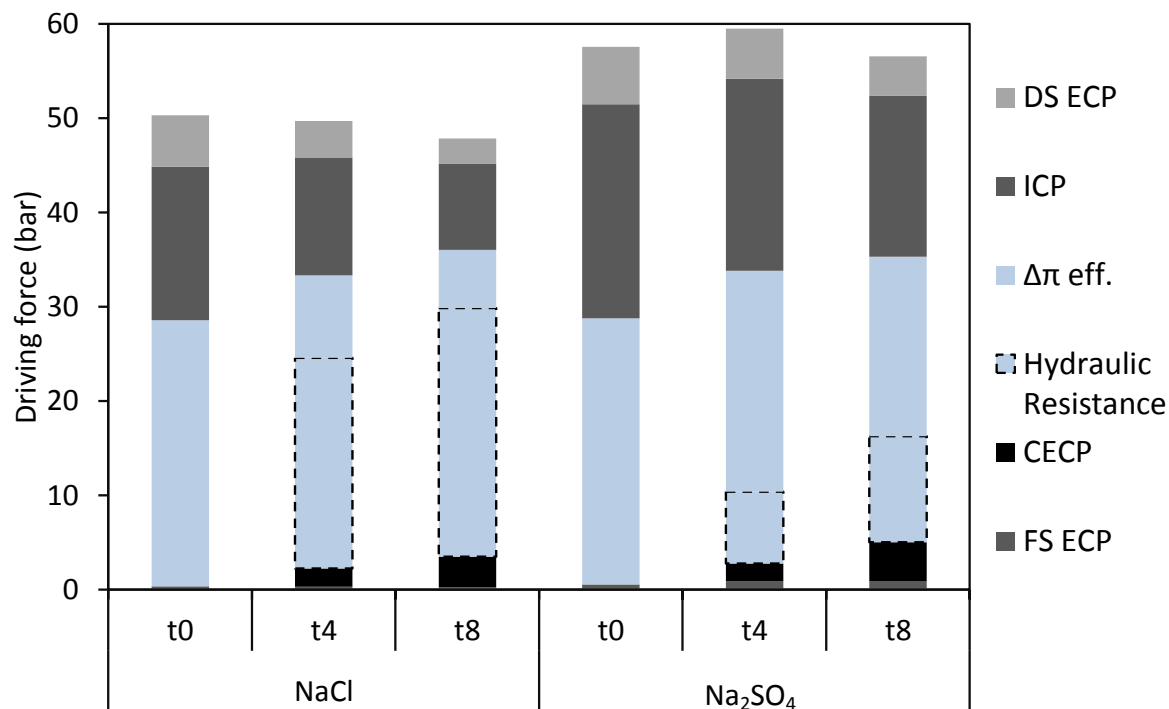


Figure 7.9 Contribution of the different concentration polarisation effects and hydraulic resistance on lowering the overall driving force to the resulting effective driving force. Again, these components were calculated for the TFC-3 membrane at three different stages of the experiment, at the beginning, after 4 hours and at the end after 8 hours. The experiments compared are FO mode with constant NaCl DS concentration and FO mode with constant Na₂SO₄ DS concentration.

The calculated CP effects and resulting effective driving force for the experiments with both draw solutions are shown in Figure 7.9. When using Na₂SO₄ as the DS, the effects of ECP and ICP were more pronounced due to the lower diffusivity of the SO₄²⁻ ion through the boundary layers and the support layer. Although less fouling accumulated on the surface of the membrane with Na₂SO₄, CECF seemed to increase, again probably due to the lower diffusivity of SO₄²⁻ ions within the cake layer. The different impact of hydraulic resistance on the effective driving force was clearly visible between the two experiments. The greater fouling resistance with NaCl reduces the water flux to a greater extent than with Na₂SO₄.

7.3.4 Effect of membrane surface properties

A comparison between the fouling propensities of the two TFC membranes from all the experiments indicates that TFC-2 leads to greater fouling accumulation. Both the alginate surface density and the cake structural parameter obtained from the majority of fouling experiments were greater for TFC-2. The membrane separation and structural properties that govern the water and salt fluxes can influence fouling behaviour. Since the initial water fluxes

were equal for both membranes, enhanced hydrodynamic drag force does not explain the results. From the membrane characterisation it has been found that TFC-2 has greater selectivity and therefore a lower RSF. This also cannot explain the obtained results as a lower RSF discourages fouling. The differences in fouling observed are likely explained by the structural and physico-chemical properties of the membranes, which influence foulant-membrane interactions and are crucial in the early stages of membrane fouling (She et al., 2015).

A greater membrane surface roughness and more hydrophilic character have been reported to enhance fouling due to the larger surface area and repulsive acid-base interactions between the foulant and the membrane (Gu et al., 2013; Tiraferri et al., 2012). Values of surface roughness and hydrophobicity are shown in the materials and methods section (Table 4.1). Although one study reports a greater surface roughness for TFC-3, another study gives a very similar value to TFC-2. In addition, both novel TFC membranes have similar hydrophobicity values. Hence, the different fouling propensity cannot be explained by these membrane properties. Another property that has been found to strongly influence the fouling severity is surface charge. Highly negatively charged membranes often exhibit strong anti-fouling tendency, because alginate gels are also negatively charged in water and are repelled by the membrane (Setiawan et al., 2012). TFC-3 has a surface charge of -58 mV compared to -13.7 mV for TFC-2 (Table 4.1). Such a large difference is likely to be the dominant cause of greater fouling for TFC-2. Nonetheless, membrane surface properties only play a role in the initial fouling stage, limiting the importance of foulant-membrane interactions in long term fouling behaviour (Tang et al., 2009). This can be seen in a plot of the first derivative of water flux against time, as shown in Figure 7.10. Strong foulant-membrane electrostatic interactions are present early in the experiment and can be only observed under mild-fouling conditions, as is the case of TFC-3 (Gu et al., 2013). For TFC-2 the influence of surface properties on fouling is not visible. Afterwards, fouling is governed by foulant-deposited-foulant interactions, which are similar for both membranes.

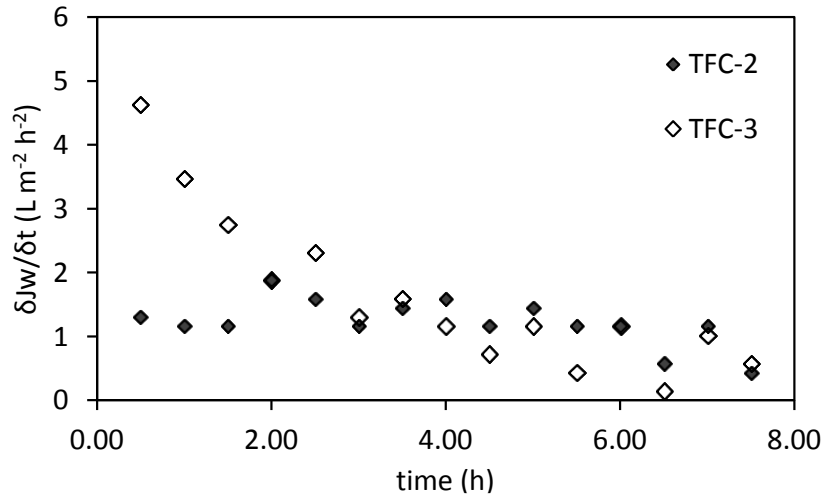


Figure 7.10 First derivative of water flux plotted against time, showing the initial effect of foulant-membrane interactions on the water flux decline. These were calculated from the FO experiments at constant DS concentration.

In conclusion, the water flux decline was proven to be an inappropriate metric for fouling propensity. Different driving forces led to similar water flux declines but different foulant accumulation, and this was attributed to the FO process unique interplay of concentration polarisation effects, RSF and effective osmotic pressure difference. More severe fouling at constant driving force was assumed to be brought on by a higher sustained effective osmotic pressure difference causing foulant compression at the active layer interface. Increased RSF was also found to encourage fouling by changing the feedwater composition and the structure of the alginate cake layer. On the other hand, the reason for why hydraulic pressure leads to a denser alginate layer was not fully understood. The general hypothesis is that hydraulic pressure stimulates the hydrostatic compaction of the cake layer, making it thinner but denser. However, it is also possible that the different response of TFC membranes to hydraulic pressure compared to osmotic pressure has a role in membrane fouling. Although more hydrophobic and with a greater surface roughness, the strong negative surface charge of TFC-3 has been found to repel alginate molecules making the membrane less prone to fouling in the initial stages of cake development.

8 Conclusions and recommendations for future research

This final section presents the conclusions and overall research findings of this thesis. In a similar way to the research objectives, the conclusions were divided into three parts, one for each of the research areas, equivalent to chapters 5-7. From the conclusions drawn, practical applications of the results, recommendations for FO membrane developers, and opportunities for future research were identified.

8.1 FO-only characterisation of novel TFC membranes

- Compared to the conventional CTA and early TFC membranes, the novel TFC membranes were composed of a more permeable active layer structure reflected by the greater A and B coefficients. This allowed for an improved water flux, easily exceeding $20 \text{ L m}^{-2} \text{ h}^{-1}$, and almost a three-fold increase in selectivity.
- Novel membranes also incorporated a thinner support layer between 100-200 μm , beneficial in reducing the adverse effects of internal concentration polarisation, particularly important at low water fluxes.
- Intrinsic membrane performance parameters for the novel TFC membranes obtained using the chosen FO-only characterisation methods were very sensitive to the variability of membrane coupons and experimental conditions, with errors of up $\pm 50\%$ in the determination of solute permeability and support layer structure.
- The duration of the characterisation experiments, the measurements' accuracy and the algorithm used in optimising the membrane parameters are the main limitations of the membrane characterisation methods.

8.2 Transport of TrOCs through novel TFC membranes

- The novel FO membranes exhibit very high rejections (above 90%) of most organic compounds due to the combination of steric hindrance and electrostatic repulsion.
- Membranes with exceptionally high negative surface charge compromise the rejection of positively charged compounds, and rejections lower than 60% can be observed for compounds such as nadolol, trimethoprim and thiabendazole. This effect is specifically pronounced on clean membranes and in the presence of low ion concentration in the feed.

- At draw solution concentrations typically used in FO which range from 0.1 to 1M, the ionic strength inside the membranes increases, shrinking the active layer pores and shielding the membrane surface charge. These changes result in a lower permeability of organic compounds as well as weaker electrostatic interactions between the membrane and the charged solutes.
- The low reverse salt fluxes that establish during typical FO operation do not have a direct impact on the permeability of organic compounds via the proposed mechanisms of hindered forward transport and Donnan dialysis. Solute-membrane interactions dominate.

8.3 Fouling propensity of novel TFC membranes with different driving forces

- It is difficult to deduce all the complex and unique fouling processes in FO from a parameter such as water flux decline, which is impacted by many different factors.
- A constant osmotic pressure driving force of 20 bar resulted in significantly higher fouling than the widely adopted approach used in FO fouling experiments whereby the osmotic pressure is not maintained constant. Almost twice as much alginate deposited on the same membrane surface of 90 cm².
- RSF-enhanced fouling and compression of the cake layer close to the active layer were identified as important FO fouling mechanisms for the novel membranes due to their enhanced permeability of water and draw salt.
- An applied hydraulic pressure in the feed solution introduces cake layer compaction even at low pressures of 1 bar in PAO mode. This is important in large FO systems as the occurrence of hydraulic pressure gradients are difficult to avoid.
- A strong negative membrane surface charge improves resistance to alginate fouling, dominating over surface roughness and hydrophobic interactions as the main parameter determining fouling propensity.
- The model for determining the cake structural parameter is over-simplified and the pore sizes, porosity and tortuosity of the foulant cake should be incorporated.

8.4 General discussion and recommendations for future research

Although accurate and comprehensive models describing mass transport in FO have been developed for conventional membranes, the applicability of these models for novel TFC

membranes was not as straightforward. Using the transport equations in the characterisation of membranes allowed for the determination of the membranes' intrinsic transport and structural parameters (A , B and S_s). These parameters are crucial for comparing the performance of membranes and consequently selecting the most appropriate membrane to use in a specific industrial process. They also aid in the design and operation of membrane installations. However, the large errors associated with the obtained parameters in this thesis and the large variability between the parameters acquired from the literature suggest that either i) the models are incomplete and inaccurate for novel TFC membranes or ii) experimental conditions, such as conductivity measurements, need to be better controlled during the characterisation experiments. More accurate characterisation methods are therefore required, tailored for specific driving forces (FO, PAO and PRO) and operating conditions (cross-flow velocity, spacers and concentration range of draw solutions). Ideally, a fundamental and reliable characterisation method for all FO membranes is needed in order to standardise and interpret the results from different labs. This involves using a standardised FO system set-up which maintains constant operating conditions, without pressure build-up along the channels and without the need of spacers allowing precise control of hydrodynamic conditions. In addition, precise measurement of conductivity and the implementation of longer experimental stages would likely reduce the experimental errors and improve the accuracy of the real membrane performance parameters. Despite the current challenges in measuring the support layer structural parameter, direct measurement of support layer thickness, porosity and tortuosity would enhance the characterisation methods and provide further information on how to best direct membrane development.

Both novel TFC membranes showed great improvements in water permeability and draw salt selectivity. This was achieved by modifying the active layer permeability and decreasing the ICP effect with thinner support layers. One of the main advantages of incorporating high-flux membranes is that low draw solution concentrations can be used, allowing for economically feasible draw solution reconcentration processes. In addition, the surface area needed for water production is reduced, limiting the capital and operational costs in large-scale applications. In the context of water reuse, these improvements in membrane permeability and selectivity are beneficial to produce more clean water with a lower draw solute loss. However, the active layer modifications to achieve these performances were found to have repercussions on the rejection of feed solutes such as organic contaminants commonly found in wastewater. Smaller pore free volumes and a higher negative surface potential contributed to a higher rejection of neutral and negatively charged compounds but adversely reduced the

rejection of positively charged compounds. In fabricating membranes, increasing membrane permeability should not be the only objective and membrane surface properties have to be properly selected for an overall improved rejection of organic compounds. In other words, it is might be more desirable to improve membrane selectivity rather than permeability. Moreover, the influence of membrane adsorption on long-term rejection behaviour of organic compounds and salting out of uncharged solutes warrants further study. So far it is widely accepted that increasing membrane hydrophilicity does reduce the adsorption capacity of hydrophobic compounds, but it might have an influence on the rejection of hydrophilic compounds and the non-steady state adsorption. Since the draw solution indirectly affects the transport of TrOCs by changing the membrane ionic strength and pore sizes, it would be interesting to investigate whether using different draw solutes further enhances the rejection of organic compounds. And even though RSF was found to have no direct impact on the permeability of the compounds, it is possible that higher reverse salt fluxes obtained with even more permeable membranes could sterically hinder the forward transport of TrOCs. Therefore additional experiments are needed using higher draw salt concentrations or using draw solutes with high RSF, to validate this mechanism. For example, using different salts in the feed and draw solutions to maintain a negligible osmotic pressure difference, avoid a water flux to establish but with the presence of a reverse salt flux.

Fouling in forward osmosis depends on many factors, from membrane properties to feedwater composition and operating conditions. Ultimately, even FO suffers from fouling which compromises the quantity of product water and is therefore a problem in large-scale water reuse applications. Maintaining a constant osmotic pressure difference across the active layer is representative of real large-scale FO processes and, because it leads to more severe fouling, future experimental set-ups aimed at studying FO fouling should include a draw re-concentration system similar to the one employed in this thesis. With regard to the applied hydraulic pressure used in PAO mode, further research is needed to pinpoint the exact cause of cake layer compaction, with specific attention on the trans-membrane pressure, and apply the knowledge obtained to improving the fouling resistance of both FO and RO water reuse systems. Hydraulic pressure is also a source of membrane deformation and its impact on water flux and subsequent fouling behaviour is not identical to that of osmotic pressure. The role of hydraulic pressure on the active layer structure needs to be fully elucidated, specifically the possibility of membrane defects shrinking or enlarging at low enough hydraulic pressures, which is suspected to be membrane specific. Nonetheless, fouling accumulation on non-

deformed membranes can be eventually estimated by considering the deviations due to hydraulic pressure.

In addition, the predictive model employed to quantify fouling needs to be extended to include variations in the hydraulic diameter of the pores and the porosity and tortuosity of alginate gels when the density increases. Ideally, the porosity of the cake layer should be measured directly and in-situ, only this way can cake compaction be confirmed. As membrane performance increases and internal mass transfer resistances decrease, external mass transfer becomes a limiting factor. As a result, module and spacer design needs to be directed to improving mass transfer and reducing fouling in the external boundary layers. Since FO modules suffer from pressure build-up in the feed and draw channels, the impact of a slight increase in hydraulic pressure on the fouling potential in FO modules needs to be explored. Particularly with state-of-the-art membranes, which are more permeable and therefore their transmembrane flux is more sensitive to pressure changes. Overall, understanding fouling is crucial in the development of new membranes with surface modifications that improve fouling resistance, and of great importance in fouling mitigation, use of spacers and designing efficient cleaning protocols.

9 References

- Achilli, A., Cath, T.Y., Childress, A.E., 2010. Selection of inorganic-based draw solutions for forward osmosis applications. *J. Memb. Sci.* 364, 233–241. doi:10.1016/j.memsci.2010.08.010
- Achilli, A., Cath, T.Y., Marchand, E. a., Childress, A.E., 2009. The forward osmosis membrane bioreactor: A low fouling alternative to MBR processes. *Desalination* 238, 10–21. doi:10.1016/j.desal.2008.02.022
- Alsvik, I.L., Hägg, M.B., 2013. Pressure retarded osmosis and forward osmosis membranes: Materials and methods. *Polymers (Basel)*. 5, 303–327. doi:10.3390/polym5010303
- Alturki, A.A., McDonald, J.A., Khan, S.J., Price, W.E., Nghiem, L.D., Elimelech, M., 2013. Removal of trace organic contaminants by the forward osmosis process. *Sep. Purif. Technol.* 103, 258–266. doi:10.1016/j.seppur.2012.10.036
- Anderson, M.G., McDonnell, J., Ximing, C., Cline, S.A., Balance, W.W., Rockstrom, J., Daily, G.C., Ehrlich, P.R., Reidy, C.A., Dynesius, M., Revenga, C., Dams, L., Reichel, E., Global, M.A., Green, P., Salisbury, J., Lammers, R.B., Kanae, S., Oki, T., Hoekstra, a Y., Eichert, P., Abbaspour, K.C., Zehnder, A.B., Kitoh, A., Hosaka, M., Dunne, K.A., Vecchia, a V, Valeo, C., Heal, K., Science, I., Bengtsson, M., Agata, Y., Kim, H., Science, E., 2006. The Challenge of Micropollutants. *Sci. Technol.* 1072–1077. doi:10.1126/science.1127291
- Ansari, A.J., Hai, F.I., Guo, W., Ngo, H.H., Price, W.E., Nghiem, L.D., 2016. Factors governing the pre-concentration of wastewater using forward osmosis for subsequent resource recovery. *Sci. Total Environ.* 566–567, 559–566. doi:http://dx.doi.org/10.1016/j.scitotenv.2016.05.139
- Arena, J.T., Manickam, S.S., Reimund, K.K., Brodskiy, P., McCutcheon, J.R., 2015. Characterization and Performance Relationships for a Commercial Thin Film Composite Membrane in Forward Osmosis Desalination and Pressure Retarded Osmosis. *Ind. Eng. Chem. Res.* 54, 11393–11403. doi:10.1021/acs.iecr.5b02309
- Awad, A.M., Jalab, R., Minier-matar, J., Adham, S., Nasser, M.S., Judd, S.J., 2019. The status of forward osmosis technology implementation. *Desalination* 461, 10–21. doi:10.1016/j.desal.2019.03.013
- Bamaga, O. a., Yokochi, a., Zabara, B., Babaqi, a. S., 2011. Hybrid FO/RO desalination system: Preliminary assessment of osmotic energy recovery and designs of new FO membrane module configurations. *Desalination* 268, 163–169. doi:10.1016/j.desal.2010.10.013
- Bellona, C., Drewes, J.E., Xu, P., Amy, G., 2004. Factors affecting the rejection of organic solutes during NF/RO treatment - A literature review. *Water Res.* 38, 2795–2809. doi:10.1016/j.watres.2004.03.034
- Bixio, D., Thoeye, C., De Koning, J., Joksimovic, D., Savic, D., Wintgens, T., Melin, T., 2006. Wastewater reuse in Europe. *Desalination* 187, 89–101. doi:10.1016/j.desal.2005.04.070
- Blandin, G., Gautier, C., Toran, M.S., Monclus, H., Rodriguez-roda, I., Comas, J., 2018. Retrofitting membrane bioreactor (MBR) into osmotic membrane bioreactor (OMBR): a pilot scale study Gaetan. *Chem. Eng. J.* doi:10.1016/j.cej.2018.01.103
- Blandin, G., Verliefe, A.R.D., Le-Clech, P., 2015. Pressure enhanced fouling and adapted anti-

- fouling strategy in pressure assisted osmosis (PAO). *J. Memb. Sci.* 493, 557–567. doi:10.1016/j.memsci.2015.07.014
- Blandin, G., Verliedde, A.R.D., Tang, C.Y., Childress, A.E., Le-Clech, P., 2013. Validation of assisted forward osmosis (AFO) process: Impact of hydraulic pressure. *J. Memb. Sci.* 447, 1–11. doi:10.1016/j.memsci.2013.06.002
- Blandin, G., Vervoort, H., D’Haese, A., Schoutteten, K., Bussche, J. Vanden, Vanhaecke, L., Myat, D.T., Le-Clech, P., Verliedde, A.R.D., 2016a. Impact of hydraulic pressure on membrane deformation and trace organic contaminants rejection in pressure assisted osmosis (PAO). *Process Saf. Environ. Prot.* 102, 316–327. doi:10.1016/j.psep.2016.04.004
- Blandin, G., Vervoort, H., Le-Clech, P., Verliedde, A.R.D., 2016b. Fouling and cleaning of high permeability forward osmosis membranes. *J. Water Process Eng.* 9, 161–169. doi:10.1016/j.jwpe.2015.12.007
- Boo, C., Lee, S., Elimelech, M., Meng, Z., Hong, S., 2011. Colloidal fouling in forward osmosis: Role of reverse salt diffusion. *J. Memb. Sci.* 390–391, 277–284. doi:10.1016/j.memsci.2011.12.001
- Braghetta, A., DiGiano, F.A., Ball, W.P., Member, ASCE, 1997. Nanofiltration of Natural Organic Matter: pH and Ionic Strength Effects. *J. Environ. Eng.* 628–641.
- Bui, N.-N., Arena, J.T., McCutcheon, J.R., 2015. Proper accounting of mass transfer resistances in forward osmosis: Improving the accuracy of model predictions of structural parameter. *J. Memb. Sci.* 492, 289–302. doi:10.1016/j.memsci.2015.02.001
- Cath, T.Y., 2009. Solute Coupled Diffusion in Osmotically Driven Membrane Processes 43, 6769–6775. doi:10.1021/es901132x
- Cath, T.Y., Childress, A.E., Elimelech, M., 2006. Forward osmosis: Principles, applications, and recent developments. *J. Memb. Sci.* 281, 70–87. doi:10.1016/j.memsci.2006.05.048
- Cath, T.Y., Elimelech, M., McCutcheon, J.R., McGinnis, R.L., Achilli, A., Anastasio, D., Brady, A.R., Childress, A.E., Farr, I. V., Hancock, N.T., Lampi, J., Nghiem, L.D., Xie, M., Yip, N.Y., 2013. Standard Methodology for Evaluating Membrane Performance in Osmotically Driven Membrane Processes. *Desalination* 312, 31–38. doi:10.1016/j.desal.2012.07.005
- Cath, T.Y., Hancock, N.T., Lundin, C.D., Hoppe-Jones, C., Drewes, J.E., 2010. A multi-barrier osmotic dilution process for simultaneous desalination and purification of impaired water. *J. Memb. Sci.* 362, 417–426. doi:10.1016/j.memsci.2010.06.056
- Cekli, L., Phuntsho, S., Kim, J.E., Kim, J., Choi, J.Y., Choi, J.S., Kim, S., Kim, J.H., Hong, S., Sohn, J., Shon, H.K., 2016. A comprehensive review of hybrid forward osmosis systems: Performance, applications and future prospects. *J. Memb. Sci.* 497, 430–449. doi:10.1016/j.memsci.2015.09.041
- Chemicalize [WWW Document], n.d. URL <https://chemicalize.com/#/> (accessed 10.20.17).
- Childress, A.E., Elimelech, M., 1996. Effect of solution chemistry on the surface charge of polymeric reverse osmosis and nanofiltration membranes. *J. Memb. Sci.* 119, 253–268. doi:https://doi.org/10.1016/0376-7388(96)00127-5
- Chung, T.S., Li, X., Ong, R.C., Ge, Q., Wang, H., Han, G., 2012. Emerging forward osmosis (FO) technologies and challenges ahead for clean water and clean energy applications. *Curr.*

Opin. Chem. Eng. 1, 246–257. doi:10.1016/j.coche.2012.07.004

- Coday, B.D., Heil, D.M., Xu, P., Cath, T.Y., 2013. Effects of Transmembrane Hydraulic Pressure on Performance of Forward Osmosis Membranes. doi:10.1021/es304519p
- Coday, B.D., Yaffe, B.G.M., Xu, P., Cath, T.Y., 2014. Rejection of trace organic compounds by forward osmosis membranes: a literature review. Environ. Sci. Technol. 48, 3612–24. doi:10.1021/es4038676
- Cornelissen, E.R., Harmsen, D., de Korte, K.F., Ruiken, C.J., Qin, J.J., Oo, H., Wessels, L.P., 2008. Membrane fouling and process performance of forward osmosis membranes on activated sludge. J. Memb. Sci. 319, 158–168. doi:10.1016/j.memsci.2008.03.048
- D’Haese, A., 2017. Mechanistic modeling of mass transport phenomena in Forward Osmosis. Ghent University, Ghent, Belgium.
- D’Haese, A., Le-Clech, P., Van Nevel, S., Verbeken, K., Cornelissen, E.R., Khan, S.J., Verliefde, A.R.D., 2013. Trace organic solutes in closed-loop forward osmosis applications: Influence of membrane fouling and modeling of solute build-up. Water Res. 47, 5232–5244. doi:10.1016/j.watres.2013.06.006
- D’Haese, A.K.H., Motsa, M.M., Meeren, P. Van Der, Verliefde, A.R.D., 2016. A refined draw solute flux model in forward osmosis: Theoretical considerations and experimental validation. J. Memb. Sci. doi:10.1016/j.memsci.2016.08.053
- Ge, Q., Ling, M., Chung, T.S., 2013. Draw solutions for forward osmosis processes: Developments, challenges, and prospects for the future. J. Memb. Sci. 442, 225–237. doi:10.1016/j.memsci.2013.03.046
- Gros, M., Rodriguez-Mozaz, S., Barceló, D., 2012. Fast and comprehensive multi-residue analysis of a broad range of human and veterinary pharmaceuticals and some of their metabolites in surface and treated waters by ultra-high-performance liquid chromatography coupled to quadrupole-linear ion trap tandem. J. Chromatogr. A 1248, 104–121. doi:10.1016/j.chroma.2012.05.084
- Gu, Y., Wang, Y.N., Wei, J., Tang, C.Y., 2013. Organic fouling of thin-film composite polyamide and cellulose triacetate forward osmosis membranes by oppositely charged macromolecules. Water Res. 47, 1867–1874. doi:10.1016/j.watres.2013.01.008
- Guo, T., Englehardt, J., Wu, T., 2014. Review of cost versus scale: Water and wastewater treatment and reuse processes. Water Sci. Technol. 69, 223–234. doi:10.2166/wst.2013.734
- Hancock, N.T., Xu, P., Heil, D.M., Bellona, C., Cath, T.Y., 2011. Comprehensive bench- and pilot-scale investigation of trace organic compounds rejection by forward osmosis. Environ. Sci. Technol. 45, 8483–8490. doi:10.1021/es201654k
- Hancock, N.T., Xu, P., Roby, M.J., Gomez, J.D., Cath, T.Y., 2013. Towards direct potable reuse with forward osmosis: Technical assessment of long-term process performance at the pilot scale. J. Memb. Sci. 445, 34–46. doi:10.1016/j.memsci.2013.04.056
- Heo, J., Boateng, L.K., Flora, J.R. V, Lee, H., Her, N., Park, Y.G., Yoon, Y., 2013. Comparison of flux behavior and synthetic organic compound removal by forward osmosis and reverse osmosis membranes. J. Memb. Sci. 443, 69–82. doi:10.1016/j.memsci.2013.04.063

- Heo, J., Chu, K.H., Her, N., Im, J., Park, Y.G., Cho, J., Sarp, S., Jang, A., Jang, M., Yoon, Y., 2016. Organic fouling and reverse solute selectivity in forward osmosis: Role of working temperature and inorganic draw solutions. *Desalination* 389, 162–170. doi:10.1016/j.desal.2015.06.012
- Hoek, E.M. V, Elimelech, M., 2003. Cake-Enhanced Concentration Polarization: A New Fouling Mechanism for Salt-Rejecting Membranes. *Environ. Sci. Technol.* 37, 5581–5588. doi:10.1021/es0262636
- Holloway, R.W., Childress, A.E., Dennett, K.E., Cath, T.Y., 2007. Forward osmosis for concentration of anaerobic digester centrate. *Water Res.* 41, 4005–4014. doi:10.1016/j.watres.2007.05.054
- Husnain, T., Liu, Y., Riffat, R., Mi, B., 2015. Integration of Forward Osmosis and Membrane Distillation for Sustainable Wastewater Reuse. *Sep. Purif. Technol.* 156, 424–431. doi:10.1016/j.seppur.2015.10.031
- Jang, D., Jeong, S., Jang, A., Kang, S., 2018. Relating solute properties of contaminants of emerging concern and their rejection by forward osmosis membrane. *Sci. Total Environ.* 639, 673–678. doi:10.1016/j.scitotenv.2018.05.078
- Jang, Y., Cho, H., Shin, Y., Choi, Y., Lee, S., Koo, J., 2016. Comparison of fouling propensity and physical cleaning effect in forward osmosis, reverse osmosis, and membrane distillation. *Desalin. Water Treat.* 3994, 1–10. doi:10.1080/19443994.2016.1152650
- Jin, X., Shan, J., Wang, C., Wei, J., Tang, C.Y., 2012. Rejection of pharmaceuticals by forward osmosis membranes. *J. Hazard. Mater.* 227–228, 55–61. doi:10.1016/j.jhazmat.2012.04.077
- Karabelas, A.J., Sioutopoulos, D.C., 2015. New insights into organic gel fouling of reverse osmosis desalination membranes. *Desalination* 368. doi:10.1016/j.desal.2015.01.029
- Kim, B., Gwak, G., Hong, S., 2017. Review on methodology for determining forward osmosis (FO) membrane characteristics: Water permeability (A), solute permeability (B), and structural parameter (S). *Desalination* 422, 5–16. doi:10.1016/j.desal.2017.08.006
- Kim, B., Lee, S., Hong, S., 2014. A novel analysis of reverse draw and feed solute fluxes in forward osmosis membrane process. *Desalination* 352, 128–135. doi:10.1016/j.desal.2014.08.012
- Kim, C., Lee, S., Shon, H.K., Elimelech, M., Hong, S., 2012. Boron transport in forward osmosis: Measurements, mechanisms, and comparison with reverse osmosis. *J. Memb. Sci.* 419–420, 42–48. doi:10.1016/j.memsci.2012.06.042
- Kim, S.J., Kook, S., O'Rourke, B.E., Lee, J., Hwang, M., Kobayashi, Y., Suzuki, R., Kim, I.S., 2017. Characterization of pore size distribution (PSD) in cellulose triacetate (CTA) and polyamide (PA) thin active layers by positron annihilation lifetime spectroscopy (PALS) and fractional rejection (FR) method. *J. Memb. Sci.* 527, 143–151. doi:10.1016/j.memsci.2016.12.064
- Kim, T.-U., Drewes, J.E., Scott Summers, R., Amy, G.L., 2007. Solute transport model for trace organic neutral and charged compounds through nanofiltration and reverse osmosis membranes. *Water Res.* 41, 3977–3988. doi:10.1016/j.watres.2007.05.055
- Kim, Y., Elimelech, M., Shon, H.K., Hong, S., 2014. Combined organic and colloidal fouling in

- forward osmosis: Fouling reversibility and the role of applied pressure. *J. Memb. Sci.* 460, 206–212. doi:10.1016/j.memsci.2014.02.038
- Kim, Y., Li, S., Chekli, L., Woo, Y.C., Wei, C.-H., Phuntsho, S., Ghaffour, N., Leiknes, T., Shon, H.K., 2017. Assessing the removal of organic micro-pollutants from anaerobic membrane bioreactor effluent by fertilizer-drawn forward osmosis. *J. Memb. Sci.* 533, 84–95. doi:10.1016/j.memsci.2017.03.027
- Kimura, K., Amy, G., Drewes, J., Watanabe, Y., 2003. Adsorption of hydrophobic compounds onto NF/RO membranes: An artifact leading to overestimation of rejection. *J. Memb. Sci.* 221, 89–101. doi:10.1016/S0376-7388(03)00248-5
- Klaysom, C., Cath, T.Y., Depuydt, T., Vankelecom, I.F.J., 2013. Forward and pressure retarded osmosis: potential solutions for global challenges in energy and water supply. *Chem. Soc. Rev.* 42, 6959. doi:10.1039/c3cs60051c
- Kong, F., Yang, H., Wang, X., Xie, Y.F., 2014a. Rejection of nine haloacetic acids and coupled reverse draw solute permeation in forward osmosis. *DES* 341, 1–9. doi:10.1016/j.desal.2014.02.019
- Kong, F., Yang, H., Wu, Y., Wang, X., Xie, Y.F., 2014b. Rejection of pharmaceuticals during forward osmosis and prediction by using the solution-diffusion model. *J. Memb. Sci.* 476, 410–420. doi:10.1016/j.memsci.2014.11.026
- Kook, S., Swetha, C.D., Lee, J., Lee, C., Fane, T., Kim, I.S., 2018. Forward Osmosis Membranes under Null-pressure Condition: Do Hydraulic and Osmotic Pressures Have Identical Nature? *Environ. Sci. Technol.* acs.est.7b05265. doi:10.1021/acs.est.7b05265
- Koutsou, C.P., Yiantsios, S.G., Karabelas, a. J., 2009. A numerical and experimental study of mass transfer in spacer-filled channels: Effects of spacer geometrical characteristics and Schmidt number. *J. Memb. Sci.* 326, 234–251. doi:10.1016/j.memsci.2008.10.007
- Kwan, S.E., Bar-Zeev, E., Elimelech, M., 2015. Biofouling in forward osmosis and reverse osmosis: Measurements and mechanisms. *J. Memb. Sci.* 493, 703–708. doi:10.1016/j.memsci.2015.07.027
- Lay, W.C.L., Chong, T.H., Tang, C.Y., Fane, A.G., Zhang, J., Liu, Y., 2010. Fouling propensity of forward osmosis: Investigation of the slower flux decline phenomenon. *Water Sci. Technol.* 61, 927–936. doi:10.2166/wst.2010.835
- Lee, J., Choi, J.Y., Choi, J.-S., Chu, K.H., Yoon, Y., Kim, S., 2016. A statistics-based forward osmosis membrane characterization method without pressurized reverse osmosis experiment. *Desalination*. doi:10.1016/j.desal.2016.04.023
- Lee, J., Kook, S., Lee, C., Kim, I.S., 2017. Effect of intermittent pressure-assisted forward osmosis (I-PAFO) on organic fouling. *Desalination* 419, 60–69. doi:10.1016/j.desal.2017.06.003
- Lee, K.Y., Mooney, D.J., 2012. Alginate: Properties and biomedical applications. *Prog. Polym. Sci.* 37, 106–126. doi:10.1016/j.progpolymsci.2011.06.003
- Lee, S., Boo, C., Elimelech, M., Hong, S., 2010. Comparison of fouling behavior in forward osmosis (FO) and reverse osmosis (RO). *J. Memb. Sci.* 365, 34–39. doi:10.1016/j.memsci.2010.08.036

- Leverenz, H.L., Tchobanoglous, G., Asano, T., 2011. Direct potable reuse: a future imperative. *J. Water Reuse Desalin.* 1, 2. doi:10.2166/wrd.2011.000
- Linares, R.V., Li, Z., Sarp, S., Bucs, S.S., Amy, G., 2014. ScienceDirect Forward osmosis niches in seawater desalination and wastewater reuse 6. doi:10.1016/j.watres.2014.08.021
- Lobo, V.M.M., 1993. Mutual Diffusion Coefficients in Aqueous Electrolyte Solutions, *Pure & Appl. Chem.* doi:10.1351/pac199365122613
- Lutchmiah, K., Cornelissen, E.R., Harmsen, D.J.H., Post, J.W., Lampi, K., Ramaekers, H., Rietveld, L.C., Roest, K., 2011. Water recovery from sewage using forward osmosis. *Water Sci. Technol.* 64, 1443–1449. doi:10.2166/wst.2011.773
- Lutchmiah, K., Verliefe, A.R.D., Roest, K., Rietveld, L.C., 2014. ScienceDirect Forward osmosis for application in wastewater treatment : A review. *Water Res.* 58, 179–197. doi:10.1016/j.watres.2014.03.045
- Manickam, S.S., McCutcheon, J.R., 2017. Understanding mass transfer through asymmetric membranes during forward osmosis: A historical perspective and critical review on measuring structural parameter with semi-empirical models and characterization approaches. *Desalination.* doi:10.1016/j.desal.2016.12.016
- Mazlan, N.M., Marchetti, P., Maples, H.A., Gu, B., Karan, S., Bismarck, A., Livingston, A.G., 2016. Organic fouling behaviour of structurally and chemically different forward osmosis membranes – A study of cellulose triacetate and thin film composite membranes. *J. Memb. Sci.* 520, 247–261. doi:10.1016/j.memsci.2016.07.065
- Mccutcheon, J.R., Elimelech, M., 2006. Influence of concentrative and dilutive internal concentration polarization on flux behavior in forward osmosis 284, 237–247. doi:10.1016/j.memsci.2006.07.049
- Mi, B., Elimelech, M., 2013. Silica scaling and scaling reversibility in forward osmosis. *Desalination* 312, 75–81. doi:10.1016/j.desal.2012.08.034
- Mi, B., Elimelech, M., 2010. Organic fouling of forward osmosis membranes: Fouling reversibility and cleaning without chemical reagents. *J. Memb. Sci.* 348, 337–345. doi:10.1016/j.memsci.2009.11.021
- Mi, B., Elimelech, M., 2008. Chemical and physical aspects of organic fouling of forward osmosis membranes. *J. Memb. Sci.* 320, 292–302. doi:10.1016/j.memsci.2008.04.036
- Nagy, E., 2014. A general, resistance-in-series, salt- and water flux models for forward osmosis and pressure-retarded osmosis for energy generation. *J. Memb. Sci.* 460, 71–81. doi:10.1016/j.memsci.2014.02.021
- Nagy, E., Hegedüs, I., Tow, E.W., Lienhard V, J.H., 2018. Effect of fouling on performance of pressure retarded osmosis (PRO) and forward osmosis (FO). *J. Memb. Sci.* doi:10.1016/j.memsci.2018.08.039
- Nghiem, L.D., Schäfer, A.I., Elimelech, M., 2006. Role of electrostatic interactions in the retention of pharmaceutically active contaminants by a loose nanofiltration membrane. *J. Memb. Sci.* 286, 52–59. doi:10.1016/j.memsci.2006.09.011
- Nghiem, L.D., Schäfer, A.I., Elimelech, M., 2004. Removal of natural hormones by nanofiltration membranes: measurement, modeling, and mechanisms. *Environ. Sci. Technol.* 38, 1888–

96. doi:10.1021/es034952r

- Nguyen, T.-T., Kook, S., Lee, C., Field, R.W., Kim, I.S., 2018. Critical flux-based membrane fouling control of forward osmosis: Behavior, sustainability, and reversibility. *J. Memb. Sci.* doi:10.1016/j.memsci.2018.10.062
- Nguyen, T.P.N., Jun, B.M., Lee, J.H., Kwon, Y.N., 2015. Comparison of integrally asymmetric and thin film composite structures for a desirable fashion of forward osmosis membranes. *J. Memb. Sci.* 495, 457–470. doi:10.1016/j.memsci.2015.05.039
- Phillip, W. a, Schiffman, J.D., Elimelech, M., 2010. High Performance Thin-Film Membrane 44, 3812–3818.
- Plakas, K. V., Karabelas, A.J., 2012. Removal of pesticides from water by NF and RO membranes - A review. *Desalination* 287, 255–265. doi:10.1016/j.desal.2011.08.003
- Rastgar, M., Shakeri, A., Salehi, H., 2017. Study of polyamide thin film characteristics impact on permeability/selectivity performance and fouling behavior of forward osmosis membrane. *Environ. Sci. Pollut. Res.* doi:10.1007/s11356-017-0043-x
- Ren, J., Mccutcheon, J.R., 2014. A new commercial thin fi lm composite membrane for forward osmosis. *Des* 343, 187–193. doi:10.1016/j.desal.2013.11.026
- S Manickam, S., McCutcheon, J.R., 2012. Characterization of polymeric nonwovens using porosimetry, porometry and X-ray computed tomography. *J. Memb. Sci.* 407–408, 108–115. doi:10.1016/j.memsci.2012.03.022
- Schock, G., Miquel, A., 1987. Mass transfer and pressure loss in spiral wound modules. *Desalination* 64, 339–352.
- Schwarzenbach, R.P., Escher, B.I., Fenner, K., Hofstetter, T.B., Johnson, C.A., Von Gunten, U., Wehrli, B., 2006. The challenge of micropollutants in aquatic systems. *Science* (80-). 313, 1072–1077.
- Setiawan, L., Wang, R., Li, K., Fane, A.G., 2012. Fabrication and characterization of forward osmosis hollow fiber membranes with antifouling NF-like selective layer. *J. Memb. Sci.* 394–395, 80–88. doi:10.1016/j.memsci.2011.12.026
- Shaffer, D.L., Werber, J.R., Jaramillo, H., Lin, S., Elimelech, M., 2015. Forward osmosis : Where are we now ? 356, 271–284.
- Shannon, M.A., Bohn, P.W., Elimelech, M., Georgiadis, J.G., Marin, B.J., Mayes, A.M., 2008. Science and technology for water purification in the coming decades 452, 301–310. doi:10.1038/nature06599
- She, Q., Hou, D., Liu, J., Tan, K.H., Tang, C.Y., 2013. Effect of feed spacer induced membrane deformation on the performance of pressure retarded osmosis (PRO): Implications for PRO process operation. *J. Memb. Sci.* 445, 170–182. doi:10.1016/j.memsci.2013.05.061
- She, Q., Jin, X., Li, Q., Tang, C.Y., 2012. Relating reverse and forward solute diffusion to membrane fouling in osmotically driven membrane processes. *Water Res.* 46, 2478–2486. doi:10.1016/j.watres.2012.02.024
- She, Q., Wang, R., Fane, A.G., Tang, C.Y., 2015. Membrane Fouling in Osmotically Driven Membrane Processes: A Review. *J. Memb. Sci.* 499, 201–233.

doi:10.1016/j.memsci.2015.10.040

- Siddiqui, F.A., She, Q., Field, R.W., Fane, A.G., 2018. Exploring the Differences between Forward Osmosis and Reverse Osmosis Fouling. *J. Memb. Sci.* 565, 241–253.
- Simpliciano, C., Mercado, M., Mobed-Miremadi, M., Clark, L., Asi, B., Diaz, S., Chu, N., Goedert, M., 2013. Cross-Linked Alginate Film Pore Size Determination Using Atomic Force Microscopy and Validation Using Diffusivity Determinations. *J. Surf. Eng. Mater. Adv. Technol.* 3, 1–12. doi:10.4236/jsemat.2013.34a1001
- Smidsrod, A.H.O., 1965. The Effect of Divalent Metals on the Properties of Alginate Solutions. *Acta Chem. Scand* 19, 329–340.
- Tang, C.Y., Chong, T.H., Fane, A.G., 2011. Colloidal interactions and fouling of NF and RO membranes : A review. *Adv. Colloid Interface Sci.* 164, 126–143. doi:10.1016/j.cis.2010.10.007
- Tang, C.Y., Kwon, Y.N., Leckie, J.O., 2009. The role of foulant-foulant electrostatic interaction on limiting flux for RO and NF membranes during humic acid fouling-Theoretical basis, experimental evidence, and AFM interaction force measurement. *J. Memb. Sci.* 326, 526–532. doi:10.1016/j.memsci.2008.10.043
- Tang, C.Y., She, Q., Lay, W.C.L., Wang, R., Fane, A.G., 2010. Coupled effects of internal concentration polarization and fouling on flux behavior of forward osmosis membranes during humic acid filtration. *J. Memb. Sci.* 354, 123–133. doi:10.1016/j.memsci.2010.02.059
- Tiraferri, A., Kang, Y., Giannelis, E.P., Elimelech, M., 2012. Superhydrophilic Thin-Film Composite Forward Osmosis Membranes for Organic Fouling Control: Fouling Behavior and Antifouling Mechanisms.
- Tiraferri, A., Yip, N.Y., Phillip, W. a., Schiffman, J.D., Elimelech, M., 2011. Relating performance of thin-film composite forward osmosis membranes to support layer formation and structure. *J. Memb. Sci.* 367, 340–352. doi:10.1016/j.memsci.2010.11.014
- Tiraferri, A., Yip, N.Y., Straub, A.P., Romero-Vargas Castrillon, S., Elimelech, M., 2013. A method for the simultaneous determination of transport and structural parameters of forward osmosis membranes. *J. Memb. Sci.* 444, 523–538. doi:10.1016/j.memsci.2013.05.023
- Tow, E.W., Lienhard, J.H., 2016. Quantifying osmotic membrane fouling to enable comparisons across diverse processes. *J. Memb. Sci.* 511, 92–107. doi:10.1016/j.memsci.2016.03.040
- Tow, E.W., Lienhard V, J.H., 2017. Unpacking compaction: Effect of hydraulic pressure on alginate fouling. *J. Memb. Sci.* 544, 221–233. doi:10.1016/j.memsci.2017.09.010
- Tow, E.W., Rencken, M.M., Lienhard, J.H., 2016. In situ visualization of organic fouling and cleaning mechanisms in reverse osmosis and forward osmosis. *Desalination* 399, 138–147. doi:10.1016/j.desal.2016.08.024
- Valladares Linares, R., Yangali-Quintanilla, V., Li, Z., Amy, G., 2011. Rejection of micropollutants by clean and fouled forward osmosis membrane. *Water Res.* 45, 6737–6744. doi:10.1016/j.watres.2011.10.037
- Verliefde, A.R.D.D., Cornelissen, E.R., Heijman, S.G.J.J., Verberk, J.Q.J.C.J.C., Amy, G.L., Van Der Bruggen, B., Van Dijk, J.C., 2008. The role of electrostatic interactions on the rejection of

- organic solutes in aqueous solutions with nanofiltration. *J. Memb. Sci.* 322, 52–66. doi:10.1016/j.memsci.2008.05.022
- Wang, J., Dlamini, D.S., Mishra, A.K., Pendergast, M.T.M., Wong, M.C.Y., Mamba, B.B., Freger, V., Verliefde, A.R.D., Hoek, E.M.V., 2014. A critical review of transport through osmotic membranes. *J. Memb. Sci.* 454, 516–537. doi:10.1016/j.memsci.2013.12.034
- Wang, Y.N., Wei, J., She, Q., Pacheco, F., Tang, C.Y., 2012. Microscopic characterization of FO/PRO membranes - A comparative study of CLSM, TEM and SEM. *Environ. Sci. Technol.* 46, 9995–10003. doi:10.1021/es301885m
- Wijmans, J.G., Baker, R.W., 1995. The solution-diffusion model : a review. *J. Memb. Sci.* 107, 1–21. doi:10.1016/0376-7388(95)00102-I
- Wong, M.C.Y., Martinez, K., Ramon, G.Z., Hoek, E.M.V., 2012. Impacts of operating conditions and solution chemistry on osmotic membrane structure and performance. *Desalination* 287, 340–349. doi:10.1016/j.desal.2011.10.013
- Xie, M., Lee, J., Nghiem, L.D., Elimelech, M., 2015. Role of pressure in organic fouling in forward osmosis and reverse osmosis. *J. Memb. Sci.* 493, 748–754. doi:10.1016/j.memsci.2015.07.033
- Xie, M., Nghiem, L.D., Price, W.E., Elimelech, M., 2014. Relating rejection of trace organic contaminants to membrane properties in forward osmosis: Measurements, modelling and implications. *Water Res.* 49, 265–274. doi:10.1016/j.watres.2013.11.031
- Xie, M., Nghiem, L.D., Price, W.E., Elimelech, M., 2013. Impact of humic acid fouling on membrane performance and transport of pharmaceutically active compounds in forward osmosis. *Water Res.* 47, 4567–4575. doi:10.1016/j.watres.2013.05.013
- Xie, M., Nghiem, L.D., Price, W.E., Elimelech, M., 2012. Comparison of the removal of hydrophobic trace organic contaminants by forward osmosis and reverse osmosis. *Water Res.* 46, 2683–2692. doi:10.1016/j.watres.2012.02.023
- Xu, W., Chen, Q., Ge, Q., 2017. Recent advances in forward osmosis (FO) membrane: Chemical modifications on membranes for FO processes. *Desalination* 419, 101–116. doi:10.1016/j.desal.2017.06.007
- Zhang, M., Hou, D., She, Q., Tang, C.Y., 2013. Organic Fouling in pressure retarded osmosis: Experiments, mechanisms and implications. *J. Memb. Sci.* 428, 181–189. doi:10.1016/j.watres.2013.09.051
- Zheng, L., Price, W.E., Nghiem, L.D., 2018. Effects of fouling on separation performance by forward osmosis: the role of specific organic foulants. *Environ. Sci. Pollut. Res.* 1–12. doi:10.1007/s11356-018-2277-7
- Zhou, Z., Lee, J.Y., Chung, T.S., 2014. Thin film composite forward-osmosis membranes with enhanced internal osmotic pressure for internal concentration polarization reduction. *Chem. Eng. J.* 249, 236–245. doi:10.1016/j.cej.2014.03.049